INFLUENCE OF METALLIC AND BASIC SITES OF NI-PROMOTED SBA-15 ON THE MECHANISTIC PATH OF CO$_2$-METHANATION
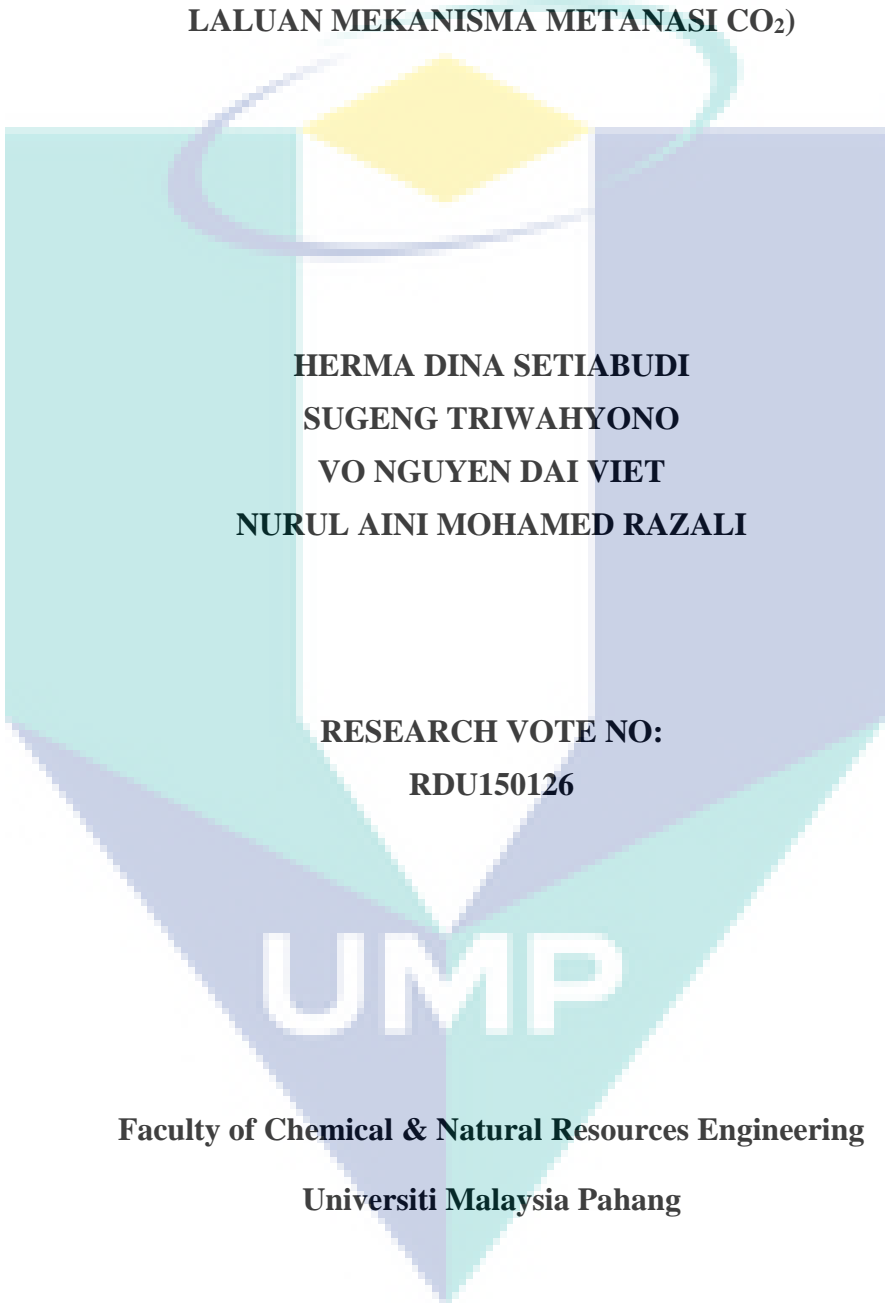
(PENGARUH LOGAM DAN TAPAK BES NI-PEMANGKIN SBA-15 KE ATAS LALUAN MEKANISMA METANASI CO$_2$)

HERMA DINA SETIABUDI

SUGENG TRIWAHYONO

VO NGUYEN DAI VIET
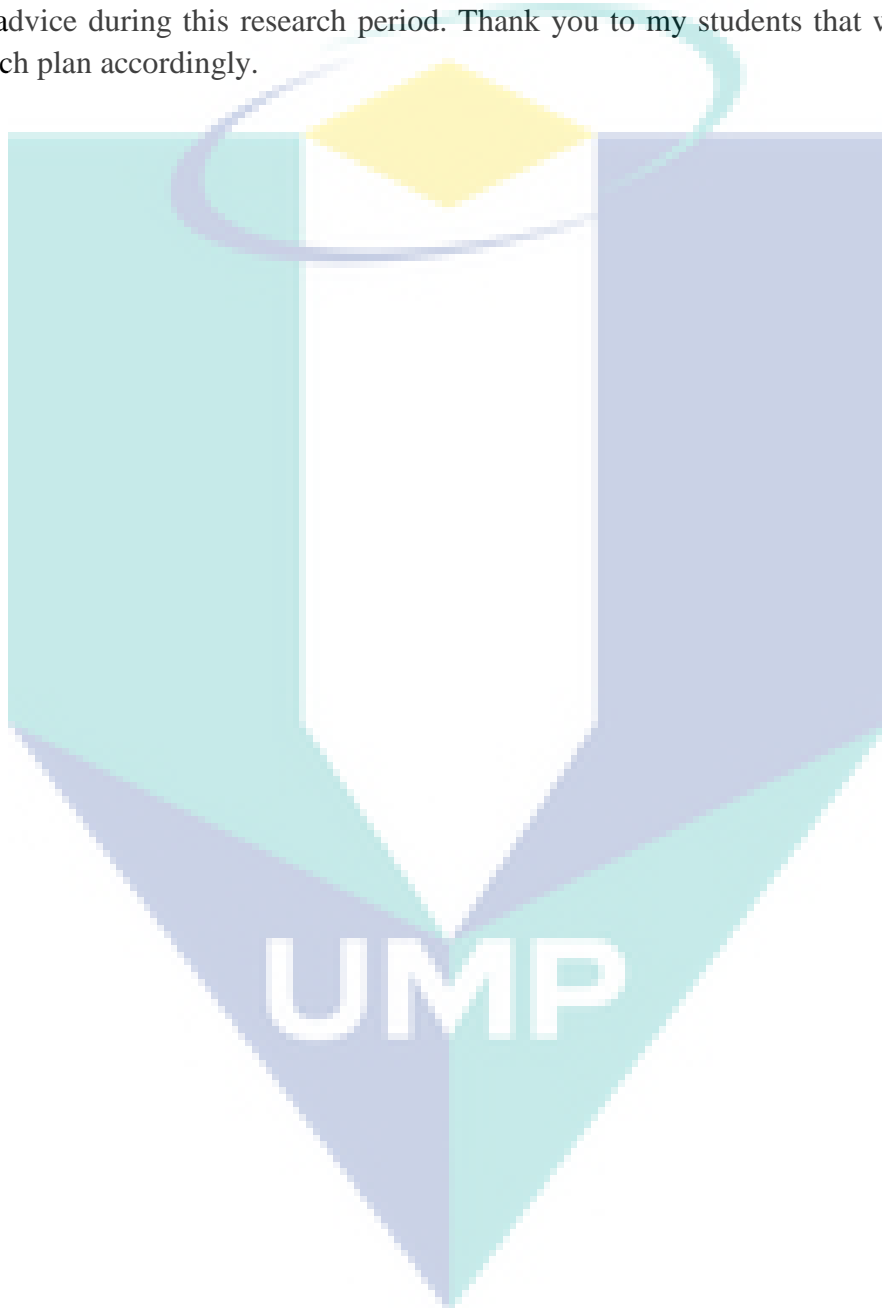
NURUL AINI MOHAMED RAZALI

RESEARCH VOTE NO:

RDU150126

Faculty of Chemical & Natural Resources Engineering

Universiti Malaysia Pahang

2018

ACKNOWLEDGEMENTS

ABSTRACT

INFLUENCE OF METALLIC AND BASIC SITES OF NI-PROMOTED SBA-15 ON THE MECHANISTIC PATH OF CO$_2$ METHANATION

The utilization of carbon dioxide (CO$_2$) has become an important topic in recent years. As CO$_2$ is one of the main contributors to greenhouse effect and hence to climate change, there is a growing interest in its use as a feedstock in chemical processes. The conversion of CO$_2$ into methane (CH$_4$) has been investigated extensively, using variety of supported metal catalysts including Ni/SBA-15. However, proper design of catalyst preparation is needed to prepare well-dispersed Ni/SBA-15. In addition, the real function of metal and basic sites on the CO$_2$ methanation process over Ni/SBA-15 is still unclear. Therefore, the objective of this study is to synthesis the well-dispersed Ni/SBA-15 for CO$_2$ methanation and investigates the influence of metallic and basic sites of Ni/SBA-15 on the mechanistic path of CO$_2$ methanation. The well-dispersed Ni/SBA-15 were synthesized by studying the effect of TEOS/P123 mass ratios (R1.5, R2.21, R3.0), hydrothermal techniques (Reflux (R) and Teflon (T)) and Ni content (1 – 10 wt%). The properties of Ni/ SBA-15 were determined by XRD, BET, FTIR, TEM, FESEM-EDX, H$_2$-TPR. The CO$_2$ methanation were carried out in a stainless steel fixed-bed reactor and the role of metallic and basic sites on mechanistic path of CO$_2$ methanation were clarified using in-situ FTIR adsorbed pyrrole, H$_2$, CO$_2$ and H$_2$ + CO$_2$. The results revealed that the well-dispersed Ni/SBA-15 was successfully synthesized at TEOS/P123 = 2.21, reflux hydrothermal technique and 5 wt.% Ni, with CO$_2$ conversion = 99.7% and CH$_4$ yield = 98.2% at T = 673 K. The in-situ FTIR studies of adsorbed H$_2$, CO$_2$, and H$_2$ + CO$_2$ confirmed that the CO$_2$ methanation of Ni/SBA-15 proceeded by CO dissociative reaction pathway. Firstly, the CO$_2$ and H$_2$ molecule were dissociated to CO, O, and H atoms on the surface of Ni metal active sites and spillover onto the support to form unidentate carbonates, bidentate carbonates and linear carbonyl as the main adsorption species. Then, these intermediate species were further undergoing hydrogenation with the atomic hydrogen to form CH$_4$ and H$_2$O. In conclusion, well dispersed Ni/SBA-15 was successfully synthesized and the role of metallic and basic sites of Ni/SBA-15 on CO$_2$ methanation were successfully discovered. The metal sites were responsible in the dissociation of CO$_2$ and H$_2$, while the concentration of basic sites influenced the CO$_2$ adsorption ability of the catalyst.

Key researchers: Herma Dina Setiabudi, Sugeng Triwahyono, Nguyen Dai Viet, Nurul Aini Mohamed Razali

E-mail : herma@ump.edu.my; Tel. No.: 09-5492836; Vote No.: RDU150126

ABSTRAK

PENGARUH LOGAM DAN TAPAK BES NI-PEMANGKIN SBA-15 KE ATAS LALUAN MEKANISMA METANASI CO_2

*(**Kata** kunci: Ni/SBA-15, metanasi CO_2; Ni/SBA-15; laluan mekanisma, tapak **logam**, tapak bes)*

Penggunaan karbon dioksida (CO_2) telah menjadi topik penting dalam beberapa tahun kebelakangan ini. Oleh kerana CO_2 adalah salah satu penyumbang utama kepada kesan rumah hijau dan membawa kepada perubahan iklim, terdapat minat yang semakin meningkat dalam penggunaannya sebagai bahan mentah dalam proses kimia. Penukaran CO_2 ke metana (CH_4) telah diselidik secara meluas, menggunakan pelbagai pemangkin logam yang disokong termasuk Ni/SBA-15. Walau bagaimanapun, reka bentuk penyediaan pemangkin yang tepat diperlukan untuk menyediakan Ni/SBA-15 yang baik. Di samping itu, fungsi sebenar logam dan tapak bes pada proses metanasi CO_2 terhadap Ni/SBA-15 masih tidak jelas. Oleh itu, objektif kajian ini adalah untuk sintesis yang Ni/SBA-15 yang baik untuk metanasi CO_2 dan menyiasat pengaruh tapak logam dan bes Ni/SBA-15 ke atas laluan mekanisma metanasi CO_2. Ni-SBA-15 yang baik telah disediakan dengan mengkaji kesan nisbah TEOS/P123 (R1.5, R2.21, R3.0), teknik hidroterma (Refluks (R) dan Teflon (T)) dan kandungan Ni (1 - 10%). Sifat Ni/SBA-15 ditentukan oleh XRD, BET, FTIR, TEM, FESEM-EDX, H2-TPR. Metanasi CO_2 telah dilakukan dalam reaktor padatan-tetap keluli tahan karat, dan peranan logam dan tapak bes ke atas laluan mekanisma metanasi CO_2 telah dijelaskan dengan menggunakan *in-situ* FTIR pirol dan *in-situ* FTIR (H_2 dan CO_2)**.** Keputusan menunjukan Ni/SBA-15 yang baik telah berjaya disintesis pada TEOS/P123 = 2.21, teknik hidrotermal refluks dan beban 5% Ni, dengan penukaran CO_2 = 99.7% dan hasil CH_4 = 98.2% pada T = 673 K. Kajian *in-situ* FTIR jerap H_2, CO_2, dan $H_2 + CO_2$ mengesahkan bahawa metanasi CO_2 untuk Ni/SBA-15 melalui laluan tindak balas CO dissociative. Pertama, molekul CO_2 dan H_2 telah dipisahkan kepada CO, O, dan atom H di permukaan tapak aktif logam Ni dan dilimparkan pada sokongan untuk membentuk karbonat unidentat, karbonat bidentat dan karbonil lurus sebagai spesies penyerapan utama. Kemudian, spesies perantaraan ini terus menjalani hidrogenasi dengan atom hidrogen membentuk CH_4 dan H_2O. Sebagai kesimpulan, Ni/SBA-15 yang baik berjaya disintesis dan peranan metallic dan tapak bes Ni / SBA-15 pada metanasi CO_2 telah berjaya ditemui. Tapak logam bertanggungjawab dalam pemisahan CO_2 and H_2, sementara kepekatan tapak asas mempengaruhi keupayaan penjerapan CO_2 pemangkin.

Penyelidik utama: Herma Dina Setiabudi, Sugeng Triwahyono, Nguyen Dai Viet, Nurul Aini Mohamed Razali

E-mail : herma@ump.edu.my; Tel. No.: 09-5492836; Vote No.: RDU150126

TABLE OF CONTENT

vii

LIST OF TABLES

LIST OF FIGURES

LIST OF SYMBOLS

%	Percentage
wt%	Weight percentage
ml	millilitre
θ	Angle
X_{CO2}	Conversion of carbon dioxide
X_{CH4}	Conversion of methane
F	Molar flow rate
P	Partial pressure
Ps	Saturated pressure
A	Area
m	Mass
λ	Wavelength of ray
˚C	Degrees Celsius
kg	kilogram
g	gram
h	hour
mL	mililiter
min	minute

LIST OF ABBREVIATIONS

Al_2O_3	Aluminium oxide
BET	Breneuer-Emmett Teller
CH_4	Methane
CO	Carbon monoxide
Co	Cobalt
CO_2	Carbon dioxide
FTIR	Fourier-transform infrared spectroscopy
H_2	Hydrogen
H_2O	Water
H_2SO_4	Sulphuric acid
MCM-41	Mobil Catalytic Material Number 41
N_2	Nitrogen
N_2O	Nitrous Oxide
Na	Sodium
Na_2O_3	Sodium dioxide
Ni	Nickel
NiO	Nickel oxide
O_3	Ozone
P123	Pluronic triblock copolymer
Pt	Platinum
Rh	Rhodium
Ru	Ruthenium
SBA-15	Santa-Barbara Amorphous 15
SiO_2	Silicon dioxide
TEM	Transmission electron microscope
XRD	X-Ray diffraction

CHAPTER 1

INTRODUCTION

1.1   Background of the study

Climate change has become one of the main concerns of humanity in recent century. The negative effects of greenhouse gas (GHG) emission on people health are unavoidable fact. As CO_2 is one of the main contributors to GHGs in Malaysia, the recycling of CO_2 has become an important topic in recent years. There are several ways of adding value of CO_2, one of which is CO_2 hydrogenation to form CH_4. The CO_2 methanation reaction is an important catalytic process of fundamental academic interest with potential commercial applications and it is recognized as a green technology (Takht & Sahebdelfar, 2014). The CH_4 produced by this reaction can be sent to chemical industries or can be utilized as an energy vector, which is an important advantage considering that the infrastructure for transport and storage of methane is already present.

The conversion of CO_2 into CH_4 has been extensively studied, using variety of supported metal catalysts. Mesoporous SBA-15 is preferred as a support material due to its large pore size, high thermal stability, uniformly arranged mesopores and very high surface area. This high surface area can be exploited to create highly dispersed active species on support surfaces (Abdullah et al., 2010; Lu & Kawamoto, 2013; Rahmat et al., 2010; Wang et al., 2015). Regarding the choice of metal, it has been reported that nickel (Ni) shows good activity for methanation, and the presence of supports can markedly improve catalytic activity (Aziz et al, 2015a; Pan et al., 2014). Because the support has a significant influence on the morphology of the active phase and catalytic properties (Lu & Kawamoto, 2013; Wang & Gong, 2011), preparation of highly dispersed supported metal catalysts has been the focus of considerable research. Therefore, it is desirable to synthesis the well-dispersed Ni/SBA-15 for the CO_2 methanation.

Aziz et al. studied the CO_2 methanation over metal supported on mesoporous silica material prepared by alkaline media synthesis (MSN), and reported that the metal sites were responsible in the dissociation of CO_2 and H_2 (Aziz et al., 2014), while the concentration of basic sites influenced the CO_2 adsorption ability of the catalyst (Aziz et al., 2014). However, the different metals and supports used in CO_2 methanation will give different effects on the properties and mechanism of reaction (Aziz et al., 2014; Aziz et al., 2014). Thus, it is desirable to study the influence of metallic and basic sites on the mechanistic path of CO_2 methanation over metal supported on mesoporous silica material prepared by acidic media synthesis (SBA-15), owing to the fact that the synthesis condition will greatly influence the properties of catalyst.

1.2   Objectives

The objectives of this research are as follows:

1. To synthesis and characterize well dispersed Ni-promoted SBA-15.

2. To investigate the catalytic activity of the synthesized catalysts on CO_2 methanation.

3. To determine the influence of metallic and basic sites of Ni/SBA-15 on the mechanistic path of CO_2 methanation

1.3   Scopes of study

The scopes of this research as follows:

Work scopes for objective 1

Preparation of well dispersed Ni/SBA-15 by:

i) Studying the effect of TEOS/P123 ratio (1.5, 2.21 & 3.0).
ii) Studying the effect preparation techniques of SBA-15 (without hydrothermal, hydrothermal using reflux method and hydrothermal using Teflon-lined stainless-steel autoclave).
iii) Studying the effect of Ni loading (0, 3, 5 & 10 wt%).

Determination of the physical and chemical properties of synthesized catalyst by using x-ray diffraction (XRD), brunauer-emmett-teller (BET) specific surface area and porosity

2

analyser, fourier transform infra-red (FTIR) spectroscopy, uv-vis diffuse reflectance spectroscopic (UV-Vis DRS), scanning electron microscopy equipped with energy dispersive x-ray spectroscopy (SEM-EDX), transmission electron microscopy (TEM), hydrogen - temperature programmed reduction (H_2-TPR), and thermogravimetric analyser (TGA).

Work scopes for objective 2

Investigation of the catalytic performance of Ni/SBA-15 towards CO_2 methanation using stainless steel fixed-bed reactor and gas chromatography (GC).

Work scopes for objective 3

Determination of the role of metallic and basic sites of Ni/ SBA-15 on mechanistic path of CO_2 methanation using:

i)   In-situ FTIR pyrrole
ii) In-situ FTIR (H_2 and CO_2).

CHAPTER 2

LITERATURE REVIEW

2.1 Carbon Dioxide (CO_2)

Carbon dioxide (CO_2) is defined as a colourless gas which composed of one carbon atom bonded covalently to two oxygen atoms. It is very stable, non-toxic and non-flammable molecule. CO_2 is one of the major contributors to the greenhouse gases. It is also known as sour gas which promotes the corrosion especially in the steel-pipelines, and thus reducing the quality and price of the natural gas. In fact, the degradation of natural gas quality can be occurred by the appearance of uncontrolled carbon dioxide (CO_2). However, CO_2 capturing and recycling are significantly recognized as the great interest techniques for mitigating the emission of greenhouse gases at controlled level into the atmosphere and converting the waste CO_2 into more valuable, marketable and economical feedstocks. Currently, there are various ranges of CO_2 applications including the production of methane, formic acid, dimethyl ether, alkyl formates, alkyl formamides, carbon monoxide, syngas, methanol, and oxalic acid.

2.2 CO_2 Methanation

Methanation of carbon dioxide also called the Sabatier reaction is an important catalytic hydrogenation process. It is an exothermic reaction ($\Delta H_{298K} = -165.0$ kJ/mol, $\Delta G_{298K} = -113.2$ kJ/mol). Catalytic CO_2 methanation not only enhances the CO_2 removal, but it promotes an efficient and green technology pathway for the development of CO_2 recycling towards more valuable and sustainable use such as for the synthesis of methane (chemicals), which can indeed reduce the greenhouse gases emissions. Thus, CO_2 methanation is considered as the most efficient and green technology process to remove high content of CO_2 present in the natural gas. Equation 2.1 represents the reaction of CO_2 methanation.
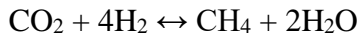
$$CO_2 + 4H_2 \leftrightarrow CH_4 + 2H_2O \qquad\qquad\qquad 2.1$$

Besides, as compared to the methanation of carbon monoxide (CO), the methanation of CO_2 is reported to proceed with lower activation energy and a higher rate. CO_2 methanation is also categorized as a simple reaction for the methane production whereby it is operated under atmospheric compared with other productions such as methanol and dimethyl ether (DME), directly injected into natural gas pipeline and can be used as a raw material for the chemical production (Aziz et al., 2015).

2.2.1 Plausible mechanism of CO2 methanation

Insight into the mechanism of CO_2 methanation has been studied either by using fourier transform infrared (FTIR) spectroscopy or diffuse reflectance infrared fourier transform (DRIFT) spectroscopy. Several authors have discussed the mechanism of CO_2 methanation over supported metal catalysts. One of the most cited mechanism proposes that CO_2 reacts with H_2 at the interface between the metal and supports, in which reverse water-gas shift (RWGS) reaction is involved (as shown in Equation 2.2). RWGS reaction is defined as a reaction whereby it forms CO as an intermediate. This reaction occurs on metal sites and is followed by the hydrogenation of CO into methane and water (as shown in Equation.2.3) (Aldana et al., 2013; Tada et al., 2012).

$$CO_2 + H_2 \leftrightarrow CO + H_2O \qquad\qquad\qquad 2.2$$

$$CO(CO + 3H_2 \rightarrow CH_4 + H_2O) \qquad\qquad\qquad 2.3$$

Frontera et al. (2017) had reported that there are two paths that are usually involved in CO_2 methanation reaction. The first path is the conversion of CO_2 into CO as the intermediate of reaction continues with CO hydrogenation into methane which is same with CO methanation reaction and the second path is the direct methanation of CO_2 into methane production. The simplified reaction mechanisms of CO_2 methanation which have been mentioned by Frontera et al. (2017) is illustrated in Figure 2:1.
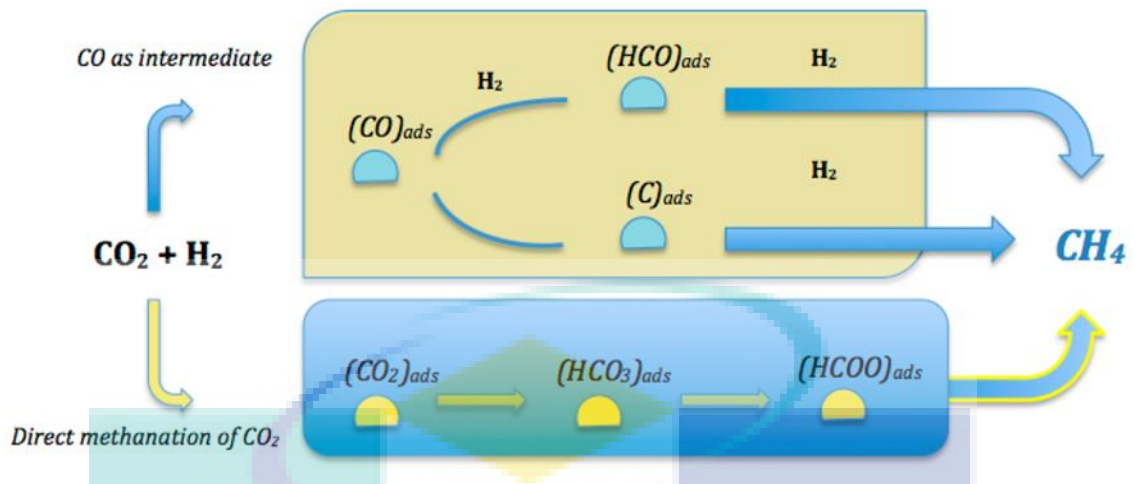
Figure 2:1   Simplified reaction mechanisms of CO_2 methanation

Source: Frontera et al. (2017)

It was in agreement with Aziz et al. (2015b) and Zheng et al. (2016). The other proposed mechanism is the formation of carbon over supported Ni-based catalyst. It can be summarized that there are six main products of CH_4, CO, H_2, CO_2, H_2O and C deposit are highly possible to be produced from CO_2 methanation. Three main independent reactions mostly involved in the CO_2 methanation process which are;

$$CO_2 + H_2 \leftrightarrow CH_4 + H_2O \qquad\qquad 2.4$$

$$CO_2 + H_2 \leftrightarrow CO + H_2O \qquad\qquad 2.5$$

$$CO_2 + 2H_2 \leftrightarrow C + 2H_2O \qquad\qquad 2.6$$

However, different opinions have been mentioned by Aziz et al. (2015a) on the nature of the intermediate towards methane production. It has been reported that either carbon in CO_2 dissociation and its hydrogenation or CH_xO interacted with hydrogen might be formed and known as the rate-limiting step. He also stated that the CO which is formed from reaction between CO_2 and H_2 might be reacted with oxide surfaces of the catalysts to form three species of bridged carbonyl, linear carbonyl, and bidentate formate as the intermediate for CO_2 methanation. The formation of bridged carbonyl, linear carbonyl, and bidentate formate as the intermediate for CO_2 methanation is shown in Figure 2:2.
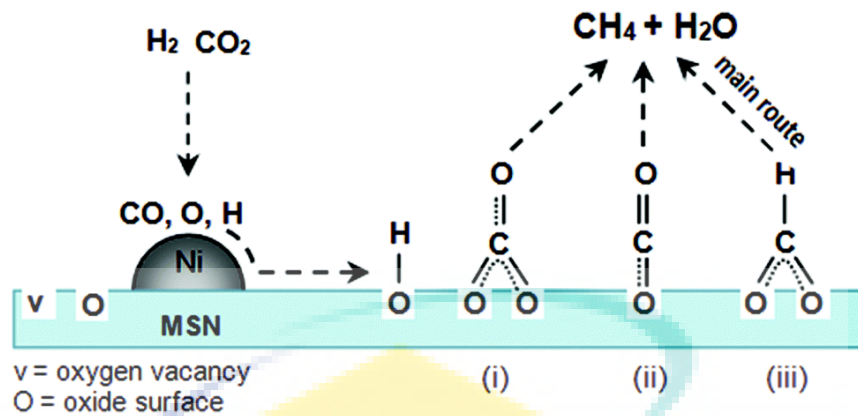
Figure 2:2   The formation of bridged carbonyl, linear carbonyl, and bidentate formate as the intermediate for CO_2 methanation

Source: Aziz et al. (2015a)

In addition, Aziz et al. (2014b) had studied about the CO_2 methanation over metal supported on mesoporous silica material prepared by alkaline media synthesis (MSN), and reported that there are two important sites contained in the surface centres of catalyst which are highly responsible for the activity sites of the reaction; metallic site and associated basic site. The metal sites were responsible in the dissociation of CO_2 and H_2 (Aziz et al., 2014b), while the concentration of basic sites influenced the CO_2 adsorption ability of the catalyst (Aziz et al., 2014a).

Consequently, the metal sites must be not existed in the oxide form. It was due to the efficiency of CO_2 conversion towards methane production might be reduced, and thus lowering the catalytic performances of the catalyst towards CO_2 methanation. Regarding to the previous study by Mutz et al. (2015) who had studied on Ni/CaO-Al_2O_3 catalyst, high performances of catalyst were observed whereas about 81% of CO_2 conversion with 99% of CH_4 selectivity had been achieved. However, when the metal particles were oxidized partly becoming to metal oxides due to dropped out of H_2, the catalytic performances of CO_2 methanation over metal-based catalyst were reduced indicating that fluctuation conditions of catalyst oxidization must be prevented and the supply of H_2 had to be considered (Mutz et al., 2015). The schematic diagram of CO_2 methanation over the supported Ni and NiO catalysts is shown in Figure 2:3.
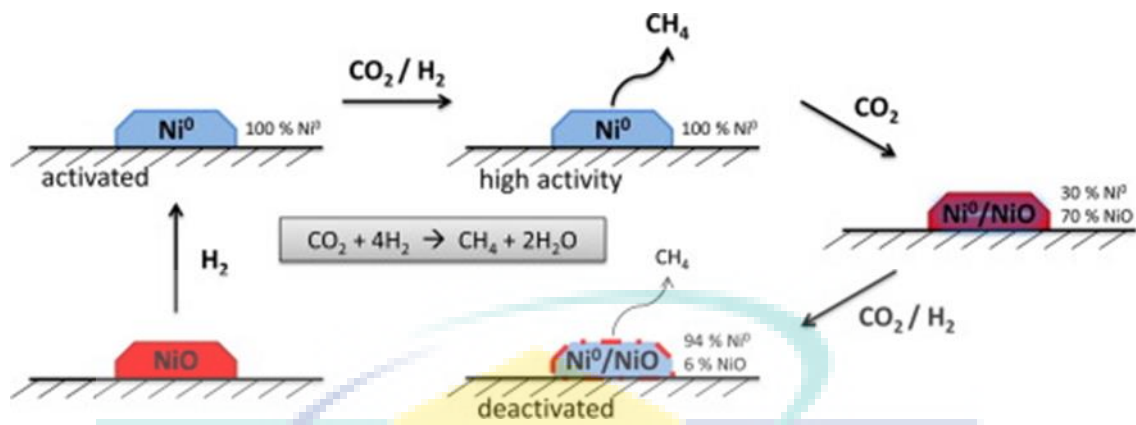
Figure 2:3   The formation of bridged carbonyl, linear carbonyl, and bidentate formate as the intermediate for CO_2 methanation

Source: Aziz et al. (2015a)

The different metals and supports used in CO_2 methanation will give the different effects on the properties and mechanism of reaction (Aziz et al., 2014a; Aziz et al., 2014b; Halim et al., 2014; Zheng et al., 2016). Furthermore, although there are many reviews and findings from the previous studies regarding the CO_2 methanation, it is difficult to conclude what is the exact mechanism involved in CO_2 methanation. There is still no general consensus regarding the reaction's mechanism of CO_2 methanation due to uncertainty rate determining step as the intermediate of reaction (Frontera et al., 2017).

2.3   Supported metal catalysis for CO_2 methanation

The CO_2 conversion into methane has been studied extensively using variety of supported metal catalysts. They are typically operated at temperatures ranging from 220 °C to 450 °C. Tada et al. (2012) reported about the catalytic performance of metal-based catalysts (Ni/CeO_2, $Ni/\alpha-Al_2O_3$, Ni/TiO_2 and Ni/MgO) towards CO_2 methanation 350 °C. They found that Ni/CeO_2 exhibited the most superior catalytic performance of CO_2 methanation whereby it possessed high CO_2 conversion and CH_4 selectivity especially at low temperature in comparable with $Ni/\alpha-Al_2O_3$, Ni/TiO_2 and Ni/MgO catalysts. It was due to the highly coverage of CO_2 species on the surface of CeO_2 and it was partially being reduced during the reaction. The catalytic properties of the metal-based catalyst (Ni-based ceria-zirconia) had also been discussed by Aldana et al. (2013). They reported that Ni-based ceria-zirconia catalyst might provide a superior performance in the CH_4 production owing to its promising Ni metals which are able to activate the Co_x

8

methanation activity, and favorable ceria-zirconia support that allowed the activation of CO_2. Cai et al. (2011) had studied about the catalytic evaluation of metal-based catalysts ($Ni/ZrO_2-Al_2O_3$) for CO_2 methanation. The effect of ZrO_2 promoter and different preparation method for the Ni metals dispersion onto the $ZrO_2-Al_2O_3$ support (impregnation-precipitation, co-precipitation, and impregnation) were synthesized as to produce the $Ni/ZrO_2-Al_2O_3$ catalysts, and then CO_2 methanation over those metal-based catalysts were investigated. The result showed that Ni incorporation into $ZrO_2-Al_2O_3$ support synthesized by the impregnation-precipitation method exhibited an outstanding catalytic behavior and stability as compared with other supports, implying better Ni dispersion and easier NiO reduction. As a result, it led an enhanced catalytic behavior of $Ni/ZrO_2-Al_2O_3$ catalyst towards CO_2 methanation

Similar observation was also reported by Ocampo et al. (2011) for the promising metal-based catalyst (Ni-based $Ce_xZr_{1-x}O_2$) for CO_2 methanation. The parameters used in their study were the influence of Ce/Zr composition and the introduction of noble metal for metal dispersion. They found that an excellent catalytic performance was achieved by the Ni-based CeO_2/ZrO_2 =60/40 Additionally, the introduction of the noble metal led the formation of homogenous and better Ni dispersion onto the framework and channels of support, and thus resulted to a higher activity and stability with a minimum rate of Ni sintering. As obtained from the previous study by Ocampo et al. (2011), it revealed that an excellent catalytic behaviour of metal-based catalyst did not only affected by the surface of available metallic nickel, but also on the composition of the support and on its modification by Ni^{2+} doping.

There are still numerous metal-based catalysts that widely being used for CO_2 methanation. The review of previous studies on CO_2 methanation over supported metal catalysts is summarized in Table 2:1. As observed, it could be summarized that the promising characteristics of metal-based catalyst is highly needed as it can provide an outstanding behavior and stability. Herein, this present work highlighted on the metal-based catalyst for an efficient methane production.

9

Table 2:1   Review of previous studies on CO_2 methanation over supported metal catalysts

Catalysts	Preparation method	T [°C]	CO_2 conversion [%]	CH_4 selectivity [%]	Advantages / Limitations	Reference
10 wt% Ni/CeO_2	Impregnation	350	93	100	Higher CO_2 conversion and CH_4 selectivity	Tada et al. (2012)
5 wt% Ni/ceria- zirconia	Pseudo sol–gel	350	67.9	98.4	Conversion decreased by 15 % after 90 h	Aldana et al. (2013)
12 wt% $Ni/ZrO_2–Al_2O_3$	Impregnation-precipitation	360	69.8	100	Conversion decreased by 1.6 % after 100 h	Cai et al. (2011)
5 wt% $Ni–Ce_xZr_{1−x}O_2$	Pseudo sol–gel	350	80	>98	Conversion decreased by 18.8 % after 140 h	Ocampo et al. (2011)
15 wt% Ni–La/SiC	Impregnation	360	85	100	Stable after 70 h	Zhi et al. (2011)
$(Co_{0.95}Ru_{0.05})_3 O_4$ nanorod	Modified wet chemistry	380	33	97	Active phases of two catalysts are metallic cobalt and bimetallic Co–Ru, respectively	Zhu et al. (2012)
35 wt% Ni/5 wt% Fe/ Alumina xerogel	Single step sol–gel	220	63.4	99.5	n/a	Hwang et al. (2012)
70 wt% Ni/SBA-15	Heat treatment	300 – 450	99.2	100	High thermal stability due to unchanged surface area after catalytic test	Lu & Kawamoto, (2013)
14 wt% Ni/USY	Impregnation	400	65.5	94.2	Stable after 10 h	Graça et al. (2014)
$Ce_{0.95}Ru_{0.05}O_2$	Combustion	450	55	99	Reaction takes place on reduced catalyst and role of dopant (Ru) is to make reduction possible at lower temperatures than on pure ceria	Sharma et al. (2011)
5 wt% Ni/2 wt% ceria/ Al_2O_3	Co–impregnating boehmite with metal solutions	300	70	100	Stable after 120 h	Liu et al. (2012)

10 wt% Ni/β-zeolite	Impregnation	360	97	n/a	n/a	Jwa et al. (2013)
10 wt% Ni/β-zeolite-with plasma	Impregnation	240	94	n/a	n/a	Jwa et al. (2013)
15 wt% Ni/TiO$_2$	Precipitation–deposition	260	96	99	Conversion decreased by 2.9 % after 81 h	Liu et al. (2013)
Ni/SiO$_2$	Impregnation method and treated by glow discharge plasma (H$_2$ atmosphere)	250	90	~100	Conversion decreased by 15.54 % after 100 h	Zhang et al. (2013a)
35Ni$_5$Fe$_{0.6}$RuAX	Single–step–sol–gel	220	68.2	98.9	Optimal ruthenium content was required for maximum methane production from carbon dioxide and hydrogen	Hwang et al. (2013)
5 wt% Ni/MSN	Wet–impregnation	300	64.1	99.9	n/a	(Aziz et al. (2014a)
20 wt% Ni/ nanocrystalline γ-Al$_2$O$_3$	Impregnation	350	78	100	Stable after 600 min	Rahmani et al. (2014)

UMP
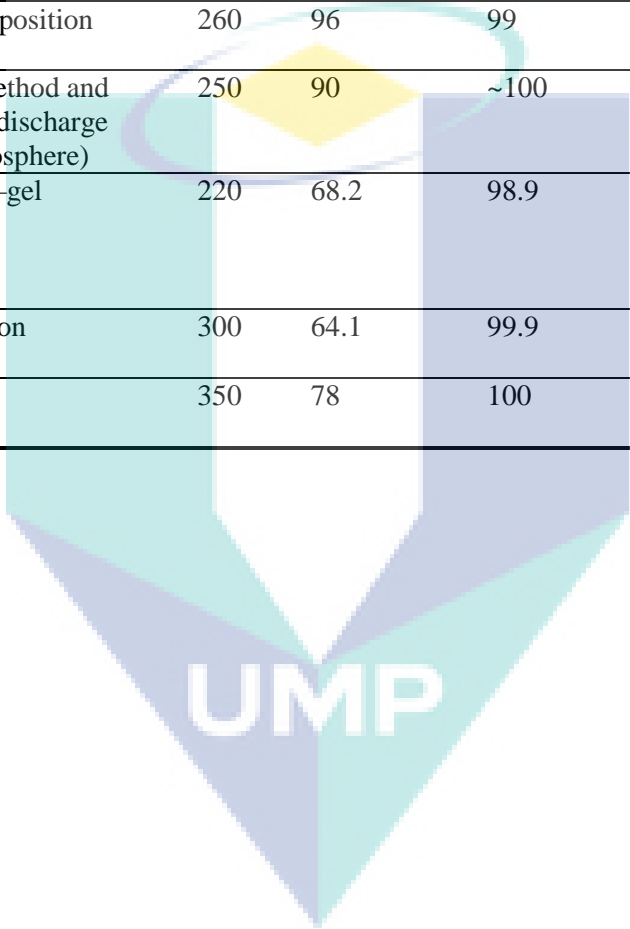
2.3.1 Mesoporous silica as support

According to IUPAC nomenclature definition, free diameter of inorganic solid pores in the range of 2-50 nm is widely known as mesoporous materials. Mesoporous materials are typically included either with alumina, carbon, silica, or transition metal oxides. Different mesoporous materials have different properties. However, mesoporous silica is one of the promising materials which have attracted an intense interest since 1990 (Rahmat et al.. Its first discovery was founded by researchers in Japan and later in Mobil Corporation Laboratories.

Mesoporous silica has attracted increasing attentions due to the large, uniform and tuning pore sizes and diameters, very high surface area, thicker pore walls, high thermal stability, hexagonal arrays of regular channel type structures, chemically inert, harmless and high potentiality of functionalization (Abdullah et al., 2010; Lu & Kawamoto, 2013; Rahmat et al., 2010). This high surface area can be exploited to create highly dispersed active species on interacting and non-interacting support materials. The relatively synergistic effect between metal and support can markedly ameliorate catalytic behaviour and stability, and thus yield high formation of products (Aziz et al., 2014a; Pan et al., 2014). Additionally, anti-sintering property of metallic metal might also be triggered owing to a better confinement of metal particles onto the mesoporous support (Liu et al., 2018b; Liu & Tian, 2017a; Liu et al., 2017b). In contrast, poorer structural of support that occupied the small pores' diameter might affect the poorer dispersion of metal particles whereby metal particles mostly deposited at the outer coverage of support rather than being anchored into the pores of the support. It has been declared that the metal dispersion onto the pores of support is less prone to metal sintering than metal mounted at the exterior surface of the support, and thus a higher catalytic behavior and stability can be accomplished with the least quantity of carbon deposition (Ma et al., 2013). In fact, the properties of the metal active phase with homogenous and better dispersion onto the framework and channels of support are directly affected by the type of support formed (Hou et al., 2006; Lu & Kawamoto, 2013; Wang et al., 2015). The favourable support with a large surface area and large pores' diameter is demonstrated to be an effective approach to produce well-dispersed metal-based catalyst and thus increase the possibility of metal dispersion inside the pores.

From the previous study, the most often used family of mesoporous silicas are Santa Barbara Amorphous (SBA-15), Mesoporous Materials (M41S) and Mesoporous Silica Nanoparticles (MSN). Mobil Composition of Matter (MCM) such as MCM-41, MCM-48, and MCM-50 are some of mesoporous silica coming from M41S family. They consist of good control of pore size diameter (2-50 nm) and the thickness of pore walls (8-10 nm). Their various potential applications are for the production of catalysis, separations, sensors, drug delivery, optical coating, and fuel cell electrodes. Meanwhile, for MSN support, it was also widely being used by the researchers especially for drug delivery system, cancer therapy, and inflammatory cardiovascular treatment owing to its specific physical properties; surface area (588-995 m^2/g), pore size diameter (3.37-4.00 nm) and particle size (70-120 nm). **Error! Reference source not found.** represents the various types of mesoporous silica with its properties and application.

Table 2:2　　　Various types of mesoporous silica with its physical properties and application

Mesoporous silica	Physical properties	Application	Reference
SBA-15	• Surface area (600-1,000 m^2/g) • Pore size diameter (5-30 nm) • Particle size (70-120 nm) • Thickness of pore walls (3-6 nm) • Better hydrothermal stability	Catalysts and catalytic supports	Abdullah et al. (2010), Rahmat et al. (2010), Rodrigues et al. (2015)
M41S - MCM-41 - MCM-48 - MCM-50	• Pore size diameter (2-50 nm) • Thickness of pore walls (8-10 nm)	• Catalysis • Separations • Sensors • Drug delivery • Optical coating • Fuel cell electrodes	Abdullah et al. (2010), Rahmat et al. (2010)
MSN	• Surface area (588-995 m^2/g) • Pore size diameter (3.37-4.00 nm) • Particle size (70-120 nm)	• Drug delivery system • Cancer therapy • Inflammatory cardiovascular treatment	Sazegar et al. (2014)

2.3.1.1　Mesoporous SBA-15

The selection of support with the most promising properties is significant for providing well dispersion and interaction with the metal which is also known as active

site, thus yielding high catalytic activity and selectivity performances towards CO_2 methanation over synthesized catalyst. In this study, mesoporous SBA-15 known as Santa Barbara Amorphous 15 is the most promising support for the synthesis of supported metal catalyst which leads toward higher catalytic performances of CO_2 methanation due to it has the excellent properties compared with other mesoporous silica which are large, uniform and tuning pore sizes and diameters (5-30 nm), thicker pore walls (3-6 nm), very high specific surface areas (600-1,000 m^2/g), higher thermal and hydrothermal stability as well as highly uniform-arranged mesopores (Zhao et al., 1998).

According to Vradman et al. (2006), the synthesis of mesoporous SBA-15 consists of four main steps of reaction which are: (1) synthesis of silica-organic polymer nanocomposite using silica source and amphiphilic triblock copolymers (P123) as the organic structure-directing agent (surfactant template), (2) aging the composite at elevated temperature, (3) filtration (and optionally washing) the obtained solid and (4) removing the surfactant template either by solvent extraction, calcination or microwave digestion. The formation of regularly spaced mesopores channels surrounded with the microporous walls could be obtained, in agreement with Gibson (2014). The network of micropore-mesopore SBA-15 is shown in Figure 2:4.
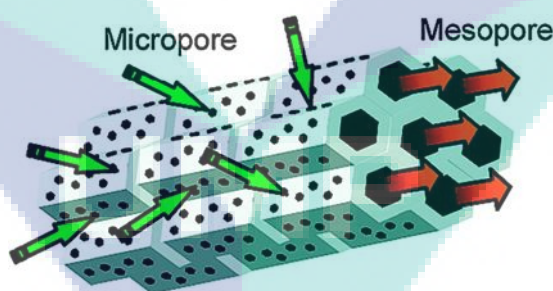
Figure 2:4   Network of micropore-mesopore SBA-15.

Source: Gibson (2014)

2.3.2   Nickel as active site and its role

CO_2 methanation has been extensively studied over variety of metal-based catalysts. Regarding the choice of metal, it has been reported that the non-noble transition

metal supported with catalysts such as nickel (Ni) is very reactive and often preferred in industrial applications owing to the facts that it can possess a higher catalytic activity towards methane production, and the presence of supports can markedly improve catalytic activity (Aziz et al., 2014a; Pan et al., 2014). According to Rossetto et al. (2015), nickel complexes have relatively outstanding catalytic activity and stability to form the specific products. They can agglomerate well even when reacted in homogenous media and form the strong metal-support interaction. It is also widely used as type of metal to be incorporated with the support because of its low cost, easily available, and high performance (Kathiraser et al., 2015; Pan et al., 2014).

Recently, Pudukudy et al. (2015a) reported about the SBA-15 supported metal-based catalysts for CH_4 decomposition reaction. The metals used in their study were Ni, Co and Fe. They found that an outstanding H_2 yield of approximately 56% could be obtained upon the implementation of SBA-15 supported Ni-based catalysts within 30 min time-on-stream as compared with other metals (Co and Fe). Meanwhile, in the case of Ni-based catalyst with the employment of noble metal such as Pd could also improve its catalytic behaviour towards CH_4 decomposition whereby a higher yield of hydrogen about 59% was achieved over Ni/SBA-15 catalyst implemented with 0.4% Pd within 30 min time-on-stream (Pudukudy et al., 2015b). It could be summarized that the superior characteristics of Ni/-based catalysts might impacted on the outstanding catalytic behaviour and thus yielded higher formation of products.

CHAPTER 3

METHODOLOGY

3.1 Chemicals

The list of chemicals that were used in thus study including with their molecular formula and manufacturer are shown in Table 3:1.

Table 3:1   List of Chemicals

Chemical	Molecular Formula	Manufacturer
Pluronic P123, M_W: 5800	EO_{20}-PO_{70}-EO_{20}	Aldrich
Tetraethylorthosilicate, 98%	TEOS	Merck
Hydrochloric acid, 37%	HCl	Merck
Nickel (II) nitrate hexahydrate, 99%	$Ni(NO_3)_2 \cdot 6H_2O$	Merck
Hexadecyltrimethylammonium bromide, 99%	$C_{19}H_{42}BrN$	Aldrich
Hydrogen cylindrical tank, >99.99%	H_2	-
Carbon dioxide cylindrical tank, >99.99%	CO_2	-
Methane cylindrical tank, >99.99%	CH_4	-
Nitrogen cylindrical tank, >99.99%	N_2	-

3.2 Catalyst preparation

3.2.1 Synthesis of SBA-15 support

The SBA-15 was prepared according to the method reported by Zhao et al. (1998). The P123 was dissolved in the solution of deionized water and 2M hydrochloric acid solution, and stirred at 40 °C for 1 h. The TEOS was slowly added to the mixture with vigorous stirring at 40 °C for 24 h, and the white precipitate product was obtained. The precipitate product was filtered, washed with deionized water and dried overnight at 110

°C. The sample was calcined at 550 °C for 3 h to remove the triblock copolymer to produce SBA-15(W). For the effect of TEOS/P123 ratios, a series of samples with different mass ratios of TEOS/P123 (1.5, 2.21 and 3.0) were prepared.

For the preparation of SBA-15 with hydrothermal, the resulting solution formed after the addition of TEOS was heated at 80 °C for 4 h using different techniques of hydrothermal treatment which are Teflon-lined stainless-steel autoclave (T) and reflux (R) method. After hydrothermal treatment, deionized water was used to rinse the solution and the samples were exposed to dry air at 110 °C for 12 h. Then, calcination was done at 550 °C for 3 h. SBA-15 sample prepared using Teflon-lined stainless-steel autoclave named as SBA-15(T), while the SBA-15 sample prepared using reflux method named as SBA-15(R). The mass ratio of TEOS/P123 used is 2.21.

3.2.2 Preparation of Ni/SBA-15

The Ni/SBA-15 catalyst was prepared by impregnation of SBA-15 powder with an aqueous solution of 5 wt% Ni salt precursor, $Ni(NO_3)_2 \cdot 6H_2O$ (Merck, 99%). The resulting slurry was heated slowly at 80 °C under continuous stirring and maintained at that temperature until all the water nearly evaporated. The solid residue was dried overnight at 110 °C followed by calcination at 550 °C for 3 h. For the effect of Ni loading, a series of sample with different Ni loading (3,5 and 10 wt%) were prepared.

3.3 Catalyst characterization

XRD was performed in order to identify the crystallinity structure of the catalysts. X-ray diffraction (XRD) (Philips X' Pert MPD, 3 kW) was performed at room temperature using a Cu Kα radiation ($\lambda = 1.5405$Å) in low-angle (0.5–3.0°) and wide-angle (30.0–80.0°) range as to identify the crystallinity conformation of the catalysts. The primary NiO crystallite size (D_{NiO}) was determined using Scherrer equation (Chen et al., 2014; Tada et al., 2014; Tao et al., 2017):

$$D_{NiO} = \frac{0.9\lambda}{B\cos\theta} \qquad\qquad 3.1$$

Where,

λ = x-ray wavelength corresponding to Cu-Kα radiation (0.15405 nm)

B = broadening (in radians) of the nickel (200) reflection

θ = angle of diffraction corresponding to peak broadening.

In order to validate the exact content of Ni loadings that were dispersed onto the framework and channels of the SBA-15 support, it was done by using the inductive coupling plasma-atomic emission spectroscopy (ICP-AES).

The Bruneuer-Emmett-Teller (BET) analysis of the catalyst was performed using AUTOSORB-1 model AS1 MP-LP instrument at liquid nitrogen temperature of 77 K as to identify the textural properties (i.e., specific BET surface area and porosity) of the catalysts. 100 mg of the samples was evacuated at a pressure below 250 mTorr with a temperature of 300 °C for 3 hours before the measurement was done.

FTIR is the most useful technique in determining the presence and absence of specific functional groups as well as chemical interaction involved in the structural of sample. Fourier Transform Infrared (FTIR) spectra (Agilent Cary 640 FTIR Spectrometer) was used to determine the presence of functional groups in catalysts and the chemical bonding of Ni species with support using the KBr matrix within the scan range of 500–1400 cm^{-1} with a resolution of 5 cm^{-1}. Prior to the analysis, 1 mg catalysts were mixed with 100 mg KBr as to increase the transparency of the sample.

The UV-Vis Diffuse Reflectance Spectroscopic (UV-Vis DRS) analysis is another technique to further examine the interaction between metal and support in the sample instead of FTIR analysis. The analysis was recorded in the wavelength range of 200 to 800 nm using Varian CARY 3E double beam spectrophotometer at room temperature.

Scanning Electron Microscope (ZEISS SEM EVO-50) was used to examine the surface morphological properties of the catalyst, while its elemental composition and metal distribution was performed using Energy Dispersion X-ray (EDX) Spectroscopy.

It was operated at 10 kV. Prior to the analysis, the samples were coated with the platinum using a sputter coater.

Field Emission Scanning Electron Microscopy (FESEM) equipped with the elemental distribution mapping (JEOL JSM7800F Electron Microscope) was performed in order to identify the morphological structural of metal-based catalysts as well as its metal distribution.

Transmission electron microscopy (TEM) is a very powerful technique which typically used for imaging the morphology structure of solid samples including the finest solid by using a high resolution. TEM equipped with a tungsten filament at an operating range of 50 to 100 kV. Prior to the TEM measurement, the samples were grounded into powders and dispersed into 100% ethanol by ultrasonic treatment for approximately 15 min, and then were left for 5 min to allow the particles to settle down. Only a drop of solution was deposited onto amorphous, porous carbon-coated TEM copper grid. The sample must be very thin enough deposited on the grid as to prevent energy loss during the transmission of electrons producing TEM image. Then, the grid that deposited with the sample was dried in air at room temperature.

Temperature-programmed reduction (TPR) was utilized to identify the reducibility of the catalyst. 10% H_2/Ar was employed as a reductant with a flow rate of 20 mL/min. The specimen was treated at a heating rate of 10 K/min from ambient temperature to 1173 K.

3.4 Reaction studies of CO_2 methanation

CO_2 methanation was carried out on a stainless steel fixed-bed reactor at atmospheric pressure and in a temperature range of 523 to 723 K. Prior to the reaction, 0.2 g of catalyst supported with quartz wool was placed at the centre of reactor tubing and treated in a flow of high purity hydrogen stream ($F_{Hydrogen} = 20$ mL/min) for 1 h at 973 K and cooled down to the desired temperature before the H_2 gas flow.is switched. A mixture of H_2 and CO_2 were fed into the reactor at gas hourly space velocity (GHSV) of 24,900 mL g_{cat}^{-1} h^{-1} and H_2/CO_2 ratio range of 1:1 to 1:6. The composition of the outlet gases were collected by gas sampling bag and were analysed by Agilent gas chromatography equipped with a GS-Carbon PLOT column and a thermal conductivity detector (TCD). For each analysis, about 30 bubbles were injected into the sample loop

and were analysed. The duration of the analysis using GC is between 20 to 30 min for each sample.

The percentage of CO_2 conversion, CH_4 selectivity, and CH_4 yield were calculated using Equation 3.2, 3.3, and 3.4 respectively. The process flow diagram of CO_2 methanation is shown in Figure 3:1.

$$CO_2 \text{ conversion, } X_{CO_2}(\%) = \frac{F_{CO_2,in} - F_{CO_2,out}}{F_{CO_2,in}} \times 100\% \qquad 3.2$$

$$CH_4 \text{ selectivity, } S_{CH_4}(\%) = \frac{F_{CH_4,out}}{F_{CO_2,in} - F_{CO_2,out}} \times 100\% \qquad 3.3$$

$$CH_4 \text{ yield, } Y_{CH_4}(\%) = \frac{X_{CO_2} \times S_{CH_4}}{100\%} \qquad 3.4$$

Where F is the molar flow rate for particular compound (mol/s).
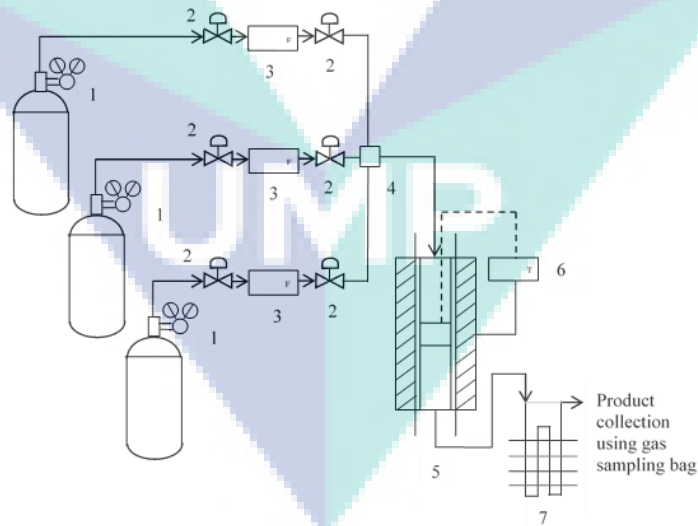
Figure 3:1   Process flow diagram of the CO_2 methanation. (1) Regulator, (2) valve, (3) mass flow controller, (4) gas chamber, (5) vertical tube furnace, (6) temperature controller, (7) condenser.

3.5   Influence of Metallic and Basic Sites of Catalysts on The Mechanistic Path of CO_2 Methanation

3.5.1   In-situ IR pyrrole

The basicity of catalysts was identified by in-situ FTIR adsorbed pyrrole. Pyrrole is an amphoteric molecule which can either interact with the Lewis basic oxygen of silicate framework via the NH group by hydrogen bonding or with the Lewis acidic cation via the aromatic π-electrons interaction. In this project, pyrrole was used as a probe molecule for a characterization of basic sites because it can be adsorbed reversibly due to its weak acidity. The Agilent Cary 640 FTIR spectrometer was equipped with a high-temperature stainless steel cell with CaF_2 windows. Prior to the pre-treatment of analysis, 30 mg of catalyst was prepared as a self-supported wafer and reduced under H_2 stream (100 mL/min) at 673 K for 1 h, followed by cooling to room temperature. 4 Torr of pyrrole was then oriented with the reduced catalyst at ambient temperature for 5 min, continued with evacuating at ambient temperature, 323 K, 373 K, 423 K and 473 K for 5 min, respectively. All spectra were conditioned and obtained at ambient temperature with a resolution of 5 cm^{-1}.

3.5.2   In-situ IR H_2, CO_2 and $H_2 + CO_2$

To study the mechanistic path of CH_4 production, in-situ FTIR adsorbed H_2, CO_2, and $H_2 + CO_2$ were conducted on an Agilent Cary 640 FTIR spectrometer equipped with a high-temperature stainless steel cell with CaF_2 windows. The pretreatment of catalyst was done using the same procedure as mentioned in the in-situ FTIR adsorbed pyrrole. Then the activated catalyst was introduced with the reactant gas (H_2, CO_2 or $H_2 + CO_2$) at ambient temperature and followed by subsequent heating to 623 K. All the spectra were collected using FTIR spectrometer at room temperature.

CHAPTER 4

RESULTS AND DISCUSSION

4.1 Effect of TEOS/P123 Mass Ratios on the Properties and Catalytic Activity of Ni/SBA-15 Towards CO$_2$ Methanation

4.1.1 Characterization of the Ni/SBA-15(R1.5), Ni/SBA-15(R2.21) and Ni/SBA-15(R3.0) Catalysts

Figure 4:1(A) shows the low-angle XRD patterns of Ni/SBA-15 with different TEOS/P123 mass ratio. The pattern of Ni/SBA-15 prepared with 2.21 TEOS/P123 mass ratio exhibited three peaks, indexed as (100), (110) and (200) which are reflection of typically two dimensional, hexagonally ordered mesostructures (*p*6mm), demonstrating the high quality of the mesopore packing (Zhao et al., 1998). When a lower (1.5) and a higher (3.0) mass ratio of TEOS/P123 were applied, the intensity of (100) peak was slightly decreased and did not feature the (110) and (200) peaks. Moreover, it was observed that the (100) peak slightly shifted to the left indicating the reduction of *d*(100) spacing and unit cell parameter. The slight decreased of (100) peak and the disappearance of the (110) and (200) peaks at lower TEOS/P123 mass ratio (TEOS/P123 = 1.5) might be due to the incomplete structural formation of SBA-15 as the amount of the TEOS was insufficient to form highly ordered hexagonal structure. Meanwhile, a reduction in the intensity of the (100) peak and the disappearance of the (110) and (200) peaks at higher TEOS/P123 mass ratio (TEOS/P123 = 3.0) might be due to a relatively poorer structural ordering of samples with a higher TEOS/P123 mass ratio because of the presence of disordered silica. The results observed in this study clearly indicated that the TEOS/P123 mass ratios (1.5 - 3.0) remarkably affected the structure of Ni/SBA-15.

The presence of crystalline NiO on the catalysts was characterized using wide-angle XRD, as shown in Figure 4:1(B), in which the peaks at 37.3º, 43.2º, 62.9º, 75.4º and 79.3º can be attributed to face-centered cubic crystalline NiO structure (Aziz et al., 2015b).
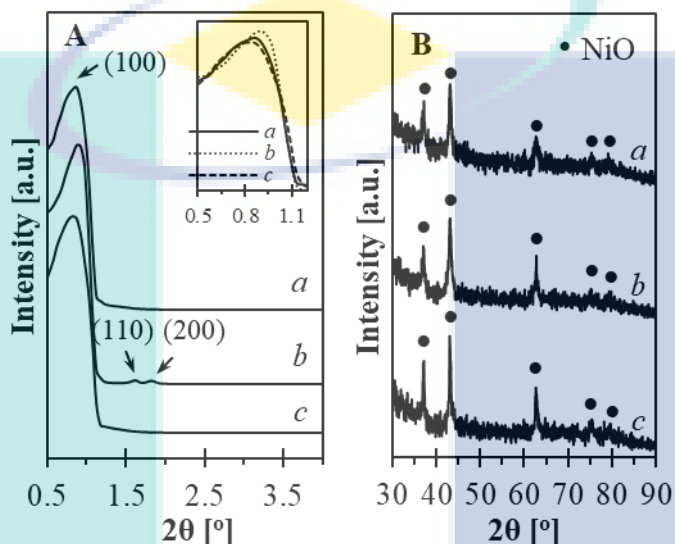
Figure 4:1   (A) Low-angle and (B) wide-angle XRD patterns of Ni/SBA-15 with TEOS/P123 mass ratios of (a) 1.5, (b) 2.21 and (c) 3.0.

An increase of TEOS/P123 mass ratio resulted in a slight increase of the peaks, suggesting that with higher TEOS/P123 mass ratio (TEOS/P123 = 3.0), most of NiO particles were aggregated on the SBA-15 outer surface, meanwhile, with lower TEOS/P123 mass ratio (TEOS/P123 = 1.5), most of NiO particles were in the SBA-15 pores. From the previous study, Lu and Kawamoto (2014) had mentioned about the influence of the synthesis method on the XRD peak intensities of NiO/SBA-15 (Lu & Kawamoto, 2014). They found that by direct synthesis method, the result showed the higher XRD peak intensities of NiO/SBA-15 as compared to those which were prepared by post synthesis method. The result indicated that with direct synthesis method, most of the NiO particles were located on the outer surface of catalyst.

The nitrogen adsorption-desorption isotherms of Ni/SBA-15 synthesized at different mass ratios of TEOS/P123 are shown in Figure 4:2. All samples exhibited type IV isotherm, which is a typical feature for mesoporous material, according to the IUPAC classification (Abdullah et al., 2010a; Dan et al., 2012; Lu & Kawamoto, 2014). For the

Ni/SBA-15 which was prepared with a TEOS/P123 mass ratio of 1.5, the isotherm exhibited a large hysteresis loop of type H3 indicating a very wide distribution of pores. However, in the case of TEOS/P123 = 2.21, the isotherm showed type H1 hysteresis loop which is a typical feature for mesoporous material which indicates a narrow distribution of relatively uniform cylindrical pores (Abdullah et al., 2010a; B. Lu & Kawamoto, 2014). Meanwhile, when the TEOS/P123 mass ratio was further increased to 3.0, the isotherm showed type H2 hysteresis loop exhibiting non-uniform pore shapes which consisting of ill-defined pore shape and wide pore size distribution. With regards to the relative pressure, it was observed that the pore size of Ni/SBA-15 was significantly decreased with an increasing TEOS/P123 mass ratio due to the excessive amount of TEOS which could interrupt the condensation of the silica network and thus could affect pore size of the sample.
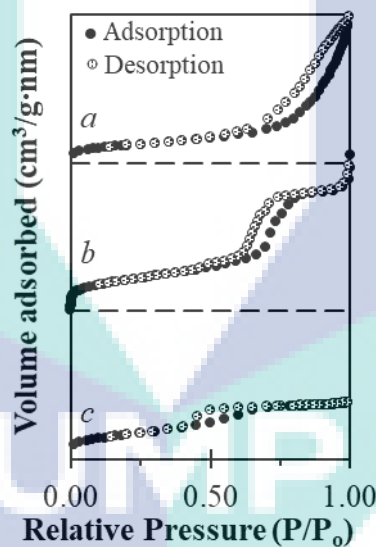
Figure 4:2   Nitrogen adsorption-desorption isotherms of Ni/SBA-15 with TEOS/P123 mass ratios of (a) 1.5, (b) 2.21 and (c) 3.0.

The surface area, pore volume and pore diameter of Ni/SBA-15 with different TEOS/P123 mass ratios are summarized in Table 4:1. With the increasing TEOS/P123 mass ratio, the surface area, pore volume and pore diameter gradually decreased. The decrease in the surface area and pore volume at higher TEOS/P123 mass ratio might be related to the excessive amount of TEOS which preferably solubilized in the copolymer micelles and condensed to form the microporous plugs. The observed trends were in a

good agreement with that observed on SBA-15 and SBA-15 PMOs as reported by Kruk et al. (2000) and Bao et al. (2004), respectively (Bao et al., 2004; Teka & Enyew, 2014). They proposed that during the assembling process, the template blocks interacted only to a limited amount of silica source and the remaining silica source preferably solubilized in the copolymer micelles and condensed to form the microporous plugs. Meanwhile, Abdullah et al. (2010b) reported that the changes in the surface area, pore volume and pore diameter of SBA-15 at higher TEOS/P123 ratio were related to the failure of Si-O-Si network formation due to the excessive amount of TEOS (Abdullah et al., 2010a). Apart from that, the condensation of the silica network on the micelles might be interrupted and thus the pore structure of the sample might also be affected.

Table 4:1   Physical properties of Ni/SBA-15(R1.5), Ni/SBA-15(R2.21) and Ni/SBA-15(R3.0)

Catalyst	TEOS/123	Surface area (m^2/g)	Pore volume (cm^3/g)	Pore diameter (nm)
Ni/SBA-15(R1.5)	1.5	508	1.121	13.91
Ni/SBA-15(R2.21)	2.21	646	0.573	5.25
Ni/SBA-15(R3.0)	3.0	425	0.369	3.70

Figure 4:3 shows the influence of the TEOS/P123 mass ratio on the Ni/SBA-15 morphology structure. SEM image of Ni/SBA-15 which was synthesized from TEOS/P123 mass ratio of 1.5 showed the irregular shape of SBA-15 which might be due to the incomplete condensation stage due to the limited amount of silica source. However, in the case of TEOS/P123 mass ratio of 2.21, the SEM image showed relatively well-ordered regular shape of SBA-15 was formed. Meanwhile, when the TEOS/P123 mass ratio was further increased to 3.0, the expended and long-connecting shape with the presence of irregular shape was observed indicating poorer structural ordering of sample with partial failure in the formation of well-ordered SBA-15. In addition, it was clearly observed that most of the NiO particles were aggregated on the outer surface of Ni/SBA-15(R3.0) which in agreement with the XRD analysis. The changes in the shape of sample with template/silica ratio were also observed on ZSM-5 samples reported by Fouad et al. (2006) (Fouad et al., 2006). They found that the samples which were prepared by 0.215 and 0.322 template/silica mole ratios crystallized in cube-like shaped crystal, whereas, sample prepared by 0.43 template/silica mole ratio crystallized in sphere-like shaped

crystals and the sample prepared by 0.537 template/silica mole ratio crystallized in network-like shaped crystals. The results observed in previous study clearly indicated that the different ratios of template/silica significantly affected the morphology and shape of synthesis sample.
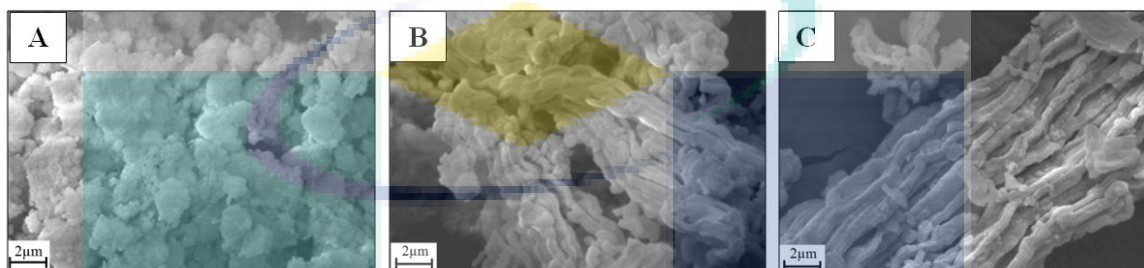
Figure 4:3   SEM images of Ni/SBA-15 with TEOS/P123 mass ratios of (A) 1.5, (B) 2.21 and (C) 3.0

The effects of mass ratio on the structure of the sample were also confirmed by the TEM analysis as shown in Figure 4:4. The images indicated that the Ni/SBA-15 synthesized from 1.5 TEOS/P123 mass ratio showed the absence of hexagonal array because of the incomplete condensation stage of silica precursor. The condensation stage was incomplete might be due to the limited amount of silica source to interact with the excess amount of surfactant, and thus facilitate the formation of irregular shape of SBA-15. However, in the case of TEOS/P123 = 2.21, the TEM image showed relatively well-ordered hexagonal mesostructures, with microporous interconnecting hexagonal, which presented the highest ordered hexagonal mesoporous structure of SBA-15. Meanwhile, when the TEOS/P123 mass ratio was further increased to 3.0, the expended and long-connecting SBA-15 structure was observed indicating poorer structural ordering of sample at higher TEOS/P123 mass ratio. Moreover, it was observed that there was the presence of ordered and disordered silica structure in 3.0 TEOS/P123 mass ratio suggesting partially hexagonal mesoporous structure formation at higher mass ratio. This could indicate the partial failure in the formation of Si–O–Si network into hexagonal array at higher TEOS/P123 mass ratio due to the excessive TEOS amount interrupting the condensation of the silica network on the micelles. This finding was in agreement with the study reported by Abdullah et al. (2010), who found that the excess of silica precursor could affect the siloxane network structure of SBA-15 (Abdullah et al., 2010a). They

stated that the large amount of silica precursor interrupting the condensation of silica network on the micelles due to the limited amount of surfactant, and thus the excess silica precursor could functionalise the silica surface to form irregular silica mesopores.
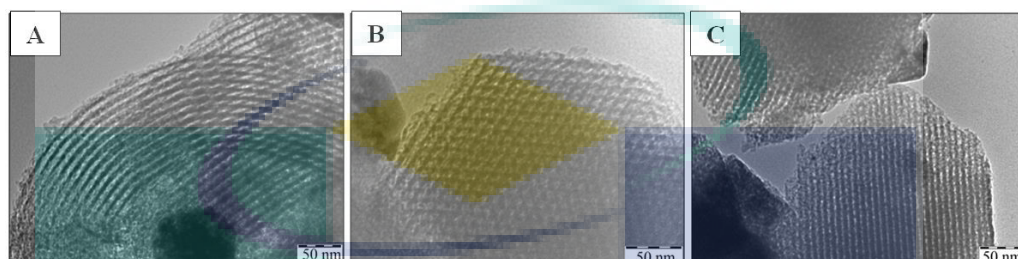
Figure 4:4   TEM images of Ni/SBA-15 with TEOS/P123 mass ratio of (A) 1.5, (B) 2.21 and (C) 3.0.

Figure 4:5 shows the FTIR spectra of KBR of Ni/SBA-15 with different TEOS/P123 mass ratios. The bands at approximately 1060, 801 and 510 cm^{-1} were corresponded to the asymmetric stretching vibrations of Si–O–Si, symmetric stretching vibrations of Si–O–Si, and tetrahedral bending vibration of Si–O–Si bonds, respectively (Fan et al., 2015; Setiabudi et al., 2016; Ye et al., 2011). It was observed that the intensity of the band at 1060 cm^{-1} was moderately decreased at higher TEOS/P123 mass ratio indicating the partial failure in the formation of Si–O–Si network at higher mass ratio due to the excessive TEOS amount interrupting the condensation of the silica network on the micelles. Based on the previous study (Brodie-Linder et al., 2010), the band around 961 cm^{-1} has been widely use to characterize the incorporation of metal ions in the silica framework in which the interaction of Ni particles with support was indicated by a decrease in the intensity of the peak and the peak becomes enveloped in the band of 1060 cm^{-1}. It was observed that incorporation of metal ions in the silica framework was following the order of Ni/SBA-15(R1.5) ≈ Ni/SBA-15(R3.0) < Ni/SBA-15(R2.21) indicating higher quantity of metal-support interaction in Ni/SBA-15 with TEOS/P123 = 2.21. At higher wavenumber, the broad adsorption band at 3440 cm^{-1} was attributed to the O-H stretching vibration mode of Si-OH involved in the hydrogen interaction with the adsorbed water molecules. An increase of TEOS/P123 mass ratios from 1.5 to 3.0 resulted in an increased of the peak, indicating higher amount of hydroxyl groups at higher TEOS/P123 mass ratio.
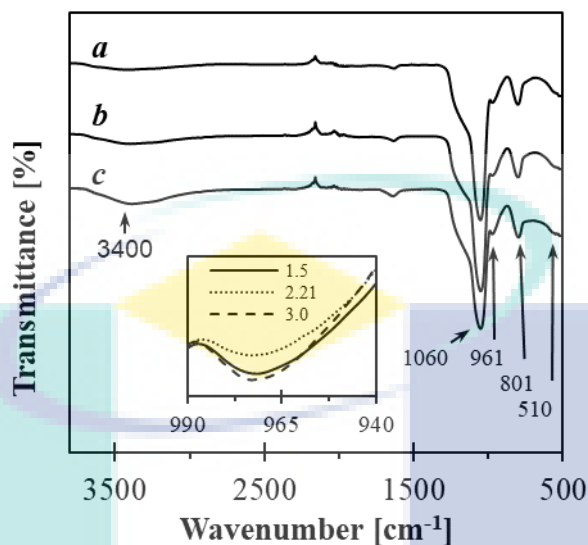
Figure 4:5   FTIR spectra of KBr of Ni/SBA-15 with TEOS/P123 mass ratio of (a) 1.5, (b) 2.21 and (c) 3.0.

4.1.1   Catalytic Performance of Ni/SBA-15(R1.5), Ni/SBA-15(R2.21), Ni/SBA-15(R3.0) Catalysts

Figure 4:6 shows the effects of TEOS/P123 mass ratios on the conversion of CO_2 in CO_2 methanation. At temperature studied, the catalytic activity of Ni/SBA-15 towards CO_2 reforming of CH_4 followed the order of Ni/SBA-15(R2.21) > Ni/SBA-15(R3.0) > Ni/SBA-15(R1.5). The Ni/SBA-15(R2.21) exhibited an excellent performance might be related with the well-ordered hexagonal structure of SBA-15 which provided better dispersion of Ni particles and thus resulted in higher catalytic performance. Meanwhile, the lowest catalytic performance of Ni/SBA-15(R1.5) might be related with the incomplete hexagonal structure of SBA-15 which resulted in poorer dispersion of Ni particles as supported by the characterization results. Thus, the results clearly indicated that TEOS/P123 mass ratio of 2.21 was the optimal synthesis ratio under the reaction studied.
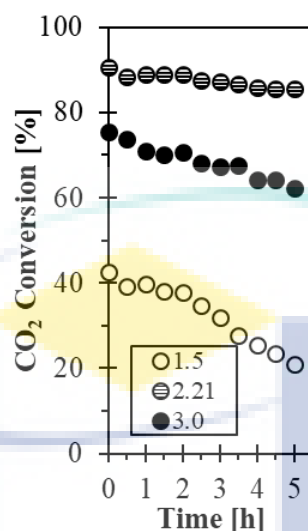
Figure 4:6   CO$_2$ conversion of Ni/SBA-15 with different TEOS/P123 mass ratios (1.5, 2.21 and 3.0) at reaction temperature of 673 K.

4.1.2   Outcomes of the study

The influences of TEOS/P123 mass ratios (1.5, 2.21 and 3.0) on the properties and catalytic activity of Ni/SBA-15 towards CO$_2$ reforming of CH$_4$ were studied, owing to the fact that TEOS/P123 has a significant influence on the morphology, metal-support interaction and catalytic performance of the catalyst. XRD, BET, SEM and TEM results indicated that the TEOS/P123 ratio of 2.21 was the optimal synthesis ratio of Ni/SBA-15 which producing the well-ordered hexagonal mesoporous structure with the highest Ni-support interaction. The catalytic activity of Ni/SBA-15 towards CO$_2$ reforming of CH$_4$ followed the order of Ni/SBA-15(R2.21) > Ni/SBA-15(R3.0) > Ni/SBA-15(R1.5). The superior catalytic behavior of Ni/SBA-15(R2.21) towards CO$_2$ reforming of CH$_4$ was related with the catalytically favorable textural properties of Ni/SBA-15(R2.21) which enhanced the dispersion of metal particles, improved the catalyst activity, increased the catalyst stability and reduced the carbon deposition. Meanwhile, the lowest catalytic performance of Ni/SBA-15(R1.5) might be related with the incomplete hexagonal structure of SBA-15 which resulted in poorer dispersion of Ni particles as supported by the characterization results. Thus, the present study confirmed that TEOS/P123 mass ratio played as an important role in the enhancement of Ni/SBA-15 catalysts properties and catalytic performance towards CO$_2$ methanation.

Since the Ni/SBA-15 with 2.21 TEOS/P123 ratio showed highest activity towards CO_2 methanation, this ratio was used in the subsequent study.

4.2 Effect of Hydrothermal Treatment Techniques on the Properties and Catalytic Activity of Ni/SBA-15 Towards CO_2 Methanation

4.2.1 Characterization of SBA-15(R), SBA-15(T), SBA-15(W), Ni/SBA-15(R), Ni/SBA-15(T) and Ni/SBA-15(W)

XRD characterization was accomplished to examine the crystallinity of the catalysts. Figure 4:7 indicates the XRD patterns of SBA-15 and Ni/SBA-15 catalysts synthesized by using different techniques of hydrothermal treatment (Reflux and Teflon) and without undergoing hydrothermal treatment. The low-angle XRD patterns of SBA-15 prepared with hydrothermal treatment (Teflon and Reflux) and without hydrothermal treatment demonstrated three peaks of (100), (110) and (200). These are the portray of typical hexagonally arranged, two-dimensional mesoporous channels of SBA-15 (*p*6mm) (Pan et al., 2015). As observed, the introduction of Ni did not alter the location of the diffraction peak of (100) planes but slightly reduced the diffraction peak's intensity evidencing the structural degradation of a hexagonal arrangement of supports due to a high quantity of metal interacted with the support. The effect becomes more prominent for Ni/SBA-15(R), implying to the higher and stronger Ni interaction with the SBA-15(R) support.

The presence of Ni particles in SBA-15 support was investigated using wide-angle XRD analysis and the result was illustrated in Figure 4:7(B). As observed, almost similar diffraction peak positions approximately at 37.3^o, 43.2^o, 62.9^o, 75.4^o, and 79.3^o were possessed by all catalysts, attributed to face-centered cubic (FCC) crystalline NiO structure (Bukhari et al., 2017; Garbarino et al., 2014). However, Ni/SBA-15(W) possessed the highest peak intensity of NiO than Ni/SBA-15(T) and Ni/SBA-15(R), indicating that without hydrothermal treatment, most of the metal particles aggregated on the outer surface of the catalyst. Scherrer equation was used to determine the crystallite sizes of NiO particles and the results were 17.92 nm, 19.86 nm and 25.00 nm for the Ni/SBA-15(R), Ni/SBA-15(T) and Ni/SBA-15(W), respectively, indicating the presence of largest NiO particles in SBA-15(W). The enlargement of NiO particles size on SBA-

15(W) revealed that the aggregation of NiO particles mostly occurred at the exterior appearance of SBA-15. It might be related to the Ni particles was being blocked from entering the SBA-15(W) support's pore channels due to the smaller pore diameter.

The influence of the synthesis method on the location and metal particles size was also mentioned by Sidik et al. (2016) for Ni/MSN catalyst synthesized by impregnation, in-situ and physical mixing techniques. They found that the Ni/MSN synthesized using physical mixing and impregnation methods have higher intensities of XRD peaks, implying the larger Ni particles was incorporated and dispersed on the external surface of the catalyst. Moreover, the calculated Ni particle size proved that the impregnation and physical mixing methods had larger Ni particles compared to the in-situ method. The same situation was also observed by Ocampo et al. (2011) who studied the catalytic performances of $Ni\text{-}Ce_{0x}Zr_{1-x}O_2$ catalysts synthesized by the different noble metal addition and Ce/Zr composition towards CO_2 methanation. It was found that higher peak intensity of NiO crystallite was detected by $5\%Ni\text{-}Ce_{0.72}Zr_{0.28}O_2$, thus exhibited a larger NiO crystallite size in $5\%Ni\text{-}Ce_{0.72}Zr_{0.28}O_2$ compared with $5\%Ni\text{-}Ce_{0.5}Zr_{0.5}O_2$ and $5\%Ni\text{-}Ce_{0.14}Zr_{0.86}O_2$.
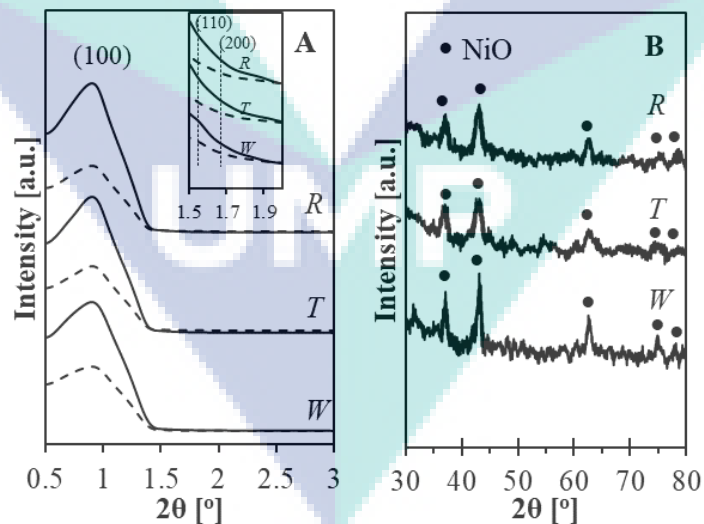
Figure 4:7   XRD patterns for (A) low-angle of SBA-15 (solid line) and Ni/SBA-15 (dash line), and (B) wide-angle of Ni/SBA-15 synthesized by reflux (R), Teflon (T) and without undergoing hydrothermal treatment (W).

The impregnation of Ni metal onto the SBA-15 support was done at the same percentage amount which is 5 wt.%. As to validate the actual amount of Ni loadings onto the different synthesized SBA-15 supports, ICP-AES analysis was performed and its results of the elemental analysis was summarized in the Table 4:2. It could be obviously seen that the amount of nickel in the fresh catalysts of Ni/SBA-15(R), Ni/SBA-15(T) and Ni/SBA-15(W) are almost similar to each other (approximately 5 wt.%), indicating the successfully Ni distribution and dispersion onto the framework and channels of SBA-15 supports either prepared from without and with hydrothermal treatment (Teflon and Reflux) as designed. It was in accordance with Zhao et al. (2016), who studied about the different methods for Ni dispersion onto ZrO_2 for CO_2 methanation and found the closeness designed value of Ni loadings onto ZrO_2 with the obtained results of real Ni from the ICP-AES analysis.

Table 4:2   Physical properties of SBA-15 and Ni/SBA-15 prepared under different techniques of hydrothermal treatment.

Catalysts	Surface area (m^2/g)	Pore volume $(cm^3/g)^a$	Pore diameter (nm)	Fresh NiO crystallite size $(nm)^b$	Spent Ni size $(nm)^b$	Ni loadings $(wt.\%)^c$
SBA-15(R)	814	0.777	5.49	-	-	-
SBA-15(T)	655	0.476	5.27	-	-	-
SBA-15(W)	646	0.573	5.25	-	-	-
Ni/SBA-15(R)	460	0.569	6.05	17.92	19.92	5.1
Ni/SBA-15(T)	460	0.608	5.96	19.86	21.89	4.9
Ni/SBA-15(W)	462	0.578	5.75	25.00	34.89	5.0

[a] Obtained from Barret-Joyner-Halenda (BJH) desorption method.
[b] Calculated from XRD result using Scherrer equation.
[c] Obtained from ICP-AES result.

The N_2 adsorption-desorption isotherms of SBA-15 and Ni/SBA-15 prepared using the different techniques of hydrothermal treatment are expressed in Figure 4:8. It could be noticed that the curves for all SBA-15 samples were identical to each other and displayed type IV isotherms with H1 hysteresis loop regarding IUPAC adsorption isotherm recommendations, suggesting a typical mesoporous structure with relatively uniform cylindrical pores (Bendahou et al., 2008; Li et al., 2015a; Newalkar & Komarneni, 2001).
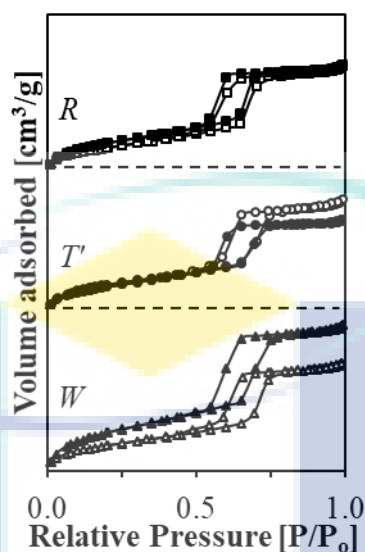
Figure 4:8   Nitrogen adsorption-desorption isotherms of SBA-15 (black marker) and Ni/SBA-15 (white marker) synthesized by reflux (R), Teflon (T) and without undergoing hydrothermal treatment (W).

The physical properties of SBA-15 and Ni/SBA-15 synthesized without and with hydrothermal treatment (Teflon and Reflux) are displayed in Table 4:2 4.2. As observed, the BET surface area, pore volume and pore diameter of the SBA-15 ranging from 646 m^2/g to 814 m^2/g, 0.573 cm^3/g to 0.777 cm^3/g and 5.25 nm to 5.49 nm, respectively. The introduction of Ni particles into SBA-15 resulted in a decrease of BET surface area and pore volume with an increment in average pore diameter. According to literature (Aziz et al., 2014a), the decrement in BET surface area was related to the partial obstruction of the pores by Ni particles deposition, while the changes of the pore size was related to the isomorphous replacement of silanol groups with Ni atoms which might be resulted in the wall contraction and subsequently, pores' expansion. Owing to the fact that the size of NiO (17.92-25.00 nm) calculated using Scherrer equation was bigger than the average pore size of SBA-15 (5.25-5.49 nm), thus, in the present study, Ni particles was expected to be mounted into the pore mouth and surface of SBA-15 which resulted to an increment of pore diameter (5.75-6.05 nm). However, the location of Ni particles either inside or outer surface of pore channels of support might not be significantly important in the reaction studies, which was in agreement with the previous study reported by Lu & Kawamoto (2013). In contrast, it had been reported in the works of literature that both factors of large pore diameter and high specific surface area of support were highly

33

correlated due to they could provide significant channels in support, and thus led to higher metal distribution and strong interaction between support and metal particles (Cheng et al., 2009; Lu & Kawamoto, 2013; Tao et al., 2017). By comparing with all methods, the changes in texture properties becomes more significant for Ni/SBA-15(R) likely owing to the highest surface area (814 m^2/g) and largest pore diameter (5.49 nm) of SBA-15(R) which provides abundance sites for Ni dispersion, and thus resulted to the yield of higher and stronger metal-support interaction. Meanwhile, low BET surface area and small pore diameter of support might cause "dead-zone" formation in the channels of catalyst (Tao et al., 2017) due to the limited spaces for metal dispersion, and thus resulting in a weaker metal-support interaction.

Figure 4:9 represents the FTIR spectra in the wavelength of 1300 – 500 cm^{-1}. The appearance of peak approximately at 1060 and 801 cm^{-1} were assigned to the asymmetric and symmetric Si–O–Si stretching vibrations, respectively (Bukhari et al., 2017; Jusoh et al., 2013). Meanwhile, the bands approximately at 961 cm^{-1} implied to the Si–O stretching vibration of Si–OH (Bukhari et al., 2017; Jusoh et al., 2013). According to the literatures (Bukhari et al., 2017; Jusoh et al., 2013; Tomer et al., 2016), the characterization of metal ion interacted with the silica framework was usually investigated from the peak of 961 cm^{-1}, in which the interaction of metal particles with support was indicated by a decrement of the peak intensity at 961 cm^{-1} and the peak becomes enveloped in the band of 1060 cm^{-1}. As observed in Figure 4:9, the introduction of Ni into SBA-15 reduced the peak intensity at 961 cm^{-1} and the peak of 961 cm^{-1} becomes enveloped in the band of 1060 cm^{-1}. This result might be related to the replacement of O–H with O–Ni to form Si–O–Ni bond, indicating the interaction of Ni ions with the silica framework. By comparing all spectra in Figure 4.9, the significant changes of the bands were observed in Ni/SBA-15(R), suggesting higher metal-support interaction occurred in Ni/SBA-15(R) framework. In brief, the trend of metal ions insertion and dispersion onto the silica framework and channels of SBA-support followed the sequence of Ni/SBA-15(R) > Ni/SBA-15(T) > Ni/SBA-15(W).
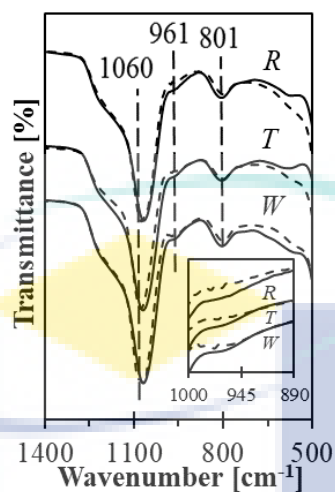
Figure 4:9   FTIR spectra of KBr in the range of 1400 – 500 cm^{-1} for SBA-15 (solid line) and Ni/SBA-15 (dash line) synthesized by reflux (R), Teflon (T) and without undergoing hydrothermal treatment (W).

To further prove the interaction between Ni and synthesized SBA-15, characterization of the catalysts was done by using UV-Vis DRS. The spectra of UV-Vis DRS in Figure 4:10 obviously showed that stretching vibration of Si-O-H in the silica framework of SBA-15 support was changed into Si-O-Ni when Ni particles were introduced into SBA-15 support indicated by the presence of band approximately at 216 nm. As reported elsewhere (Lu et al., 2015; Marakatti & Peter, 2016), an appearance of a band at 216 nm was indicated for the formation of chemical bonding between metal particles and siliceous framework of SBA-15 support through oxygen. It was in agreement with the previous assumption observed from FTIR spectra on the replacement of metal ions in the silica framework of SBA-15 support, as mentioned by Tomer et al. (2016). Additionally, it was reported elsewhere (Lu et al., 2015) that the movement of the band of 216 nm to lower wavelengths indicated the quantity and strength of metal-support interaction in the catalyst. As compared with other methods, Ni/SBA-15(R) exhibited the strongest and highest quantity of metal-support interaction as compared with Ni/SBA-15(T) and Ni/SBA-15(W) catalysts. This result was probably influenced by the high specific surface area and large pore diameters of SBA-15(R) which provide better dispersion of metal. As been reported by several researchers, the metal dispersions and metal-support interactions were correlated well with the structural properties of the support (Aziz et al., 2014a; Aziz et al., 2014b; Fihri et al., 2012; Gibson, 2014; Halim et

35

al., 2014; Tada et al., 2014; Tao et al., 2017; Zheng et al., 2016). Gibson (2014) reported that support with regularly spaced mesopores channels surrounded with the microporous walls was vital for homogeneous metal distribution and stronger metal-support interaction, in order to exhibit better metal-support structures with more edges and resulting to the formation of a promising catalyst with a higher quantity of active sites. In addition, Aziz et al. (2014a) found that the active sites of catalyst were depending on the co-existence of both inter- and intra-particle porosity of the support which could provide better dispersion of Ni particles. Therefore, it is acceptable to summarize that the structural property of SBA-15 influences the interaction between Ni metal and the SBA-15 support. In summary, in accordance with the UV-Vis DRS results, the quantity and strength of metal-support interaction was descending as Ni/SBA-15(R) > Ni/SBA-15(T) > Ni/SBA-15(W), which in accordance with the FTIR results.
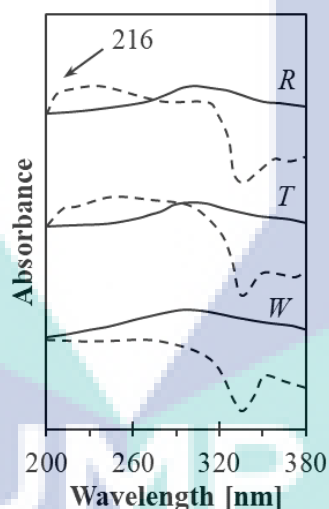
Figure 4:10   UV-Vis DRS spectra of SBA-15 (solid line) and Ni/SBA-15 (dash line) synthesized by reflux (R), Teflon (T) and without undergoing hydrothermal treatment (W).

Figure 4:11 displays the SEM-EDX illustrations of Ni/SBA-15(R). The SEM image showed the formation of the relatively rod-like shape of Ni/SBA-15, while its elemental mapping images showed the existence of metal on the catalyst. It could be obviously noticed that metallic Ni was well-distributed onto the SBA-15(R) synthesized by using reflux technique, as displayed by the grey dots shown in Figure 4.11. It might be owing to the favorable characteristics of SBA-15(R) which equipped with a high

36

specific surface area and large pore diameter, and thus might form a better Ni dispersion onto SBA-15(R) support and lead to stronger the Si-O-Ni interaction.
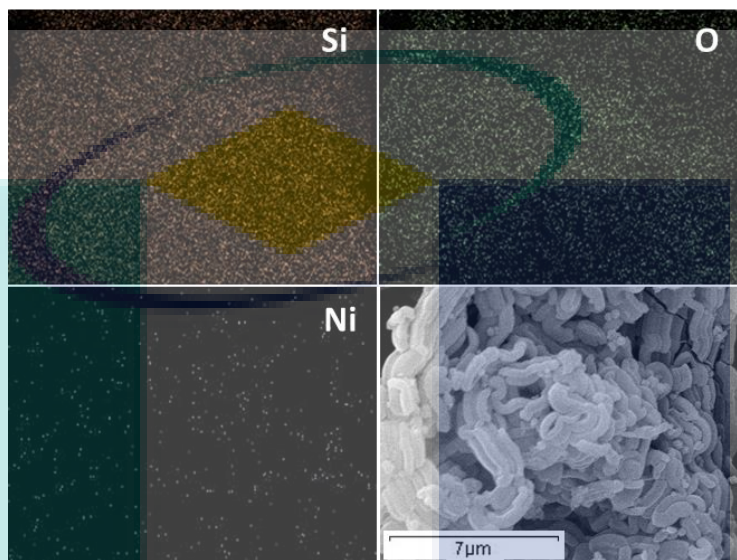
Figure 4:11   SEM-EDX images of Ni/SBA-15(R).

In order to further prove the well-distribution and dispersion of Ni onto the synthesized SBA-15(R), the structure of Ni/SBA-15(R) was viewed using TEM and its image is illustrated in Figure 4:12. It could be clearly observed that the presence of relatively high ordered hexagonal mesoporous structure of SBA-15(R) support was filled with a homogenous and better NiO dispersion upon the introduction of NiO particles. This observation was in accordance with the previous assumption on the elemental mapping of NiO onto the surface of SBA-15 support which showed the well-dispersion of Ni/SBA-15(R).
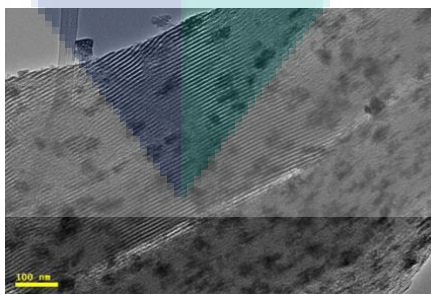
Figure 4:12   TEM image of Ni/SBA-15(R).

The basicity of each Ni/SBA-15 catalyst was determined using adsorbed pyrrole IR spectroscopy as presented in Figure 4:13. Before being adsorbed by pyrrole, all Ni/SBA-15 catalysts were degassed at 673 K for 1 h. As elucidated in Figure 4:13(A), a sharp peak at 3740 cm^{-1} coupled with a shoulder peak at 3710 cm^{-1} was exhibited by all activated Ni-based catalysts, indicating the appearance of a terminal (isolated) and internal silanol groups (Gabrienko et al., 2010). However, the peak intensity at 3740 cm^{-1} increasing as Ni/SBA-15(R) < Ni/SBA-15(T) < Ni/SBA-15(W) due to the perturbation of silica framework with Ni species (Gallo et al., 2010). The incorporation of Ni species mostly occurred onto SBA-15(R) support due to its favorable structural properties; higher surface area and larger pore size, in agreement with the previous assumptions stated above. The broad band centralized at 3550 cm^{-1} was also observed, revealing to the structural defect and/or vicinal hydroxyl groups (Lercher et al., 2007). Meanwhile, as illustrated in Figure 4:13(B-D), IR spectra obviously evidenced the existence of main broad band approximately at 3475–3200 cm^{-1}, which attributing to the interaction between N-H stretching vibrations of chemisorbed pyrrole (C$_4$H$_4$NH) with the basic sites of framework oxygen atoms, and thus resulting the C$_4$H$_4$NH-O bridges with basic oxygen to be formed (Aziz et al., 2014b). However, the intensity of the band decreased dramatically upon the increasing outgassing temperature, which might be due to poor pyrrole-SiO$_2$ interaction (Scokart & Rouxhet, 1980). The peak at the band of 3530 cm^{-1} and 3410 cm^{-1} represented the gas phase pyrrole N-H band position and liquid state like physisorbed pyrrole, respectively (Scokart & Rouxhet, 1980). Moreover, the appearance of the band at approximately 3467 cm^{-1} with a higher intensity was attributed to a higher tendency of pyrrole to blocking effect, indicating a higher basicity (Aziz et al., 2014b). The basicity of the catalysts was descending as Ni/SBA-15(R) > Ni/SBA-15(T) > Ni/SBA-15(W), representing that Ni/SBA-15(R) showed the highest concentration of basic sites. It showed that reflux method as a hydrothermal treatment technique, which allowed the formation of favorable catalytic properties of well-dispersed and strong Ni interaction with SBA-15(R), led to a higher basic sites concentration due to the higher tendency of pyrrole to blocking effect, and thus might be resulted to a higher catalytic performances of CO$_2$ methanation. Meanwhile, the lowest basicity of Ni/SBA-15(W) whereby the low tendency of pyrrole to blocking effect occurred, might be influenced by a poorer structural formation of SBA-15 support that limited the Ni particles dispersion,

lowered metal-support interaction and might be leading to the lowest catalytic performance towards CO_2 methanation.
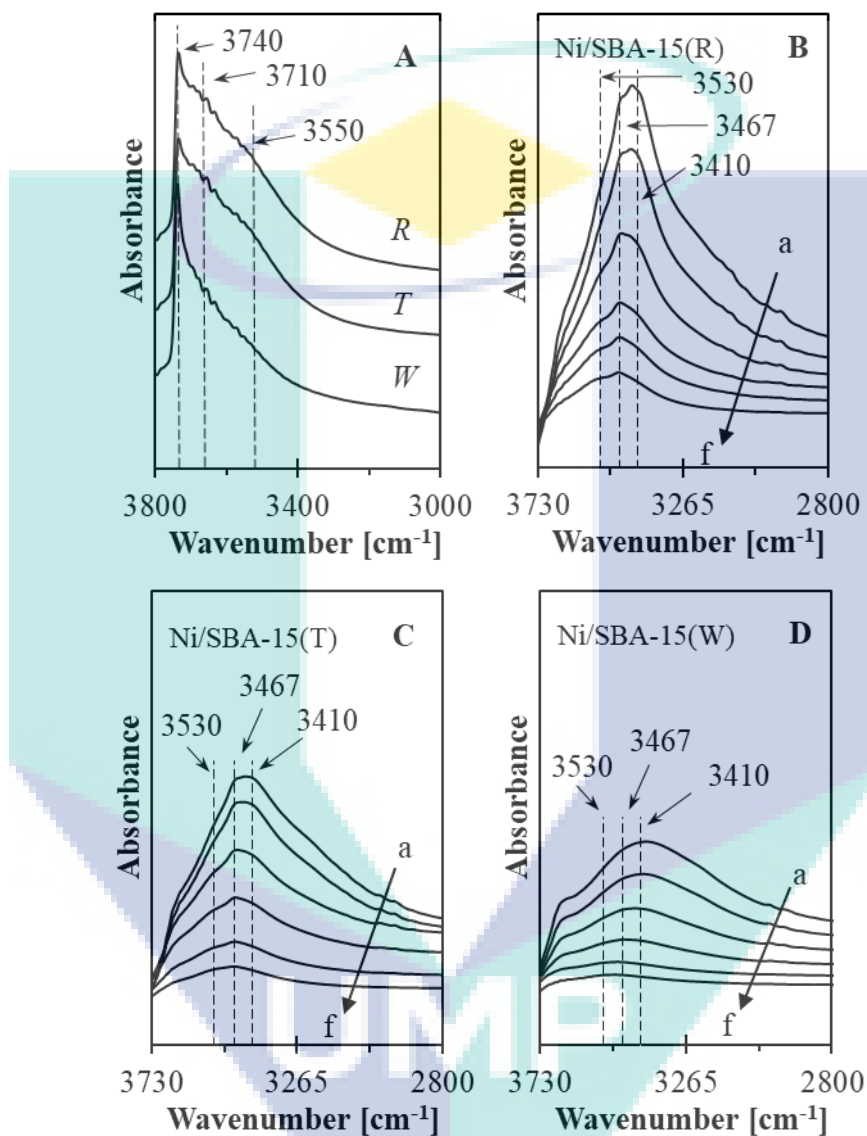
Figure 4:13   (A) IR spectra of activated Ni/SBA-15 catalysts prepared by reflux (R), Teflon (T) and without undergoing hydrothermal treatment (W). (B-D) IR spectra of pyrrole adsorbed on activated Ni/SBA-15 catalysts prepared by R, T and W at (a) room temperature followed by outgassing at (b) room temperature, (c) 323 K, (d) 373 K, (e) 423 K, and (f) 473 K.

Referring to the characterization results, the proposed reaction pathway for the substitution of Si–O–H with Si–O–Ni is illustrated in Figure 4:14. It is plausible to propose that two hydroxyl groups attached to the silica framework of SBA-15 were replaced with Ni^{2+} to form Si–O–Ni. The replacement of Si–O–H with Si–O–Ni network

was in agreement with FTIR analysis whereby the introduction of Ni reduced the peak intensity at 961 cm^{-1} and the peak becomes enveloped in the band of 1060 cm^{-1}, implying the interaction of metal particles with support. It was also found that the introduction of Ni into SBA-15 altered the specific surface area and pore size of SBA-15 representing the substitution of Ni ions into silica framework. It is suggested that the higher specific surface area and larger pore diameter of SBA-15(R) provide the significant channels in support and lead to higher and stronger metal-support interaction (Si–O–Ni). The stronger metal-support interaction reduced Ni agglomeration and thus formed finer NiO particles. The replacement of Si–O–H network into Si–O–metal network was also mentioned by Sidik et al. (2016), for Ni/MSN catalyst. They noticed that the introduction of Ni using in-situ method decreased the number of external Si–O–H groups at 956 cm^{-1} signified the subsequent substitution of silanol groups with some of the Ni^{2+} producing Si-O-Ni, as proven by FTIR analysis. Furthermore, Jusoh et al. (2015) also found that the introduction of Zn using in-situ method into MSN decreased the number of external Si–O–H groups due to the subsequent incorporation of Zn ions producing Si-O-Zn. The substitution of OH with Zn ions was confirmed by a drastic decreased of external Si-OH groups at 966 cm^{-1} upon the introduction of Zn.
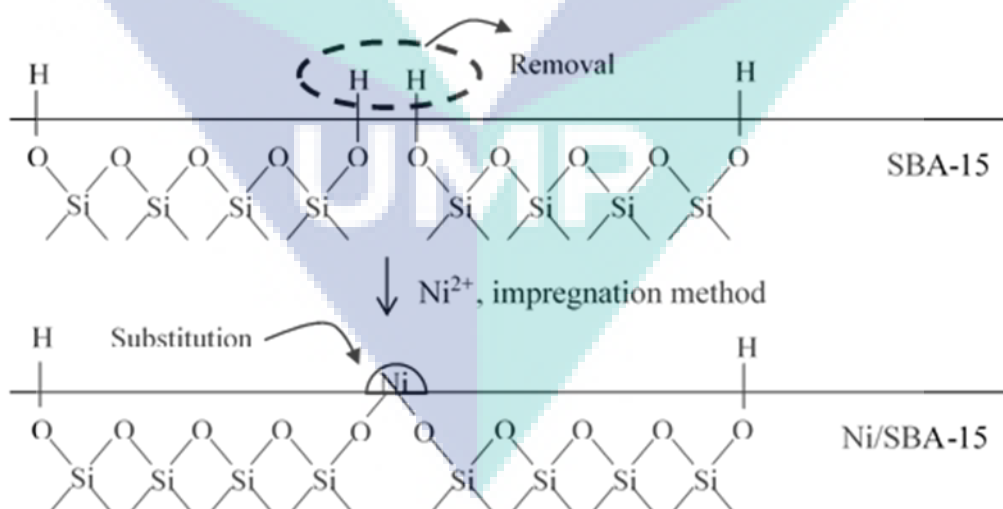
Figure 4:14   Proposed reaction pathway for the substitution of Si–O–H with Si–O–Ni.

4.2.2 Catalytic Performance of Ni/SBA-15(R), Ni/SBA-15(T) and Ni/SBA-15(W) towards CO_2 methanation

Figure 4:15 shows the (A) CO_2 conversion, (B) CH_4 selectivity, and (C) CH_4 yield of the catalysts at a temperature of 523 K, 623 K, 673 K, and 723 K. As observed, the promising performance of Ni-based catalysts significantly influenced by the reaction temperature, whereby an elevated reaction temperature increased the CO_2 conversion and CH_4 yield. The efficacy of CO_2 conversion and CH_4 yield among Ni/SBA-15 catalysts was declined as Ni/SBA-15(R) > Ni/SBA-15(T) > Ni/SBA-15(W) at different temperatures (523–623 K). It was observed that at 723 K, the CH_4 yield over all Ni/SBA-15 synthesized using the different techniques of hydrothermal treatment was slightly decreased due to the thermodynamic barrier of the catalyst was reached (Tada et al., 2014), implying the unfavorable of high reaction temperature towards CO_2 methanation. For the CH_4 selectivity (Figure 4:15(B)), it could be obviously found that its trend was declined with an increment of reaction temperature owing to the happening of reversible water gas shift (RWGS) reaction ($CO_2 + H_2 \leftrightarrow CO + H_2O$) (Zhao et al., 2016). Regarding to the RWGS reaction, the CO and liquid H_2O were usually produced, and thus might be leading to a drastically drop of catalytic behavior of the catalyst. Almost no detection of CO was exhibited by all Ni/SBA-15 catalysts at 523 K due to the closeness result of 100% CH_4 selectivity, and then their CH_4 selectivity were slightly dropped approaching the same value at reaction temperature of 623 K. However, for Ni/SBA-15(T) and Ni/SBA-15(W), both of them drastically initiated the RWGS reaction at 673 K, meanwhile, the RWGS reaction of Ni/SBA-15 (R) was began to drastically start at 723 K. It showed that the highest inhibition of RWGS reaction with the maximum product of CH_4 yield and CO_2 conversion was possessed by the most stable and promising catalytic characteristics of Ni/SBA-15(R) at 673 K, in comparable with the Ni/SBA-15(T) and Ni/SBA-15(W) catalysts.

The superior catalytic performance of Ni/SBA-15(R) could be closely depended on the favorable physical properties of SBA-15(R); highest surface area, largest pore volume, and largest pore diameter, which provide significant channels for Ni deposition, led to higher and stronger metal-support interaction, and thus possessed the highest catalytic performance of CO_2 methanation compared with Ni/SBA-15(T) and Ni/SBA-

15(W). Meanwhile, the lowest catalytic behavior of Ni/SBA-15(W) was related to the poorer structural properties of SBA-15(W); lowest surface area and lowest pore diameter, which cause "dead zone" formation in the channels due to the limited spaces for Ni deposition and thus lead to larger Ni sizes and weak metal-support interaction. The poorer structure properties of catalyst and weak metal-support interaction simultaneously resulted in lowest catalytic performance. Regarding to the results observed in this study, it is clearly revealed that favorable structure properties of support were the key success for good metal dispersion and strong metal-support interaction, resulting to an outstanding performance over the supported metal catalyst.
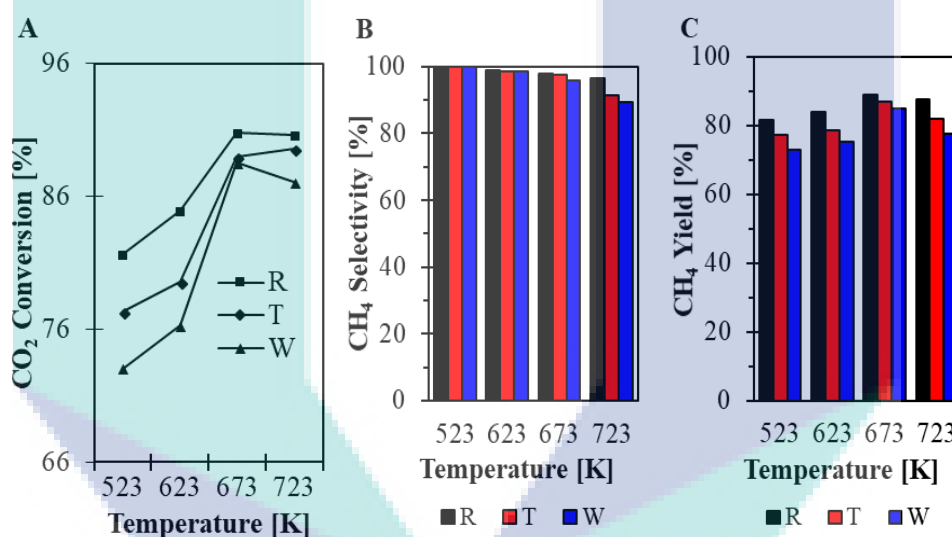
Figure 4:15   (A) CO_2 conversions, (B) CH_4 selectivity and (C) CH_4 yield of Ni/SBA-15 prepared by reflux (R), Teflon (T) and without undergoing hydrothermal treatment (W) in CO_2 methanation at the reaction temperatures of 523 K, 623 K, 673 K and 723 K.

This result was in conformity with our previous study (Bukhari et al., 2017) and reported works of literature (Aziz et al., 2014a; Zhi et al., 2011). Previously, we (Bukhari et al., 2017) have studied the influences of TEOS/P123 mass ratios on the properties of Ni/SBA-15 towards syngas production. We found that Ni/SBA-15 prepared with TEOS/P123=2.21 has the highest catalytic performance towards syngas production, owing to its well-ordered hexagonal structure which enhanced the dispersion of metal particles and thus created stronger metal-support interaction. Likewise, Aziz et al. (2014a) mentioned that excellent catalytic activity of Ni/MSN catalyst might be affected by the high surface area of MSN arose from the existence of inter and intra-particle porosity and

thus led to a better distribution of Ni on the surface of MSN. Besides, Zhi et al. (2011) found that excellent catalytic behavior of Ni-La/SiC catalyst resulted from better Ni dispersion and stronger interaction between NiO and SiC with finer Ni particle size deposited on the surface of SiC.

4.2.3   Catalytic stability of Ni/SBA-15(R), Ni/SBA-15(T) and Ni/SBA-15(W)

Upon the influence of reaction temperatures ranging from 523 to 723 K towards CO_2 methanation over all Ni/SBA-15 catalysts that had been conducted, it was found that the highly active catalytic performance of all Ni/SBA-15 catalysts towards CO_2 methanation reaction was obtained at reaction temperature of 673 K. However, the best performance of catalyst did not reveal the best stability of catalyst. Thus, the lifetime for each Ni/SBA-15 synthesized from different hydrothermal techniques were carried out at the best reaction temperature of 673 K as to know which Ni/SBA-15 achieved the best catalytic performance and stability at that reaction temperature. Figure 4:16 indicates the long-term stability test of Ni/SBA-15(R), Ni/SBA-15(T), and Ni/SBA-15(W) catalysts towards CO_2 methanation at 673 K for 120 h time-on-stream. As illustrated, the efficacy in the catalytic stability of the catalysts was Ni/SBA-15(R) > Ni/SBA-15(T) > Ni/SBA-15(W), indicating Ni/SBA-15(R) showed the most stable catalyst due to its most favorable characteristics of SBA-15(R); high surface area and large pore diameter prepared by reflux hydrothermal treatment technique which allowed a stronger Ni-support interaction and thus might produce negligible amount of coke deposition. Its catalytic performance towards CO_2 methanation was kept maintained for about 48 h time-on-stream at 673 K, but then, its catalytic stability of Ni/SBA-15(R) was declined slowly from 90.7 % to 89.9 % with a difference of 0.8 %, which might be due to the carbon formation and Ni metal sintering (Junke et al., 2009). Meanwhile, the stability of Ni/SBA-15(T) and Ni/SBA-15(W) was declined from 88.9 % to 87.1 % and 88.5 % to 86.5 % with a difference of 1.8 % and 2.0 %, respectively. According to the previous assumptions and pieces of literature, it is reasonable to conclude that the factors involved in enhancing the catalytic performances and stabilities of supported metal catalysts were well dispersion of metal, smaller size of metal and stronger metal-support interaction as a result of higher surface area and larger pore diameter of support which might inhibit the metal agglomeration of metal during the reaction.
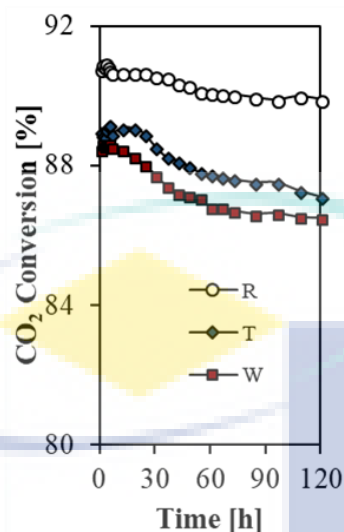
Figure 4:16   Long-term stability test of Ni/SBA-15 catalysts prepared by reflux (R), Teflon (T) and without undergoing hydrothermal treatment (W) at reaction temperature of 673 K for 120 h time-on-stream.

4.2.4   Characterization of spent Ni/SBA-15(W), Ni/SBA-15(T) and Ni/SBA-15(R)

After reacted for 120 h time-on-stream at 673 K, the metallic composition phase of spent catalysts was characterized by using XRD analysis and illustrated in Figure 4:17. It could be proclaimed that the XRD patterns of all spent catalysts attributed almost similar diffraction peak positions approximately at 44.3°, 52.5°, and 76.8°, attributed to metal Ni particles (Zhang et al., 2013b). However, the intensity of the spent catalysts was decreased as Ni/SBA-15(W) > Ni/SBA-15(T) > Ni/SBA-15(R), implying the highest peak intensity of metallic Ni exhibited by Ni/SBA-15(W). The result indicated that Ni sintering mostly occurred on the outer surface of spent Ni/SBA-15(W) after 120 h time of reaction, which might be caused by the weakest metal-support interaction. Meanwhile, spent Ni/SBA-15(R) possessed the lowest peak intensity of metallic Ni, indicating less Ni sintering occurred after 120 h time of reaction due to the strongest metal-support interaction. By calculating the size of metallic Ni using Scherrer equation, the results showed the values of 19.92 nm, 21.89 nm and 34.89 nm for the spent Ni/SBA-15(R), Ni/SBA-15(T) and Ni/SBA-15(W) catalysts, respectively, revealing the occurrence of the largest Ni sintering that existed on the spent Ni/SBA-15(W).

According to the proposed mechanism for CO_2 methanation reported in literature (Aziz et al., 2014b), active sites (Ni) were responsible to dissociate CO_2 and H_2 to CO, O

and H. Then, the linear and bridged carbonyl was formed when CO interacted with oxide surfaces of the support, while the interaction of CO with atomic H formed bidentate formate. The O atom then split over onto the support and stabilized in the oxygen vacancy site near the metal site. The adsorbed oxygen then reacted with atomic hydrogen to form hydroxyl which further reacted with another hydrogen to form the water molecule. The adsorbed carbon species were further hydrogenated to CH_4 and another H_2O molecule. Li & Gong (2014) mentioned that the dehydrogenation or scission of C-C, C-O bonds of oxygenate ($C_xH_yO_z$) into the adsorbed carbonyl groups and/or surface-bound proton, carbon, and oxygen species might be occurred on the metal surface which acted as active sites during the reaction, producing CO and further converting into either CO_2 or CH_4 through the water gas shift reaction (WGSR) or methanation reaction, respectively. It was in agreement with Westermann et al. (2015) who studied about the mechanism of NiUSY zeolites towards CO_2 methanation and found that Ni as the active sites was vital for H_2 and CO_2 dissociation into the oxygenate formation namely as monodentate formate, producing carbonyls and finally converting to CH_4. Based on this information, it is logical to presume that the smaller Ni species, better Ni species dispersion, and stronger the strength between metal and support contributed to an outstanding performance of Ni/SBA-15(R). Nonetheless, poor metal-support interaction triggered a larger formation of Ni with defective dispersion, thus Ni/SBA-15(W) marked the lowest catalytic activity. Apart from that, larger Ni species arose from weaker metal-support interaction probably enhanced the migration and coalescence of particles from the support with other metal particles resulting to the sintering phenomenon and coke formation during the reaction, and thus led to the deactivation activity of the catalyst. It was proved by XRD analysis of spent catalyst as illustrated in Figure 4.17 and assigned that the intensity of the spent catalysts after 120 h time-on-stream decreasing as Ni/SBA-15(W) > Ni/SBA-15(T) > Ni/SBA-15(R), indicating Ni/SBA-15(W) possessed the largest size of NiO (34.89 nm) than Ni/SBA-15 (R) (19.92 nm) and Ni/SBA-15(T) (21.89 nm). Previously, Junke et al. (2009) had investigated the importance of smaller metal particles, homogeneous metal dispersion and stronger metal-support interaction on $Ni/La_2O_3/Al_2O_3$ for syngas production. They found that the homogeneous small metal particles with strong metal-support interaction might prevent the metal particles being lifted easily from the external of the support and thus resulted in the coke deposition and deactivation of the catalyst. In

contrast, lower metal dispersion and weaker metal-support interaction with larger metal species might cause the Ni sintering on the surface of the support and further fluctuating the reactant conversion and product yield. Additionally, other researchers were also mentioned that a better confinement effect of metal particles into the channels of support as one of the important key for providing an excellent anti-sintering and high stability for the methanation reaction (Ai et al., 2018; Liu et al., 2016; Liu et al., 2017c). In the present study, it could be concluded that most favourable catalytic properties of SBA-15 support; higher surface area and larger pore diameter reflux method could be produced by undergoing the reflux method as a hydrothermal treatment technique which promoting towards a better Ni dispersion and stronger metal-support interaction with a finer Ni crystallites size, and thus increasing the catalytic performances and stabilities of supported metal catalysts towards CO_2 methanation with a lower tendency of Ni sintering which might be resulted to deactivation activity of catalyst.
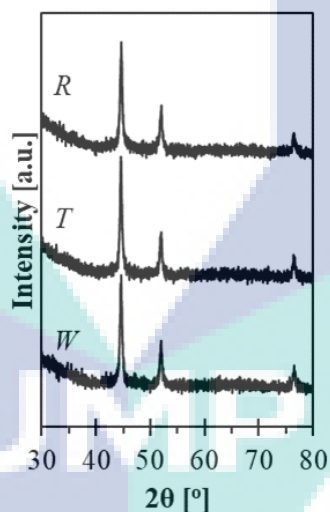
Figure 4:17   XRD patterns of spent Ni/SBA-15 catalysts prepared by reflux (R), Teflon (T) and without undergoing hydrothermal treatment (W) at reaction temperature of 400 °C for 120 h time-on-stream.

4.2.5   Outcomes of the study

The influences of Ni loading (3 – 10 wt%) on the properties of Ni/SBA-15 and CO_2 reforming of CH_4 were studied, owing to the fact that metal loading has a significant influence on the metal-support interaction and catalytic performance of the catalyst. Characterization results indicated that the formation of Ni–O–Si by substitution of surface

silanol groups with Ni species and the maximum substitution was achieved at 5 wt% loading, while further increase in Ni loading stimulate the agglomeration of Ni particles. The catalytic activity of Ni/SBA-15 towards CO_2 reforming of CH_4 followed the order of 5Ni/SBA-15 > 3Ni/SBA-15 ≈ 10Ni/SBA-15, whereas the average H_2/CO ratio followed the order of 5Ni/SBA-15 > 3Ni/SBA-15 > 10Ni/SBA-15. The superior catalytic behavior of 5Ni/SBA-15 towards CO_2 reforming of CH_4 probably was related to the presence of Ni–O–Si, which enhanced the stabilization of the active Ni species on SBA-15 and altered the properties of catalyst towards an excellent catalytic performance. In addition, the analysis of spent Ni/SBA-15 catalysts found that the presence of Ni–O–Si minimizes the growth of encapsulating graphite carbon and thus enhanced the stability of catalyst. Thus, the present study confirmed that metal-support interaction, Si–O–Ni played an important role in the enhancement of the catalytic performance of Ni/SBA-15 catalysts.

Since the Ni/SBA-15 with 5 wt% showed highest activity towards CO_2 reforming of CH_4, 5 wt% Ni loading was used in the subsequent study.

4.3 Effect of Ni-Loading On the Properties and Catalytic Activity of Ni/SBA-15 Towards CO_2 Methanation

4.3.1 Characterization of Ni/SBA-15 (3%, 5% and 10%)

Figure 4:18 indicates the (A) low-angle and (B) wide-angle XRD patterns of SBA-15 and Ni/SBA-15 (1, 3, 5 and 10 wt.%) catalysts. The low-angle XRD patterns of SBA-15 and all Ni/SBA-15 catalysts (Figure 4:18) displayed three main diffraction peaks indexed as (100), (110), and (200) reflections of typical two-dimensional, attributing to the presence of hexagonally ordered mesostructures (*p*6mm) with uniform and high quality of mesoporous packing (Patil et al., 2012). The introduction of Ni did not markedly alter the ordered mesostructured of SBA-15 support structure due to no shift in the peaks and no decreasing intensities were observed with the inclusion of metal, even with the increasing of Ni loading. The results indicated no structural degradation of SBA-15 support due to a highly ordered structural arrangement of SBA-15 support. However, as shown in Figure 4:18(B), the intensity of five main diffraction peaks at 37.3º, 43.2º,

62.9°, 75.4° and 79.3° which are corresponding to face-centred cubic (FCC) crystalline NiO structure (Pudukudy et al., 2015a), increased upon the increasing of Ni loading from 1 to 10%. The intensity of the peaks increased with a sequence of 1%Ni/SBA-15 > 3%Ni/ SBA-15 > 5%Ni/ SBA-15 > 10%Ni/ SBA-15, revealing that the highest accessibility and incorporation of bulky mass reactants of NiO crystalline phase deposited onto SBA-15 support at 10 wt.%, in agreement with Aziz et al. (2015b) for Ni/ MSN catalysts.

The NiO crystallites size was estimated using the Scherrer equation are shown in Table 4:3. Despite the increasing Ni loading onto SBA-15 support from 1 to 5%, NiO crystallites size slightly increased, representing to a higher quantity and homogenous dispersion of NiO crystallites onto the framework of SBA-15 support (Aziz et al., 2015b). However, a further increase in the amount of Ni loading (10 wt.%) onto the structure of SBA-15 support resulted to a drastically enlargement of NiO crystallites size in accordance to an aggregation of NiO crystallites located on the outer surface of the SBA-15 support. This phenomenon might be due to the limited access of the NiO crystallites entering the framework of SBA-15 or partial interruption of SBA-15 structure upon the bulk Ni phase and thus exhibited towards a poorer metal dispersion together with a weaker interaction between metal and support.
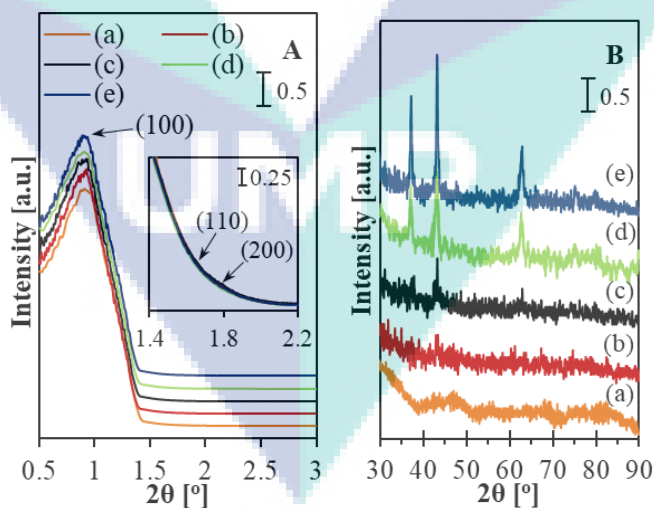
Figure 4:18   XRD patterns for (A) low-angle and (B) wide-angle of (a) SBA-15, (b) 1%Ni/SBA-15, (c) 3%Ni/ SBA-15, (d) 5%Ni/ SBA-15, and (e) 10%Ni/SBA-15.

The physical properties of SBA-15 supports and Ni/SBA-15 catalysts are listed in Table 4:3. BET surface area of SBA-15 support was 814 m^2/g. With an increase of the Ni

loading into SBA-15 from 1 to 10 wt.%, the BET surface area was found to decrease simultaneously from 746 to 329 m^2/g, respectively, attributing to SBA-15 support are incorporated by dispersing nickel oxides (Aziz et al., 2014a) which could enhance the interaction between metal and support. Moreover, the readings of the pore volume of catalysts inconsistently decreased upon the introduction of Ni loading from 1 to 5 wt.%, indicating the pore blockage with Ni species (Setiabudi et al., 2017). However, excess Ni loading into SBA-15 support (10 wt.%) significantly increased its pore volume as compared to 5%Ni/SBA-15, representing the interruption of metal-support incorporation with a poorer metal dispersion and higher insertion of 10% of Ni particles inside the pore mouth of SBA-15 support which then resulted to metal agglomeration, significant wall contraction and pores' expansion (Aziz et al., 2014a; Setiabudi et al., 2017).

Table 4:3   Physical properties of SBA-15 and Ni/SBA-15 catalysts.

Catalysts	Surface area (m^2/g)	Pore volume $(cm^3/g)^a$	Fresh NiO crystallite size $(nm)^b$	Spent Ni size $(nm)^b$
SBA-15	814	0.777	-	-
1%Ni/SBA-15	746	0.757	10.72	10.44
3%Ni/SBA-15	650	0.728	13.63	13.51
5%Ni/SBA-15	460	0.569	17.92	19.92
10%Ni/SBA-15	329	0.699	25.94	26.98

[a] Obtained from Barret-Joyner-Halenda (BJH) desorption method.
[b] Calculated from XRD result using Scherrer equation.

To investigate the functional groups and metal-support interaction of Ni/SBA-15 catalysts prepared at the different amount of Ni loadings (1, 3, 5, and 10 wt.%), FTIR spectra were collected in the wavelength ranging from 500 to 1400 cm^{-1}. As shown in Figure 4:19(A), the bands which were observed at 3450, 1635, 1060, 961 and 801 cm^{-1}, indicated the presence of -OH stretching, adsorbed water molecules retained by siliceous materials, Si-O-Si asymmetric stretching, external Si-OH groups, and Si-O-Si symmetric stretching bonds in the framework, respectively (Karim et al., 2012; Li et al., 2016; Setiabudi et al., 2017; Tomer et al., 2016). The addition of Ni loadings onto the SBA-15 support from 1 to 10% slightly altered the intensity of the band at 961 cm^{-1} and became enveloped in the band of 1060 cm^{-1}, revealing the isomorphous replacement of surface silanol groups (Si–OH) stretching with Ni species forming Si–O–Ni. Interestingly, it

could be found that the highest quantity with the strongest metal-support interaction (Si-O-Ni) was exhibited by 5%Ni/SBA-15 as it possessed the most intense peak at 961 cm^{-1} and became enveloped in the band of 1060 cm^{-1} (Figure 4:19(A)) compared with other catalysts. However, higher Ni loadings (more than 5 wt.%) onto SBA-15 support weakening the metal-support interaction, as a result of the agglomeration of abundance Ni phase. The evidence of the Si-O-Metal formation via the changes in the vibration of Si–OH groups at the band of 961 cm^{-1} was also reported by Jusoh et al. (2013) for ZnO/MSN catalyst.

In addition, reduced SBA-15 and Ni/SBA-15 catalysts possessed a sharp peak at 3740 cm^{-1} with a shoulder at 3710 cm^{-1} (Figure 4:19 (B)), attributing to the appearance of terminal (isolated) and internal silanol group (Sidik et al., 2016), respectively. The introduction of Ni species from 1 to 10 wt.% onto SBA-15 support significantly decreased the intensity of the band at 3740 cm^{-1}, which might be due to perturbation of silica framework with Ni species (Gallo et al., 2010). Meanwhile, the broad band at 3550 cm^{-1} was attributed to structural defect and/or vicinal hydroxyl groups (Lercher et al., 2007). It could be observed that increasing amount of Ni loadings onto SBA-15 influenced the minor structural defect and/or vicinal hydroxyl groups, suggesting the promising properties of SBA-15 support that allowed towards a higher incorporation and better dispersion of Ni particles into the silica framework and pore channels of support. However, upon the interaction with Ni at 10 wt.%, the structural defect and/or vicinal hydroxyl groups were slightly reduced, assigning to the perturbation of SBA-15 framework due to a bulk interaction with Ni species.
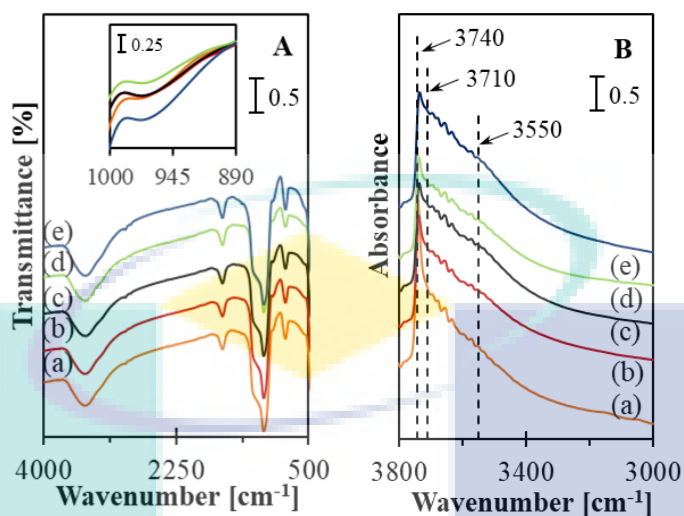
Figure 4:19   (A) FTIR spectra of KBr pellet method and (B) activated catalysts of (a) SBA-15, (b) 1%Ni/SBA-15, (c) 3%Ni/SBA-15, (d) 5%Ni/SBA-15, and (e) 10%Ni/SBA-15.

4.3.1.1   In-situ IR pyrrole

The basicity of all Ni/SBA-15 catalyst was investigated using in-situ FTIR adsorbed pyrrole and their spectra are shown in Figure 4:20. The presence of a peak at $3530\ cm^{-1}$ and $3410\ cm^{-1}$ revealed N-H band from pyrrole molecules (C_4H_4NH) in the gas phase (Camarota et al., 2011) and physisorbed pyrrole in the liquid-like state (Scokart & Rouxhet, 1980), respectively. In the spectral region of $3475–3200\ cm^{-1}$, the main broad band could be assigned to the formation of C_4H_4NH-O bridges with basic oxygen, indicating N-H stretching vibrations of chemisorbed pyrrole (C_4H_4NH) interacted with the basic sites of framework oxygen atoms. The interaction between perturbed N-H stretch of pyrrole and the basic sites of the catalysts could be investigated from the band of $3467\ cm^{-1}$ (Aziz et al., 2015b).
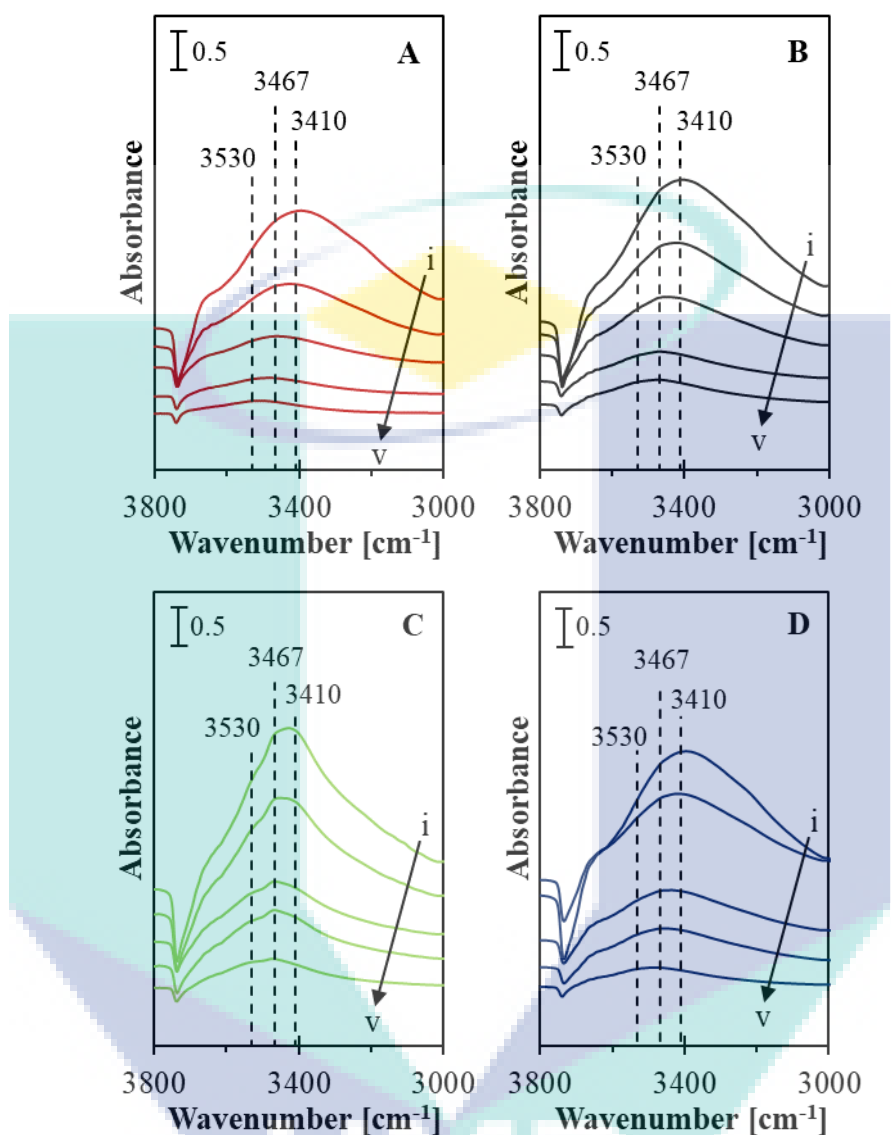
Figure 4:20   IR spectra of pyrrole adsorbed on the reduced Ni/SBA-15 catalysts, exposed to 2 Torr pyrrole at room temperature, followed by evacuated at (i) room temperature, (ii) 323, (iii) 373, (iv) 423, and (v) 473 K for (A) 1%Ni/SBA-15, (B) 3%Ni/SBA-15, (C) 5%Ni/SBA-15, and (D) 10%Ni/SBA-15 catalysts.

It was recognized that the intensity at 3467 cm^{-1} was increased upon increasing Ni loadings from 1 to 5 wt.%, attributing to an addition of Ni loadings up to 5 wt.% provided more active basic sites on the framework of the catalyst which is vital for CO_2 methanation. A lower tendency of pyrrole to the blocking effect observed in 5%Ni/SBA-15 catalyst might also correspond to the high quantity and better Ni dispersion (Aziz et al., 2014b). Notably, the number of basic sites at higher Ni loadings (10 wt.%) slightly reduced due to a poorer Ni dispersion upon bulk Ni phase. In addition, it was related to a

limited availability and accessibility of the pyrrole adsorption sites, corresponding to the limited presence of basic oxygen in the framework of support. This observation was in accordance with Kučera et al. (2004), who previously described that the basicity of ZSM-5 was highly correlated with the presence of framework oxygen atoms. However, the intensities of the bands of all supported metal catalysts with the different amount of metal loadings (1-10 wt.%) slightly decreased upon the heating process from 323 K to 473 K due to weak pyrrole-SiO_2 interaction (Scokart & Rouxhet, 1980).

4.3.2 Reaction studies of CO_2 methanation over of Ni/SBA-15 (1%, 3%, 5% and 10%)

The catalytic activity of CO_2 methanation over all Ni supported onto SBA-15 with different amount of Ni loadings (1, 3, 5, and 10 wt.%) are shown in Figure 4:21(A-C). As presented in Figure 4:21(A-C), increment of Ni loadings (1-5 wt.%) resulted in an increasing CO_2 conversion, CH_4 selectivity and CH_4 yield, representing the most excellent catalytic performance towards CO_2 methanation was possessed by 5%Ni/SBA-15, whereby it exhibited 98.9 % CO_2 conversion, 99.6 % CH_4 selectivity and 98.5 % CH_4 yield at 673 K for 6 h time-on-stream. It might be due to a favorable structure of 5%Ni/SBA-15 whereby numerous substitutions of silanol groups with larger quantity and better dispersion of Ni species and thus, resulted to a stronger metal-support interaction. However, at higher Ni loading (10 wt.%), a slight decrease in catalytic performance was observed as it possessed a slightly declined in the CH_4 selectivity. This phenomenon might be due to the agglomeration of Ni particles, indicating the limitation in substitution of Ni species into the silanol groups of SBA-15 support upon the bulk Ni phase. It could be summarized that an optimum amount of Ni loadings onto the support with better dispersion and stronger metal-support interaction was considered as an crucial role in enhancing towards an excellent catalytic performance of CO_2 methanation, in agreement with Gouveia Gil et al., 2015), who discovered about the influence of Ni loadings (5-25 wt.%) incorporated onto SBA-15 support for the combined steam methane reforming (SMR) and water gas shift (WGS) reaction.

Figure 4:21(D) shows the long-term stability test of the different amount of Ni loadings onto SBA-15 catalysts at 673 K. It was observed that the most optimum and

better stability of catalyst towards CO_2 methanation was exhibited by 5%Ni/SBA-15, whereby it remained active in CO_2 conversion during 120 h time-on-stream. This phenomenon might be due to the numerous substitutions of silanol groups with a large quantity of Ni species, thus resulted towards a better homogenous Ni dispersion and stronger metal-support interaction among Ni/SBA-15 for CO_2 methanation. Apart from that, it might be inhibited by metal sintering during the reaction as well as promoted towards an excellent catalytic performance and stability of CO_2 methanation over 5%Ni/SBA-15. Razzaq et al. (2015) had also investigated that the superior catalytic performances and stabilities towards CO and CO_2 methanation over $Co_4N/\gamma-Al_2O_3$ catalyst was highly related with the resistance of metal sintering and carbon deposition.

For 10%Ni/SBA-15, a slight reduction of catalytic stability of catalyst was observed, which closely related with the limitation substitution of silanol groups at a higher amount of Ni loading, thus lowering Ni dispersion as well as weakening the metal-support interaction. This observation was also discovered by Junke et al. (2009) and they reported that the factors which highly influenced towards the favourable catalytic performance of catalysts were due to a better and homogenous metal dispersion as well as stronger metal-support interaction. In contrast, the occurrence of poorer catalytic stability of catalyst might be due to the formation of poorer metal dispersion and weaker metal-support which triggered towards Ni agglomeration on the surface of support when reacted at the elevated reaction temperature. The metal particles were being lifted easily from the support and thus, might be resulted in the negative effects of coke formation and deactivation of catalyst (XU et al., 2009). On the other hand, with regards to Aziz et al. (2015b), decreasing in catalytic performance (activity and stability) of Ni-promoted MSN towards CO_2 methanation might be also due to the formation of coke which originated from CO disproportionation as well as from CH_4 decomposition on the catalyst surface during the reaction.
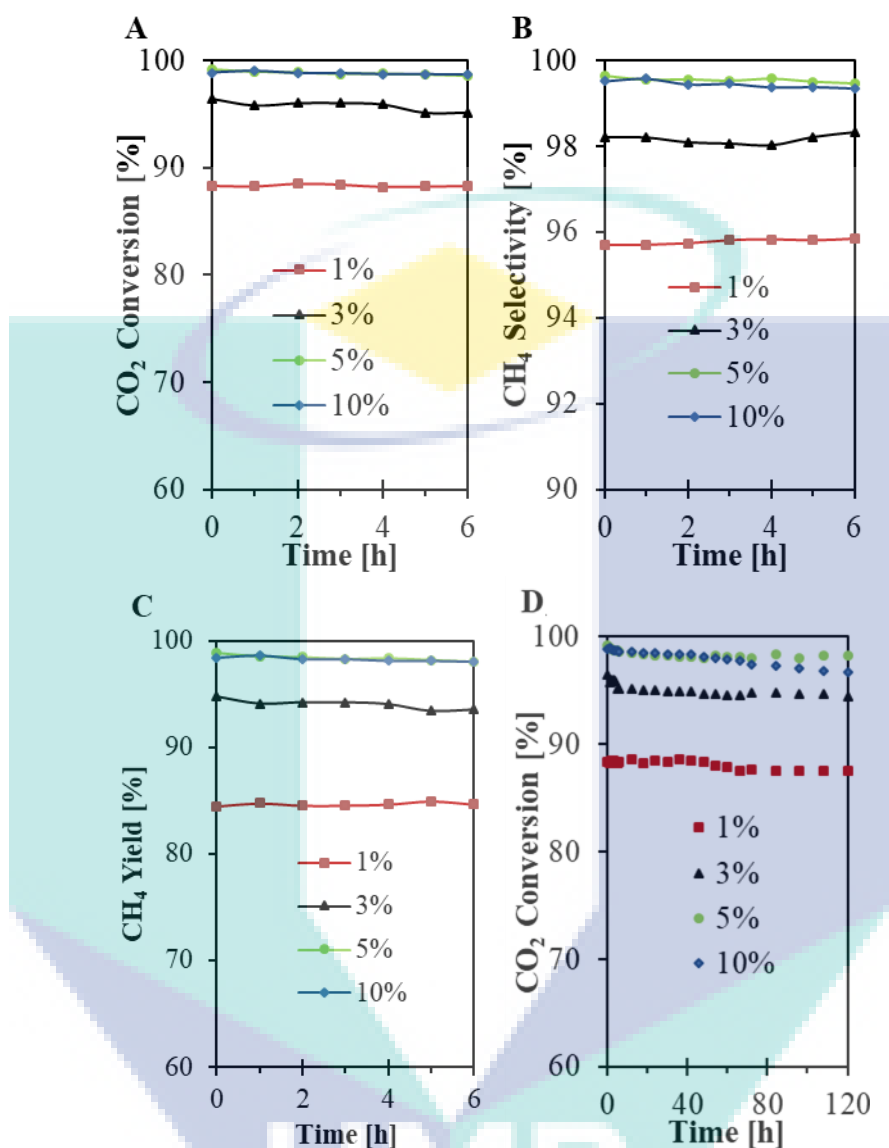
Figure 4:21   (A-C) Catalytic performances and (D) long-term stability test of all different Ni loadings onto FSBA-15 support (1, 3, 5 and 10 %) towards CO_2 methanation. Reaction conditions: T = 673 K, GHSV = 24,900 mL $g^{-1} h^{-1}$, H_2/CO_2 = 1/4, time-on-stream = 6 h.

4.3.3   Characterization of spent Ni/SBA-15 (1%, 3%, 5% and 10%)

After 120 h catalytic stability testing, the spent catalysts were then characterized using XRD analysis as to further study the reduction of NiO into Ni^o crystallites deposited onto the surface of the spent catalysts. The XRD patterns of the spent catalysts are shown in Figure 4:22. As observed, all spent Ni/SBA-15 catalysts possessed three diffraction peak positions approximately at 44.3°, 52.5°, and 76.8° which were assigned to the

presence of Ni^0 crystallite on the surface of Ni-based catalysts (Sidik et al., 2016; Zhang et al., 2013a). Those peaks became more intense upon the increasing Ni loadings (1-10 wt.%) after the 120 h of reaction towards CO_2 methanation. Their intensities increased in a sequence of 1%Ni/SBA-15 < 3%Ni/SBA-15 < 5%Ni/SBA-15 < 10%Ni/SBA-15, revealing that the highest peak intensity of Ni^0 crystallite was possessed by 10%Ni/SBA-15. This phenomenon could be described by the formation of Ni^0 crystallites species deposited onto the outer surface of the spent catalyst, indicating the poorer metal distribution and weaker metal-support interaction upon the abundance of Ni phase. No diffraction peaks of NiO crystallite were detected among all spent Ni/SBA-15 catalyst, attributing to the occurrence of completely NiO reduction into Ni^0 crystallite after the reduction at a higher reaction temperature.

The Ni^0 crystallite size of each spent supported Ni catalysts were determined using the Scherrer equation and the results are summarized in Table 4:3. The obtained results showed the readings of 8.44 nm, 9.51 nm, 10.52 nm, and 18.39 nm for the spent 1%Ni/SBA-15, 3%Ni/SBA-15, 5%Ni/SBA-15 and 10%Ni/SBA-15 catalysts, respectively. It showed that spent 10%Ni/SBA-15 was more prone towards Ni sintering, indicating the poorest Ni distribution and weaker metal-support interaction which allowed the nucleation and growth of metallic Ni crystallites, in parallel with the previous assumptions reported by Junke et al. (2009). In addition, a generation of carbon deposition was expected to occur in 10%Ni/SBA-15 upon the formation of largest Ni^0 crystallite size. According to Taherian et al. (2017), they suggested that an assembly Co species with large crystallite size on the support might cause an occurrence of metal agglomeration during the dry reforming of CH_4 attributable to relatively weak metal-support interaction, and thus triggered towards sintering activity along with more carbon deposition onto the support surface. Therefore, it was reasonable to conclude that higher Ni loading (10 wt.%) for Ni-SBA-15 generated the instability of metal crystallite with larger size whereby the Ni^0 crystallites were being lifted easily from the support due to its weak metal-support interaction, and thus expected to stimulate the carbon species deposition. Apart from that, the carbon species might block the active sites of Ni which then could decline its catalytic activity and stability towards CO_2 methanation (Figure 4:21).
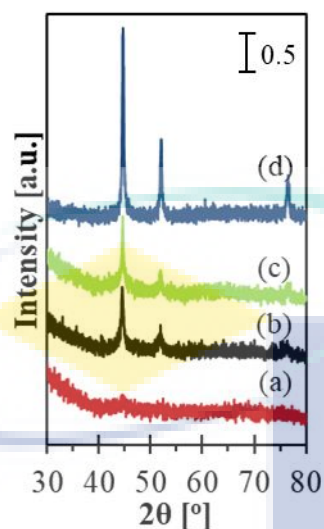
Figure 4:22   XRD analysis of all spent catalysts.

Figure 4:23 indicates the TGA profiles of all spent Ni/SBA-15 catalysts for 120 h time-on-stream. The initial weight loss appeared at a temperature below than 473 K attributing the dehydration of adsorbed H_2O (Setiabudi et al., 2017), meanwhile, the gradual weight loss appeared at a temperature above than 673 K indicating the removal (oxidation) of carbon species (Bukhari et al., 2017; Razzaq et al., 2015). There are two oxidation types of carbon species which known as amorphous carbon (673–773K) and graphite carbon (>773K) (Sidik et al., 2016). As shown in Figure 4.23, an increase in Ni loadings (1-5 wt.%) onto the framework of SBA-15 support slightly reduced the weight loss percentage, indicating the less significant formation of carbon species. However, no further decrement of weight loss percentage was noticed upon the introduction of higher metal loading (10 wt.%) onto the framework of SBA-15 support, but it began to slightly increase the weight loss percentage of carbon species as compared with 5%Ni/SBA-15, implying the growth of carbon deposition. It might be due to a poorer metal distribution and dispersion, lower metal-support interaction, and lower amount of active basic sites of the catalyst upon the presence of bulk Ni species (10 wt.%) onto the framework of SBA-15.

According to the analysis of spent catalyst, the highest resistance towards Ni sintering and the growth of coke formation were achieved at an optimum insertion of 5 wt.% Ni loading due to a homogenous and well-dispersed of Ni particles, stronger metal-

support interaction, higher surface basicity of catalyst, and thus might be affected towards a superior catalytic stability and minimized the growth of coke formation on the catalyst surface. It is believed that the better metal dispersion, stronger metal-support interaction, and higher amount of active basic sites were considered as the important factors for possessing an excellent long-term catalytic activity and stability as well as minimizing the growth of coke deposition, in compliance with the previous studies (Setiabudi et al., 2017; Sidik et al., 2016; Zhao et al., 2017).
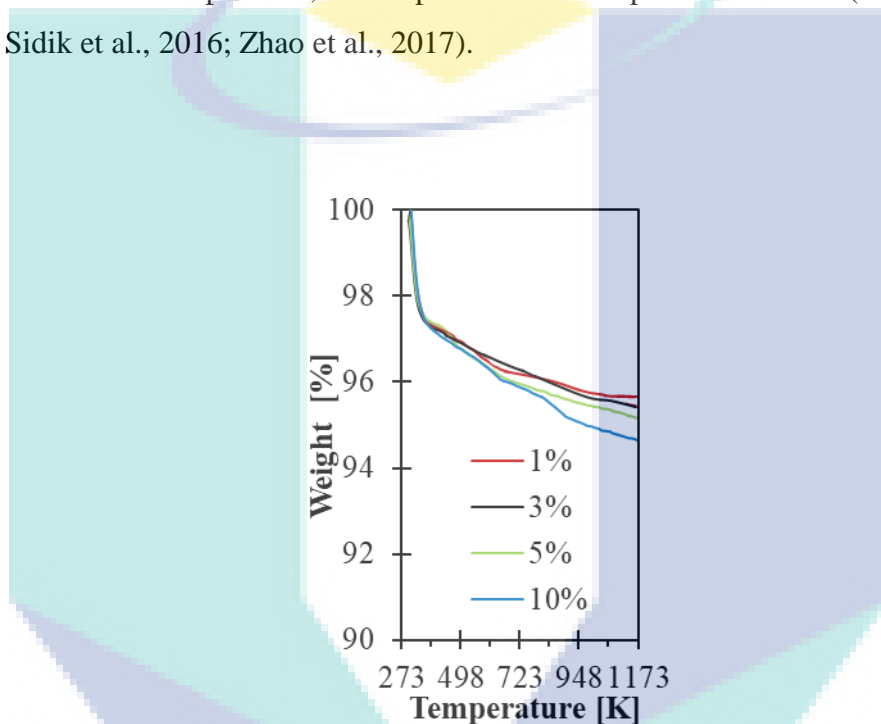
Figure 4:23   TGA analysis of all spent catalysts.

4.3.4   Mechanistic path study of CO_2 methanation

Figure 4:24 illustrates the IR spectra of adsorbed (A) CO_2 and (B) H_2 on Ni/SBA-15 catalysts from ambient temperature to 623 K. The adsorption of CO_2 on Ni/SBA-15 (Figure 4:24(A)) exhibited an intense peak at 2342 cm^{-1} with a shoulder at 2300 cm^{-1}, assigning to linearly adsorbed O=C=O species with increasing desorption from the framework of Ni/SBA-15 at elevated temperature (Hamid et al., 2017). Besides, the band at 1870 cm^{-1} was revealed to the presence of adsorbed carbonyls on Ni^0 sites (Ni^0-CO) (Teh et al., 2015). Moreover, the peaks at 1390 and 1623 cm^{-1} were related to the formation of bidentate carbonate groups (Sidik et al., 2016; Tada et al., 2014), meanwhile peak at 1470 and 1530 cm^{-1} [1] was indicated to the appearance of unidentate carbonate

species (Sidik et al., 2016; Tada et al., 2014). It was observed that the intensities of three peaks (bidentate and unidentate carbonate groups) decreased upon the increasing heating reaction from room temperature to 623 K. However, a small new band of 2055 cm^{-1} was evolved at much higher temperature of 623 K, attributing the formation of linear carbonyl from the adsorption of CO_2 onto the surface of catalyst (Chen et al., 2014). In contrast, the absence of linear carbonyl species occurred at lower heating process from room temperature up to 573 K. From this phenomenon, it could be acknowledged that the morphology of Ni/SBA-15 not only eliminated its carbonate groups originated from the wavelengths of 1390, 1530 and 1623 cm^{-1}, but it allowed the formation of new groups of linear carbonyl species as the intermediate of reaction at an elevated temperature, which is 623 K. It may be concluded that the happening of the alteration of physical CO_2 adsorption at low temperature into the allocation of linear carbonyl groups at high temperature (Chen et al., 2014; Sidik et al., 2016; Tada et al., 2014). This occurrence may also due to desorption of CO from the weaker Ni adsorption sites. For the adsorption of H_2 onto Ni/SBA-15, IR spectra as illustrated in Figure 4:24(B) revealed the appearance of bridging hydroxyl groups and perturbed Si-OH groups at 3680 cm^{-1} and 3560 cm^{-1} (Aziz et al., 2012; Hamid et al., 2017; Mirth & Lercher, 1990) respectively. Besides, the bands at 3480 and 3400 cm^{-1} are assigned to the appearance of atomic hydrogen interactions. The intensity of bridging hydroxyl groups increased upon heating, while, their absorbance bands of perturbed Si-OH groups and atomic hydrogen bonding decreased probably due to alteration of perturbed silanol species of Ni/SBA-15 with the adsorbed hydrogen to a more stable hydrogen bonded OH groups.
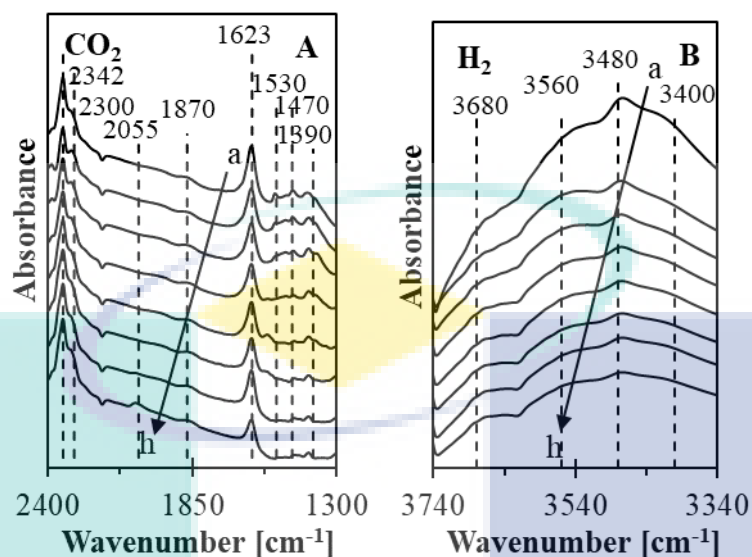
Figure 4:24 IR spectra when Ni/SBA-15 were heated in (A) 4 Torr of CO_2 and (B) 16 Torr of H_2 monitored at (a) ambient temperature, (b) 323, (c) 373, (d) 423, (e) 473, (f) 523, (g) 573, and (h) 623 K.

The changes in the IR spectra of adsorbed gases ($CO_2 + H_2$) on Ni/SBA-15 towards CO_2 methanation (Figure 4:25) was analysed using in-situ FTIR spectroscopy ($CO_2 + H_2$) as to further determine the species that involved as the reaction intermediates for CO_2 methanation mechanism. As observed in Figure 4.25(A), after $CO_2 + H_2$ adsorption on the Ni/SBA-15, the dissociation of H_2 and CO_2 mainly occurred by active sites (Ni metal) and then the formation of both bidentate and unidentate carbonates species as an intermediate was adsorbed on the surface of SBA-15 at wavelengths of 1390 and 1623 cm^{-1}, 1470 and 1530 cm^{-1} (Sidik et al., 2016; Tada et al., 2014) increased upon an elevation of reaction temperature from room temperature to 623 K towards CO_2 methanation. However, both types of peaks were slightly decomposed at an elevated temperature and evolved a development of new peak approximately at 2055 cm^{-1} over Ni/SBA-15 when the heating temperature at 623 K, which was assigned to linear carbonyl groups as an intermediate that could be also adsorbed on the surface of SBA-15 (Chen et al., 2014). Moreover, an intense peak at 2342 cm^{-1} shouldered with a small peak at 2300 cm^{-1} which was assignable to the linear O=C=O species (Hamid et al., 2017), remained unchanged from the framework of Ni/SBA-15 even reacted to a higher reaction temperature up to 623 K, indicating a stronger interaction of carbonyl species on the surface of SBA-15.
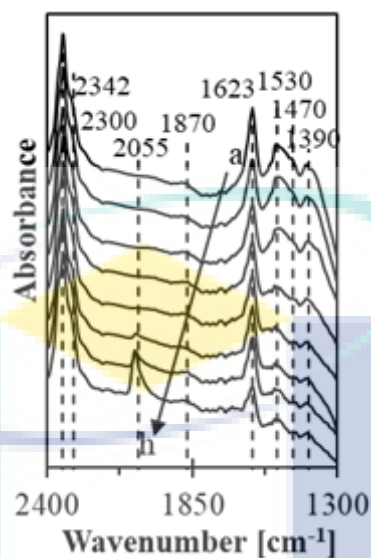
Figure 4:25   IR spectra of adsorbed gases (CO_2 + H_2) on (A) Ni/SBA-15. The samples were adsorbed at (a) ambient temperature, (b) 323, (c) 373, (d) 423, (e) 473, (f) 523, (g) 573, and (h) 623 K.

It is noteworthy that the presence of both bidentate and unidentate carbonate species as well as other bands of carbonyl groups on surface of SBA-15 revealed a large amount of CO_2 efficiently being dissociated by active sites (Ni metal) that impregnated on the SBA-15 support even though it was reacted at an elevated temperature due to favourable properties of catalysts which might significantly allow higher composition and stronger carbonate and carbonyl species of the surface of SBA-15, and thus might enhance towards a higher CO_2 methanation.

The plausible mechanism of CH_4 production through the hydrogenation of CO_2 over the Ni/SBA-15 was illustrated in Figure 4.26, in accordance with CO_2, H_2, and CO_2 + H_2 probed IR spectroscopic studies. As shown in Figure 4:26, it was suggested that CO_2 and H_2 gases were adsorbed onto the active sites (Ni metal) and further dissociated into CO, O, and H atoms. The CO migrated onto the support producing bidentate and unidentate carbonates. Besides, the linear carbonyl was also formed by the migration of CO onto the catalyst surface. Then, these three species were reacted with atomic H, followed by the hydrogenation of each bidentate carbonates, unidentate carbonates and linear carbonyl forming CH_4 and H_2O molecules.
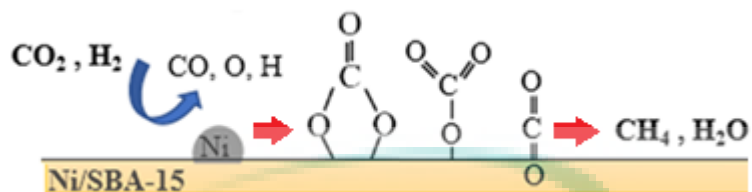
Figure 4:26   Plausible mechanism of methane production over Ni/SBA-15.

4.3.5   Outcomes of the study

In conclusion, developing new fascinating properties of Ni/SBA-15 catalysts with the varied amount of Ni loadings were discovered and synthesized. Their textural properties were investigated by XRD, BET, FTIR, FESEM-EDX, TEM and in-situ FTIR adsorbed pyrrole. It was found that the most promising and optimum amount of Ni loadings to be incorporated and dispersed onto SBA-15 support for methane production was at 5 wt.%. 5%Ni/SBA-15 possessed an excellent catalytic performance and stability with no deactivation signs up to 120 h time-on-stream. Only small amount of Ni sintering was observed whereby a smaller nucleation and growth of metallic Ni^0 crystallites occurred due to a better and homogenous NiO dispersion accompanied by stronger the metal-support interaction, in accordance with the XRD result over the spent catalyst. Addition of 5 wt.% Ni loading onto the SBA-15 support provided the higher presence of active basic sites on the catalyst surface which then might possess better stability even after 120 h time-on-stream. However, a trivial reduction in the catalytic performance and stability of CO_2 methanation was achieved by 10%Ni/SBA-15 due to its limitation spaces and substitution of Ni species with the silanol groups of SBA-15 support upon the bulk Ni phase, attributing to a poorer Ni distribution and weaker metal-support interaction. The agglomeration of NiO crystallites might cover the active basic sites of the surface of the catalyst which then continuously declined the stability of the catalyst towards CO_2 methanation after 120 h time-on-stream. The coke deposition might also occur onto the surface of 10%Ni/SBA-15, as proven by the TGA analysis. The plausible mechanism of CO_2 methanation over Ni/SBA-15 and Ni/SBA-15 was confirmed by the in-situ FTIR studies of adsorbed H_2, CO_2, and $H_2 + CO_2$. Firstly, the CO_2 and H_2 molecule were dissociated to CO, O, and H atoms on the surface of Ni metal active sites and spillover

onto the support to form unidentate carbonates, bidentate carbonates and linear carbonyl as the main adsorption species for Ni/SBA-15. Then, these intermediate species were further undergoing hydrogenation with the atomic hydrogen to form CH_4 and H_2O. In conclusion, the metal sites were responsible in the dissociation of CO_2 and H_2, while the concentration of basic sites influenced the CO_2 adsorption ability of the catalys.
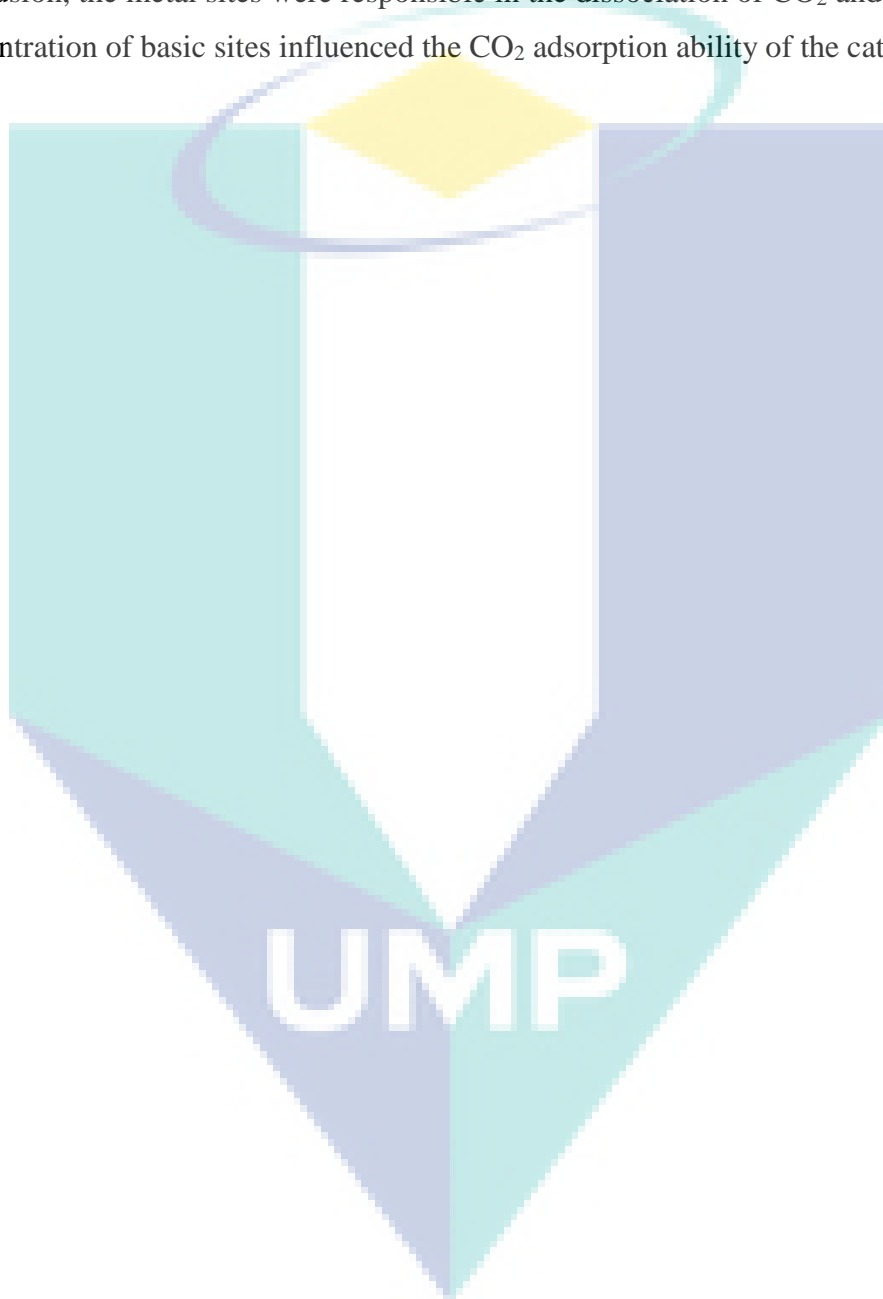
CHAPTER 5

CONCLUSION

5.1   Conclusion

In this study, Ni/SBA-15 catalysts have been successfully prepared and characterized. The effects of TEOS/P123 mass ratios on the properties and catalytic activity of Ni/SBA-15 were studied by varying the TEOS/mass ratio (1.5, 2.21 and 3.0). Characterization results indicated that the TEOS/P123 ratio of 2.21 was the optimal synthesis ratio of Ni/SBA-15 which producing the well-ordered hexagonal mesoporous structure with the highest Ni-support interaction. The catalytic activity of Ni/SBA-15 towards CO_2 methanation followed the order of Ni/SBA-15(R2.21) > Ni/SBA-15(R3.0) > Ni/SBA-15(R1.5). The superior catalytic behavior of Ni/SBA-15(R2.21) towards CO_2 reforming of CH_4 was related with the catalytically favorable textural properties of Ni/SBA-15(R2.21) which enhanced the dispersion of metal particles, improved the catalyst activity, increased the catalyst stability and reduced the carbon deposition. Meanwhile, the lowest catalytic performance of Ni/SBA-15(R1.5) might be related with the incomplete hexagonal structure of SBA-15 which resulted in poorer dispersion of Ni particles as supported by the characterization results.

The effects of hydrothermal techniques (Reflux (R) and Teflon (T)) revealed that Ni/SBA-15(R) exhibited the most fascinating characteristics owing to the highest surface area (814 m^2/g) and pore diameter (5.49 nm) of SBA-15(R), finest metal particles (17.92 nm), strongest metal-support interaction and highest concentration of basic sites. The efficacy of Ni/SBA-15 towards CO_2 methanation was descending as Ni/SBA-15(R) > Ni/SBA-15(T) > Ni/SBA-15(W), implying the excellent behaviour of Ni/SBA-15(R). The lowest performance of Ni/SBA-15(W) was due to the poorest properties of support; lowest surface area and pore diameter, largest Ni sizes, weakest metal-support interaction

and lowest concentration of basic sites. This study successfully showed that a fascinating Ni-based catalyst through the reflux hydrothermal treatment technique for CO_2 methanation. However, a sign of deactivation was detected over Ni/SBA-15(R) towards CO_2 methanation up to 120 h

The effects of Ni content on the properties and catalytic activity of Ni/SBA-15 were studied by varying the amount of Ni content (1 – 10 wt%). The synthesized catalysts were characterized using XRD, BET, FTIR, FESEM-EDX, TEM and in-situ FTIR adsorbed pyrrole. The result on the influence of Ni loadings showed that the efficacy in CO_2 methanation over Ni/SBA-15 increased with a sequence of 1%Ni/SBA-15 < 3%Ni/SBA-15 < 5%Ni/SBA-15 ≈ 10%Ni/SBA-15, indicating the most optimum Ni loadings onto the framework and channels of SBA-15 support towards an outstanding behaviour and stability of CH_4 production was at 5 wt.%. It proved that the promising support enhanced the quantity of Si-O-Ni bond, triggered better Ni dispersion, strengthen metal-support interaction, and increased the basicity. However, higher Ni loadings (10 wt.%) onto SBA-15 slightly declined the performance and stability of CO_2 methanation due to the limited spaces for substitution of Ni species with the silanol groups of SBA-15 upon the bulk Ni phase, poorer Ni dispersion, weaker metal-support interaction, and lower basicity.

The plausible mechanism of CO_2 methanation over Ni/SBA-15 was confirmed by the in-situ FTIR studies of adsorbed H_2, CO_2, and $H_2 + CO_2$. Firstly, the CO_2 and H_2 molecule were dissociated to CO, O, and H atoms on the surface of Ni metal active sites and spillover onto the support to form unidentate carbonates, bidentate carbonates and linear carbonyl as the main adsorption species for Ni/SBA-15. Then, these intermediate species were further undergoing hydrogenation with the atomic hydrogen to form CH_4 and H_2O.

In conclusion, well-dispersed Ni/SBA-15 was successfully synthesized with an optimum of TEOS/P123 = 2.21, reflux hydrothermal treatment technique and 5 wt.% Ni loadings. The role of basic and metallic sites of Ni/SBA-15 on CO_2 methanation were successfully discovered in this study. The metal sites were responsible in the dissociation of CO_2 and H_2, while the concentration of basic sites influenced the CO_2 adsorption ability of the catalyst.

5.2 Recommendation for future work

As an extension of this study, a modification of surface morphology with fibrous structure can be done for studying the effect of structure morphology on properties, catalytic activity and mechanistic patch of reaction.
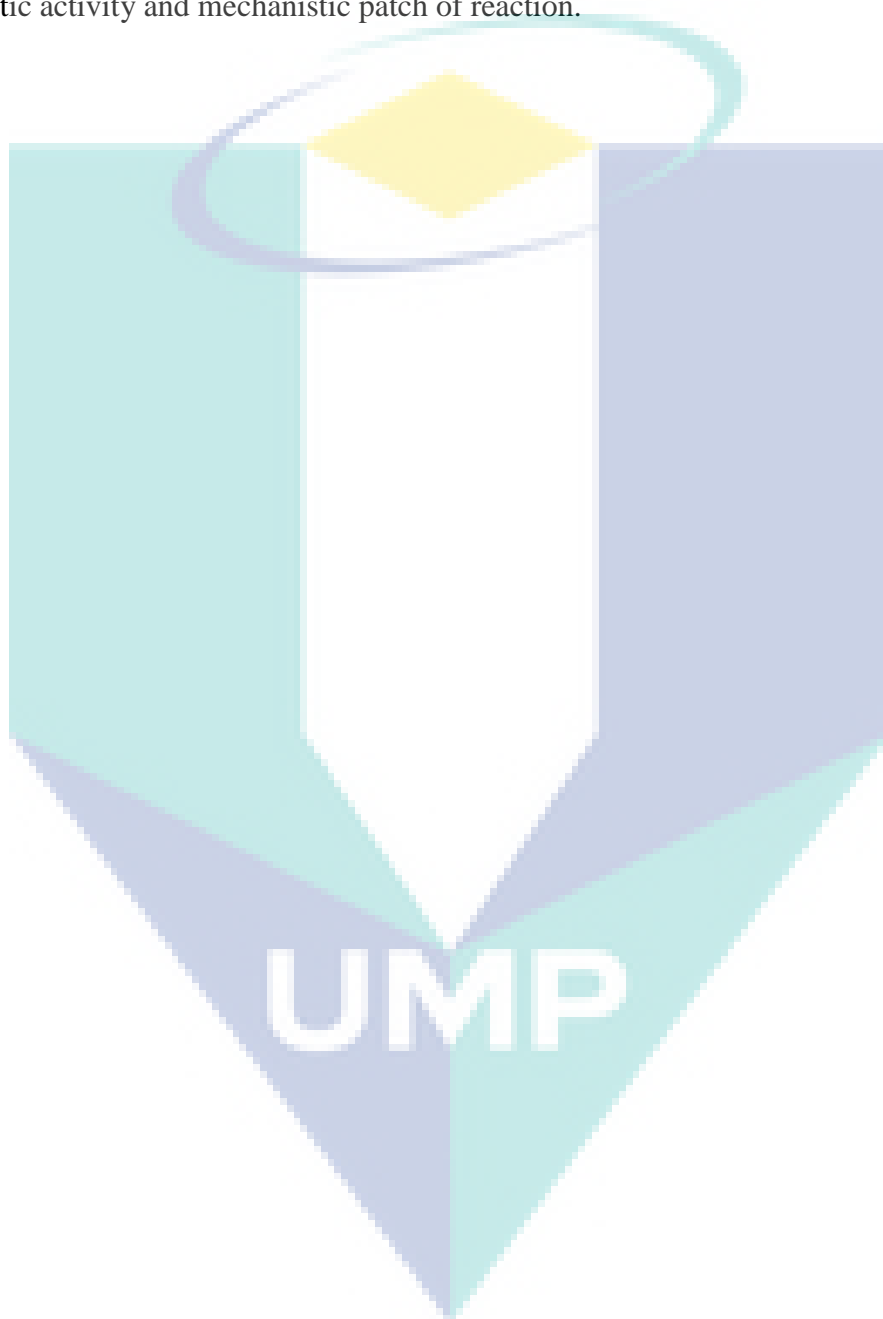
REFERENCES

Abdullah, A. Z., Razali, N., & Lee, K. . (2010a). Optimization of mesoporous K/SBA-15 catalyzed transesterification of palm oil using response surface methodology. *J. Phys. Sci.*, *21*(2), 13–27.

Abdullah, A. Z., Razali, N., & Lee, K. T. (2010b). Influence of the Silica-to-Surfactant Ratio and the pH of Synthesis on the Characteristics of Mesoporous SBA-15. *Journal of Physical Science*, *21*(2), 13–27.

Ai, H., Yang, H., Liu, Q., Zhao, G., Yang, J., & Gu, F. (2018). ZrO_2-modified Ni/LaAl$_{11}$O$_{18}$ catalyst for CO methanation: Effects of catalyst structure on catalytic performance. *Chinese Journal of Catalysis*, *39*(2), 297–308.

Aldana, P. A. U., Ocampo, F., Kobl, K., Louis, B., Thibault-Starzyk, F., Daturi, M., … Roger, A. C. (2013). Catalytic CO_2 valorization into CH_4 on Ni-based ceria-zirconia. Reaction mechanism by operando IR spectroscopy. *Catalysis Today*, *215*, 201–207.

Aziz, M. A. A., Jalil, A. A., Triwahyono, S., & Ahmad, A. (2015). CO_2 methanation over heterogeneous catalysts: recent progress and future prospects. *Green Chem.*, *17*(5), 2647–2663.

Aziz, M. A. A., Jalil, A. A., Triwahyono, S., Mukti, R. R., Taufiq-Yap, Y. H., & Sazegar, M. R. (2014). Highly active Ni-promoted mesostructured silica nanoparticles for CO_2 methanation. *Applied Catalysis B: Environmental*, *147*(September 2013), 359–368.

Aziz, M. A. A., Jalil, A. A., Triwahyono, S., Mukti, R. R., Taufiq-Yap, Y. H., & Sazegar, M. R. (2014). Highly active Ni-promoted mesostructured silica nanoparticles for CO_2 methanation. *Applied Catalysis B: Environmental*, *147*, 359–368.

Aziz, M. A. A., Jalil, A. A., Triwahyono, S., & Saad, M. W. A. (2015a). CO_2 methanation over Ni-promoted Mesostructured Silica Nanoparticles: Influence of Ni Loading and Water Vapor on Activity and Response Surface Methodology Studies. *Chemical Engineering Journal*, *260*, 757–764.

Aziz, M. A. A., Jalil, A. A., Triwahyono, S., & Saad, M. W. A. (2015b). CO_2 reforming of methane over ni supported on mesostructured silica nanoparticles (Ni/MSN): effect of ni loading. *Chemical Engineering Journal*, *260*, 757–764.

Aziz, M. A. A., Jalil, A. A., Triwahyono, S., & Sidik, S. M. (2014). Methanation of carbon dioxide on metal-promoted mesostructured silica nanoparticles. *Applied Catalysis A: General*, *486*, 115–122.

Aziz, M. A. A., Kamarudin, N. H. N., Setiabudi, H. D., Hamdan, H., Jalil, A. A., & Triwahyono, S. (2012). Negative effect of Ni on PtHY in n-pentane isomerization evidenced by IR and ESR studies. *Journal of Natural Gas Chemistry*, *21*(1), 29–36.

Bacariza, M. C., Graça, I., Bebiano, S. S., Lopes, J. M., & Henriques, C. (2018). Micro- and mesoporous supports for CO_2 methanation catalysts: A comparison between SBA-15, MCM-41 and USY zeolite. *Chemical Engineering Science*, *175*, 72–83.

Bao, X., Zhao, X. S., Li, X., & Li, J. (2004). A novel route toward the synthesis of high-quality large-pore periodic mesoporous organisilicas. *Appl. Surf. Sci*, *237*, 380–386.

Bendahou, K., Cherif, L., Siffert, S., Tidahy, H. L., Benaïssa, H., & Aboukaïs, A. (2008). The effect of the use of lanthanum-doped mesoporous SBA-15 on the performance of Pt/SBA-15 and Pd/SBA-15 catalysts for total oxidation of toluene. *Applied Catalysis A: General*, *351*(1), 82–87.

Brodie-Linder, N., Caër, S. Le, Alam, M. S., Renault, J. P., & Alba-Simionesco, C. (2010). Physical Chemistry. *Phy. Chem.*, *12*, 14188–12195.

Bukhari, S. N., Chin, C. Y., Setiabudi, H. D., & Vo, D. N. (2017). Journal of Environmental Chemical Engineering Tailoring the properties and catalytic activities of Ni / SBA-15 via di ff erent TEOS / P123 mass ratios for CO 2 reforming of CH$_4$. *Journal of Environmental Chemical Engineering*, *5*(4), 3122–3128.

Cai, M., Wen, J., Chu, W., Cheng, X., & Li, Z. (2011). Methanation of carbon dioxide on Ni/ZrO$_2$-Al$_2$O$_3$ catalysts: Effects of ZrO$_2$ promoter and preparation method of novel ZrO$_2$-Al$_2$O$_3$ carrier. *Journal of Natural Gas Chemistry*, *20*(3), 318–324.

Camarota, B., Goto, Y., Inagaki, S., & Onida, B. (2011). Basic sites on periodic mesoporous organosilicas investigated by XPS and in situ FTIR of adsorbed pyrrole. *Langmuir*, *27*(3), 1181–1185.

Chen, X., Jin, J., Sha, G., Li, C., Zhang, B., Su, D., Williams, C. T., & Liang, C. (2014). Silicon-nickel intermetallic compounds supported on silica as a highly efficient catalyst for CO methanation. *Catalysis Science and Technology*, *4*(1), 53–61.

Cheng, M., Pan, C., & Hwang, B. (2009). Highly-dispersed and thermally-stable NiO nanoparticles exclusively confined in SBA-15 : Blockage-free nanochannels, 5193–5200.

Dan, M., Lazar, M. D., Mihet, M., Almasan, V., Rednic, V., & Borodi, G. (2012). Hydrogen production by low temperature methane steam reforming using Ag and Au modified alumina supported nickel catalysts. *Reaction Kinetic Mechanical Catalyst*, *105*(1), 173–193.

Fan, X. L., Zhao, J. Z., Wei, Y., Liu, J., Duan, A., & Jiang, G. (2015). Insights into the effects of steam on propane dehydrogenation over a Pt/Al2O3 catalyst. *Catal. Sci. Technology*, *5*(1), 339–350.

Fihri, A., Bouhrara, M., Patil, U., Cha, D., Saih, Y., & Polshettiwar, V. (2012). Fibrous nano-silica supported ruthenium (KCC-1/Ru): A sustainable catalyst for the hydrogenolysis of alkanes with good catalytic activity and lifetime. *ACS Catalysis*, *2*(7), 1425–1431.

Fouad, O. A., Mohamed, R. M., M. S. Hassan, I., & Ibrahim, A. (2006). Synthesis and modification of ZSM-5 with manganese and lanthanum and their effects on decolorization of indigo carmine dye. *Catal. Today*, *116*, 82–87.

Frontera, P., Macario, A., Ferraro, M., & Antonucci, P. (2017). Supported Catalysts for CO$_2$ Methanation : A Review, (1), 1–28.

Gabrienko, A. A., Danilova, I. G., Arzumanov, S. S., Toktarev, A. V., Freude, D., & Stepanov, A. G. (2010). Strong acidity of silanol groups of zeolite beta: Evidence from the studies by IR spectroscopy of adsorbed CO and 1H MAS NMR. *Microporous and Mesoporous Materials*, *131*(1–3), 210–216.

Gallo, J. M. R., Bisio, C., Gatti, G., Marchese, L., & Pastore, H. O. (2010). Physicochemical characterization and surface acid properties of mesoporous [Al]-SBA-15 obtained by direct synthesis. *Langmuir*, *26*(8), 5791–5800.

Garbarino, G., Riani, P., Magistri, L., & Busca, G. (2014). A study of the methanation of carbon dioxide on Ni/Al$_2$O$_3$ catalysts at atmospheric pressure. *International Journal of Hydrogen Energy*, *39*(22), 11557–11565.

Gibson, L. T. (2014). Mesosilica materials and organic pollutant adsorption: part A removal from air. *Chemical Society Reviews*, *43*(15), 5163–72.

Gouveia Gil, A., Wu, Z., Chadwick, D., & Li, K. (2015). Ni/SBA-15 Catalysts for combined steam methane reforming and water gas shift - Prepared for use in catalytic membrane reactors. *Applied Catalysis A: General*, *506*, 188–196.

Graça, I., González, L. V., Bacariza, M. C., Fernandes, A., Henriques, C., Lopes, J. M., & Ribeiro, M. F. (2014). CO$_2$ hydrogenation into CH$_4$ on NiHNaUSY zeolites. *Applied Catalysis B: Environmental*, *147*, 101–110.

Halim, A. Z. A., Ali, R., & Bakar, W. A. W. A. (2014). CO$_2$/H$_2$ methanation over M*/Mn/Fe-Al$_2$O$_3$ (M*: Pd, Rh, and Ru) catalysts in natural gas; optimization by response surface methodology-central composite design. *Clean Technol. Environ. Policy*, *17*, 627–636.

Hamid, M. Y. S., Firmansyah, M. L., Triwahyono, S., Jalil, A. A., Mukti, R. R., Febriyanti, E., Suendo, V., Setiabudi, H. D., Mohamed, M., & Nabgan, W. (2017). Oxygen vacancy-rich mesoporous silica KCC-1 for CO2 methanation. *Applied Catalysis A: General*, *532*, 86–94.

Hou, Z., Chen, P., Fang, H., Zheng, X., & Yashima, T. (2006). Production of synthesis gas via methane reforming with CO2on noble metals and small amount of noble-(Rh-) promoted

Ni catalysts. *International Journal of Hydrogen Energy*, *31*(5), 555–561.

Hwang, S., Hong, U. G., Lee, J., Baik, J. H., Koh, D. J., Lim, H., & Song, I. K. (2012). Methanation of carbon dioxide over mesoporous nickel-m-alumina (M 5 Fe, Zr, Ni, Y, and Mg) xerogel catalysts: Effect of second metal. *Catalysis Letters*, *142*(7), 860–868.

Hwang, S., Hong, U. G., Lee, J., Seo, J. G., Baik, J. H., Koh, D. J., Lim, H., & Song, I. K. (2013). Methanation of carbon dioxide over mesoporous Ni-Fe-Al2O3 catalysts prepared by a coprecipitation method: Effect of precipitation agent. *Journal of Industrial and Engineering Chemistry*, *19*(6), 2016–2021.

Jusoh, N. W. C., Jalil, A. A., Triwahyono, S., Setiabudi, H. D., Sapawe, N., Satar, M. A. H., Karim, A. H., Kamarudin, N. H. N., Jusoh, R., Jaafar, N. F., Salamun, N., & Efendi, J. (2013). Sequential desilication-isomorphous substitution route to prepare mesostructured silica nanoparticles loaded with ZnO and their photocatalytic activity. *Applied Catalysis A: General*, *468*, 276–287.

Jusoh, N. W. C., Jalil, A. A., Triwahyono, S., Karim, A. H., Salleh, N. F., Annuar, N. H. R., Jaafar, N. F., Firmansyah, M. L., Mukti, R. R., & Ali, M. W. (2015). Structural rearrangement of mesostructured silica nanoparticles incorporated with ZnO catalyst and its photoactivity: effect of alkaline aqueous electrolyte concentration. *Applied Surface Science*, *330*, 10–19.

Jwa, E., Lee, S. B., Lee, H. W., & Mok, Y. S. (2013). Plasma-assisted catalytic methanation of CO and CO2 over Ni-zeolite catalysts. *Fuel Processing Technology*, *108*, 89–93.

Karim, A. H., Jalil, A. A., Triwahyono, S., Sidik, S. M., Kamarudin, N. H. N., Jusoh, R., Jusoh, N. W. C., & Hameed, B. H. (2012). Amino modified mesostructured silica nanoparticles for efficient adsorption of methylene blue. *Journal of Colloid and Interface Science*, *386*(1), 307–314.

Kathiraser, Y., Oemar, U., Saw, E. T., Li, Z., & Kawi, S. (2015). Kinetic and mechanistic aspects for CO2 reforming of methane over Ni based catalysts. *Chemical Engineering Journal*, *278*, 62–78.

Kruk, M., Jaroniec, M., & Sayari, A. (2000). New insights into pore-size expansion of mesoporous silicates using long-chain amines. *Microporous and Mesoporous Materials*, *35–36*, 545–553.

Kučera, J., Nachtigall, P., Kotrla, J., Košová, G., & Čejka, J. (2004). Pyrrole as a probe molecule for characterization of basic sites in ZSM-5: A combined FTIR spectroscopy and computational study. *Journal of Physical Chemistry B*, *108*(41), 16012–16022.

Lercher, J. A., Jentys, A., Cejka, I., Bekkum, H. van, Corma, A., & Schuth(Eds.), F. (2007). Introduction to Zeolite Science and Practice. *Third Ed., Elsevier, Amsterdam*, 452.

Li, D., Zeng, L., Li, X., Wang, X., Ma, H., Assabumrungrat, S., & Gong, J. (2015). Ceria-promoted Ni/SBA-15 catalysts for ethanol steam reforming with enhanced activity and resistance to deactivation. *Applied Catalysis B: Environmental*, *176–177*, 532–541.

Li, S., & Gong, J. (2014). Strategies for improving the performance and stability of Ni-based catalysts for reforming reactions. *Chemical Society Reviews*, *43*(21), 7245–7256.

Li, S., Li, K., Hao, J., Ning, P., Tang, L., & Sun, X. (2016). Acid modified mesoporous Cu/SBA-15 for simultaneous adsorption/oxidation of hydrogen sulfide and phosphine. *Chemical Engineering Journal*, *302*, 69–76.

Liu, H., Zou, X., Wang, X., Lu, X., & Ding, W. (2012). Effect of CeO_2 addition on Ni/Al2O3 catalysts for methanation of carbon dioxide with hydrogen. *Journal of Natural Gas Chemistry*, *21*(6), 703–707.

Liu, J., Li, C., Wang, F., He, S., Chen, H., Zhao, Y., Wei, M., Evans, D. G., & Duan, X. (2013). Enhanced low-temperature activity of CO_2 methanation over highly-dispersed Ni/TiO_2 catalyst. *Catalysis Science and Technology*, *3*(10), 2627–2633.

Liu, Q., Bian, B., Fan, J., & Yang, J. (2018). Cobalt doped Ni based ordered mesoporous catalysts for CO_2 methanation with enhanced catalytic performance. *International Journal of Hydrogen Energy*, 1–9.

Liu, Q., Qiao, Y., Tian, Y., Gu, F., Zhong, Z., & Su, F. (2017). Ordered Mesoporous Ni-Fe-Al Catalysts for CO Methanation with Enhanced Activity and Resistance to Deactivation. *Industrial and Engineering Chemistry Research*, *56*(35), 9809–9820.

Liu, Q., & Tian, Y. (2017). One-pot synthesis of NiO/SBA-15 monolith catalyst with a three-dimensional framework for CO2methanation. *International Journal of Hydrogen Energy*, *42*(17), 12295–12300.

Liu, Q., Tian, Y., & Ai, H. (2016). RSC Advances. *RSC Advances*, *6*, 20971–20978.

Liu, Q., Wang, S., Zhao, G., & Yang, H. (2017). ScienceDirect CO_2 methanation over ordered mesoporous enhanced catalytic performance. *International Journal of Hydrogen Energy*, *43*(1), 239–250.

Lu, B., Ju, Y., Abe, T., & Kawamoto, K. (2015). RSC Advances. *RSC Adv.*, *5*, 56444–56454.

Lu, B., & Kawamoto, K. (2013). Preparation of the highly loaded and well-dispersed NiO/SBA-15 for methanation of producer gas. *Fuel*, *103*, 699–704. h

Lu, B., & Kawamoto, K. (2014). NiO/SBA15. *Inter. Coal Sci. Technol*, *1*(2), 315–320.

Ma, Q., Wang, D., Wu, M., Zhao, T., Yoneyama, Y., & Tsubaki, N. (2013). Effect of catalytic site position: Nickel nanocatalyst selectively loaded inside or outside carbon nanotubes for methane dry reforming. *Fuel*, *108*, 430–438.

Marakatti, V. S., & Peter, S. C. (2016). Nickel-antimony nanoparticles confined in SBA-15 as highly efficient catalysts for the hydrogenation of nitroarenes. *New J. Chem*, *40*(6), 5448–5457.

Mirth, G., & Lercher, J. A. (1990). Adsorption Complexes of Methanol on Zeolite ZSM-5, *86*(17), 3039–3044.

Mutz, B., Carvalho, H. W. P., Mangold, S., Kleist, W., & Grunwaldt, J. D. (2015). Methanation of CO_2: Structural response of a Ni-based catalyst under fluctuating reaction conditions unraveled by operando spectroscopy. *Journal of Catalysis*, *327*, 48–53.

Newalkar, B. L., & Komarneni, S. (2001). Control over microporosity of ordered microporous-mesoporous silica SBA-15 framework under microwave-hydrothermal conditions: Effect of salt addition. *Chemistry of Materials*, *13*(12), 4573–4579.

Ocampo, F., Louis, B., Kiwi-Minsker, L., & Roger, A. C. (2011). Effect of Ce/Zr composition and noble metal promotion on nickel based CexZr1-xO2 catalysts for carbon dioxide methanation. *Applied Catalysis A: General*, *392*(1–2), 36–44.

Pan, Q., Peng, J., Wang, S., & Wang, S. (2014). In situ FTIR spectroscopic study of the CO $_2$ methanation mechanism on Ni/Ce $_{0.5}$ Zr $_{0.5}$ O $_2$. *Catal. Sci. Technol.*, *4*(2), 502–509.

Pan, W., Zhang, S., He, F., Gai, S., Sun, Y., & Yang, P. (2015). A cheap and efficient catalyst with ultra-high activity for reduction of 4-nitrophenol. *CrystEngComm*, *17*(30), 5744–5750.

Patil, U., Fihri, A., Emwas, A.-H., & Polshettiwar, V. (2012). Silicon oxynitrides of KCC-1, SBA-15 and MCM-41 for CO2 capture with excellent stability and regenerability. *Chemical Science*, *3*(7), 2224.

Pudukudy, M., Yaakob, Z., & Akmal, Z. S. (2015a). Direct decomposition of methane over Pd promoted Ni/SBA-15 catalysts. *Applied Surface Science*, *353*, 127–136.

Pudukudy, M., Yaakob, Z., & Akmal, Z. S. (2015b). Direct decomposition of methane over SBA-15 supported Ni, Co and Fe based bimetallic catalysts. *Applied Surface Science*, *330*, 418–430.

Rahmani, S., Rezaei, M., & Meshkani, F. (2014). Preparation of promoted nickel catalysts supported on mesoporous nanocrystalline gamma alumina for carbon dioxide methanation reaction. *Journal of Industrial and Engineering Chemistry*, *20*(6), 4176–4182.

Rahmat, N., Abdullah, A. Z., & Mohamed, A. R. (2010). A review: Mesoporous Santa Barbara amorphous-15, types, synthesis and its applications towards biorefinery production. *American Journal of Applied Sciences*, *7*(12), 1579–1586.

Razzaq, R., Li, C., Usman, M., Suzuki, K., & Zhang, S. (2015). A highly active and stable Co4N/γ-Al2O3 catalyst for CO and CO_2 methanation to produce synthetic natural gas (SNG). *Chemical Engineering Journal*, *262*, 1090–1098.

https://doi.org/10.1016/j.cej.2014.10.073

Rodrigues, J. J., Marinho, J. C., Eduardo, R. S., Lima, E. G., & Rodrigues, M. G. F. (2015). Study of the application of MO/SBA-15 and Ni/SBA-15 catalysts, prepared by microwave heating, in the synthesis of biodiesel. *Brazilian Journal of Petroleum and Gas*, *9*(1), 11–18. https://doi.org/10.5419/bjpg2015-0002

Rossetto, E., Nicola, B. P., De Souza, R. F., Pergher, S. B. C., & Bernardo-Gusmão, K. (2015). Anchoring via covalent binding of β-diimine-nickel complexes in SBA-15 and its application in catalytic reactions. *Applied Catalysis A: General*, *502*, 221–229.

Sazegar, M. R., Jalil, A. A., Triwahyono, S., Mukti, R. R., Aziz, M., Aziz, M. A. A., Setiabudi, H. D., & Kamarudin, N. H. N. (2014). Protonation of Al-grafted mesostructured silica nanoparticles (MSN): Acidity and catalytic activity for cumene conversion. *Chemical Engineering Journal*, *240*, 352–361.

Scokart, P. O., & Rouxhet, P. G. (1980). Characterization of the basicity of oxides through the infrared study of pyrrole adsorption. *Journal of the Chemical Society, Faraday Transactions 1: Physical Chemistry in Condensed Phases*, *76*, 1476–1489.

Setiabudi, H. D., Lim, K. H., Ainirazali, N., & Chin, S. Y. (2017). CO_2 reforming of CH_4 over Ni / SBA-15 : Influence of Ni loading on the metal- support interaction and catalytic activity. *Journal of Materials and Environmental Sciences*, *8*(2), 573–581.

Setiabudi, H. D., Razak, N. S. A., Suhaimi, F. R. M., & Pauzi, F. N. (2016). CO_2 reforming of CH_4 over Ni/SBA-15: Influence of Ni-loading methods. *Malaysian Journal of Catalyst*, *1*, 1–6.

Sharma, S., Hu, Z., Zhang, P., McFarland, E. W., & Metiu, H. (2011). CO_2 methanation on Ru-doped ceria. *Journal of Catalysis*, *278*(2), 297–309.

Sidik, S. M., Triwahyono, S., Jalil, A. A., Aziz, M. A. A., & Fatah, N. A. (2016). Tailoring the properties of electrolyzed Ni/mesostructured silica nanoparticles (MSN) via different Ni-loading methods for CO_2 reforming of CH_4. *Journal of CO_2 Utilization*, *13*, 71–80.

Tada, S., Ochieng, O. J., Kikuchi, R., Haneda, T., & Kameyama, H. (2014). Promotion of CO_2 methanation activity and CH_4 selectivity at low temperatures over $Ru/CeO_2/Al_2O_3$ catalysts. *International Journal of Hydrogen Energy*, *39*(19), 10090–10100.

Tada, S., Shimizu, T., Kameyama, H., Haneda, T., & Kikuchi, R. (2012). Ni/CeO2 catalysts with high CO_2 methanation activity and high CH_4 selectivity at low temperatures. *International Journal of Hydrogen Energy*, *37*(7), 5527–5531.

Taherian, Z., Yousefpour, M., Tajally, M., & Khoshandam, B. (2017). Catalytic performance of Samaria-promoted Ni and Co/SBA-15 catalysts for dry reforming of methane. *International Journal of Hydrogen Energy*, *42*(39), 24811–24822.

Takht Ravanchi, M., & Sahebdelfar, S. (2014). Carbon dioxide capture and utilization in petrochemical industry: potentials and challenges. *Applied Petrochemical Research*, *4*(1), 63–77.

Tao, M., Xin, Z., Meng, X., Bian, Z., & Lv, Y. (2017). Highly dispersed nickel within mesochannels of SBA-15 for CO methanation with enhanced activity and excellent thermostability. *Fuel*, *188*, 267–276. https://doi.org/10.1016/j.fuel.2016.09.081

Teh, L. P., Triwahyono, S., Jalil, A. A., Mamat, C. R., Sidik, S. M., Fatah, N. A. A., Mukti, R. R., & Shishido, T. (2015). Nickel-promoted mesoporous ZSM5 for carbon monoxide methanation. *RSC Advances*, *5*(79), 64651–64660.

Teka, T., & Enyew, S. (2014). Study on effect of different parameters on adsorption efficiency of low cost activated orange peels for the removal of methylene blue dye. *International Journal of Innovation and Scientific Research*, *8*(1), 106–111.

Tomer, V. K., Devi, S., Malik, R., Nehra, S. P., & Duhan, S. (2016). Fast response with high performance humidity sensing of Ag-SnO2/SBA-15 nanohybrid sensors. *Microporous and Mesoporous Materials*, *219*, 240–248.

Vradman, L., Titelman, L., & Herskowitz, M. (2006). Size effect on SBA-15 microporosity. *Microporous and Mesoporous Materials*, *93*(1–3), 313–317.

Wang, J., Ge, H., & Bao, W. (2015). Synthesis and characteristics of SBA-15 with thick pore wall and high hydrothermal stability. *Materials Letters*, *145*, 312–315.

Wang, W., & Gong, J. (2011). Methanation of carbon dioxide: An overview. *Frontiers of Chemical Engineering in China*, *5*(1), 2–10.

Westermann, A., Azambre, B., Bacariza, M. C., Graça, I., Ribeiro, M. F., Lopes, J. M., & Henriques, C. (2015). Insight into CO_2 methanation mechanism over NiUSY zeolites: An operando IR study. *Applied Catalysis B: Environmental*, *174–175*, 120–125.

Xu, J., Zhou, W., Wang, J., Li, Z., & Ma, J. (2009). Characterization and Analysis of Carbon Deposited during the Dry Reforming of Methane over $Ni/La_2O_3/Al_2O_3$ Catalysts. *Chinese Journal of Catalysis*, *30*(11), 1076–1084.

Ye, W., Lin, Z., Dong, B., Kang, J., Zheng, X., & Wang, X. (2011). Preparation and Catalytic Properties of Ti-SBA-15 Mesoporous Materials. *Material Science and Application*, *2*, 661–668.

Zhang, J., Xin, Z., Meng, X., & Tao, M. (2013). Synthesis, characterization and properties of anti-sintering nickel incorporated MCM-41 methanation catalysts. *Fuel*, *109*, 693–701.

Zhang, X., Sun, W., & Chu, W. (2013). Effect of glow discharge plasma treatment on the performance of Ni/SiO_2 catalyst in CO_2 methanation. *Journal of Fuel Chemistry and Technology*, *41*(1), 96–101.

Zhao, B., Chen, Z., Chen, Y., & Ma, X. (2017). Syngas methanation over Ni/SiO_2 catalyst prepared by ammonia-assisted impregnation. *International Journal of Hydrogen Energy*, *42*(44), 27073–27083.

Zhao, D., Feng, J., Huo, Q., Melosh, N., Fredrickson, G. H., Chmelka, B. F., & Stucky, G. D. (1998). Triblock Copolymer Syntheses of Mesoporous Silica with Periodic 50 to 300 Angstrom Pores. *Science*, *279*, 548–552.

Zhao, K., Wang, W., & Li, Z. (2016). Highly efficient Ni/ZrO_2 catalysts prepared via combustion method for CO_2 methanation. *Journal of CO_2 Utilization*, *16*, 236–244.

Zheng, J., Wang, C., Chu, W., Zhou, Y., & Köhler, K. (2016). CO_2 Methanation over Supported Ru/Al_2O_3 Catalysts: Mechanistic Studies by *In situ* Infrared Spectroscopy. *ChemistrySelect*, *1*(12), 3197–3203.

Zhi, G., Guo, X., Guo, X., Wang, Y., & Jin, G. (2011). Effect of La_2O_3 modification on the catalytic performance of Ni/SiC for methanation of carbon dioxide, Catal. *Catalysis Communications*, *16*(1), 56–59.

Zhu, H., Razzaq, R., Jiang, L., & Li, C. (2012). Low-temperature methanation of CO in coke oven gas using single nanosized Co_3O_4 catalysts. *Catalysis Communications*, *23*, 43–47.

RESEARCH OUTPUTS

List of Publications

1. H.D. Setiabudi, K.H. Lim, N. Ainirazali, S.Y. Chin, N.H.N. Kamarudin, CO_2 reforming of CH_4 over Ni/SBA-15: Influence of Ni loading on the metal-support interaction and catalytic activity, Journal of Materials and Environmental Sciences 8(2) (2017) 573-581. (ISSN: 2028-2508, Scopus Indexed Journal, SJR: 0.295)

2. N. Ainirazali, N.A.N. AbGhazab, H.D. Setiabudi, C.S. Yee, CO_2 reforming of methane over Ni/Ce-SBA-15: Effects of Ce Addition, Indian Journal of Science and Technology, 10(17) 2017. (ISSN: 0974-5645, Indexed Journal)

3. S.N. Bukhari, C.Y. Chin, H.D. Setiabudi, D.V.N. Vo, Tailoring the properties and catalytic activites of Ni/SBA-15 via different TEOS/P123 mass ratios for CO_2 reforming of CH_4, Journal of Environmental Chemical Engineering, 5(4) (2017) 3122-3128. (ISSN: 2213-3437, Scopus Indexed Journal, SJR: 0.924)

4. H.D. Setiabudi, C.C. Chong, S.M. Abed, L.P. Teh, S.Y. Chin, Comparative study of Ni-Ce loading method: Beneficial effect of ultrasonic-assisted impregnation method in CO_2 reforming of CH_4 over Ni-Ce/SBA-15, Journal of Environmental Chemical Engineering 6(1) (2018) 745-753. (ISSN: 2213-3437, Scopus Indexed Journal, SJR: 0.924)

5. S.N. Bukhari, C.C. Chong, L.P. Teh, D.V.N. Vo, N. Ainirazali, S. Triwahyono, A.A. Jalil, H.D. Setiabudi, Promising hydrothermal technique for efficient CO_2 methanation over Ni/SBA-15, International Journal of Hydrogen Energy. (ISSN: 0360-3199, ISI Journal, IF = 4.229, Available Online, https://doi.org/10.1016/j.ijhydene.2018.07.018)

6. C.C. Chong, L.P. Teh, H.D. Setiabudi, Promotional effect of Mg, Ce, and Zr on Ni-based SBA-15 catalysts for CO_2 reforming of CH_4, Journal of Environmental Chemical Engineering (ISSN: 2213-3437, Scopus Indexed Journal, SJR: 0.924, Under Review, Manuscript No. JECE-D-18-01172)

7. M.A.A. Aziz, H.D. Setiabudi, L.P. Teh, N.H.R. Annuar, S. Triwahyono, A.A. Jalil, Recent Development On Heterogeneous Catalysts for Syngas Production Via CO_2 Utilization, Catalysis Today (ISSN 0920-5861, ISI Journal, IF = 4.667, In revision, Manuscript No. CATTOD_2018_269)

8. S.N. Bukhari, C.C. Chong, H.D. Setiabudi, L.P. Teh, N. Ainirazali, S. Triwahyono, A.A. Jalil, Ni/Fibrous SBA-15: Superb catalytic performance and coke resistance catalyst

towards CO_2 methanation, Catalysis Today (ISSN 0920-5861, ISI Journal, IF = 4.667, Under Review, Manuscript No. CATTOD_2018_367)

List of Conferences

1. S.N. Bukhari, A.H.K. Owgi, N. Ainirazali, D.N. Vo, H.D. Setiabudi, Enhanced catalytic performance of Ni/SBA-15 towards CO_2 methanation via P123-assisted method. *The 3rd International Conference on Green Chemical Engineering and Technology (3rd GCET):* 07-08 November 2017, Melaka, Malaysia. (Accepted in Material Today: Proceedings, ISSN: 2214-7853, Indexed Journal, SJR: 0.314).

2. C.C. Chong, A.H.K. Owgi, N. Ainirazali, S.Y. Chin, H.D. Setiabudi, CO_2 Reforming of CH_4 over Ni/SBA-15 Prepared by Surfactant-Assisted Impregnation Method: Comparative Study of Surfactant Types. *The 3rd International Conference on Green Chemical Engineering and Technology (3rd GCET),* 07-08 November 2017, Melaka, Malaysia. (Accepted in Material Today: Proceedings, ISSN: 2214-7853, Indexed Journal, SJR: 0.314).

3. S.N. Bukhari, C.C. Chong, H.D. Setiabudi, N. Ainirazali, M.A.A. Aziz, L.P. Teh, N.H.R. Annuar, Comparative Study of Ni Loading Methods Towards Superior CO_2 Conversion over Ni/SBA-15. *5th International Conference on Business, Science and Technology (ICBST 2018),* 13-15 April 2018, Ho Chi Minh City, Vietnam. (under consideration in Journal of Engineering and Applied Science, ISSN: 1110-1903, Indexed Journal, SJR: 0.101).

Exhibitions

1. Chin Chia Yun, Herma Dina Setiabudi, Design and development of Ni/SBA-15 for CO_2 reforming of CH_4, 2016 Creation, Innovation, Technology & Research Exposition (CITREX 2016), 7-8 March 2016, Universiti Malaysia Pahang, Pahang. (Bronze)

2. Lim Kiang Hoo, Herma Dina Setiabudi, Nurul Aini Mohamed Razali, Development of Ni/SBA-15 catalyst and its potential in enhancing syngas production, 2016 Creation, Innovation, Technology & Research Exposition (CITREX 2016), 7-8 March 2016, Universiti Malaysia Pahang, Pahang. (Bronze)

3. Siti Nuraihan Mohd Arof, Nurul Aini Mohamed Razali, Herma Dina Setiabudi, Production of Hydrogen over Ni/SBA-15 catalyst, 2016 Creation, Innovation, Technology & Research Exposition (CITREX 2016), 7-8 March 2016, Universiti Malaysia Pahang, Pahang. (Bronze)

List of Students

Master Research

1. Syahida Nasuha Mohd Bukhari (MKC16031), Synthesis and Evaluation of Catalytic Performance of Ni Supported On Fibrous Morphology of SBA-15 (F-Ni/SBA-15) For CO_2 Methanation, Master Research, 2018.

Master Project

1. Saad Mohsin Abed (KKK14005), Production of Syngas from CO_2 Reforming of CH_4 using Ni-Ce/SBA-15 Catalyst, Master Project, 2016.
2. Abderahman Hamad Khalifa Owgi (KKE16007), Synthesis and Characterization of Surfactant-Assisted Ni/SBA-15 Catalysts for CO_2 Dry Reforming of CH_4, Master Project, 2016.

Undergraduate Research Project

1. Chin Chia Yun (KA12108), Carbon Dioxide Reforming of Methane over Ni-promoted SBA-15: Effect of TEOS/P123 Mass Ratio, Undergraduate Research Project, 2016.
2. Lim Kiang Hoo (KA12105), CO_2 Reforming over Nickel/SBA-15 Catalyst: Effect of Nickel Loading, Undergraduate Research Project, 2016.
3. Noor Syahira bt Abd Razak (KA12057), CO_2 Reforming Methane over Nickel/SBA-15 Catalyst: Effect of the Preparation Method, Undergraduate Research Project, 2016.